

BIOPHYSICAL AND FUNCTIONAL CHARACTERIZATION OF THE PERSULFIDE
SENSOR CstR FROM *Staphylococcus aureus*

Justin L. Luebke

Submitted to the faculty of the University Graduate School in partial fulfillment of the
requirements for the degree Doctor of Philosophy in the Department of Chemistry,
Indiana University

April 2015

Accepted by the Graduate Faculty, Indiana University, in partial fulfillment of the requirements for the degree of Doctor of Philosophy

Doctoral Committee

David, P. Giedroc, Ph.D.

Charles E. Dann III, Ph.D.

Martha Oakley, Ph.D.

James Reilly, Ph.D.

March, 12th, 2015

I dedicate this body of work to my family who has always encouraged me to pursue the highest academic achievements, my friends who brought balance, and Danielle Fanslow who has seen me through from beginning to end. This would not have been possible without you.

ACKNOWLEDGEMENTS

I would like to thank my advisor, Dr. David P. Giedroc for his support, guidance, and dedication throughout my graduate career at Indiana University. I also would like to thank the member of the Giedroc laboratory and in particular Dr. Khadine Higgins, Dr. Joseph Braymar, Dr. Katie Edmonds, Jiangchun Shen, John Lisher, Kevin Bruce, and Dr. Yue Fu. Their helpful insights and discussions have proved to be invaluable. Finally, I wish to thank my undergraduate advisor Dr. Ted Wilson (Winona State University) for directing me toward graduate school before I knew that this was what I wanted to do.

Justin L. Luebke

BIOPHYSICAL AND FUNCTIONAL CHARACTERIZATION OF THE PERSULFIDE
SENSOR CstR FROM *Staphylococcus aureus*

How cells regulate the intracellular bioavailable pool of sulfur while mitigating its toxic effects is poorly understood. Major components of this pool, collectively referred to as reactive sulfur species (RSS), include hydrogen sulfide (H₂S) and low molecular weight per- and polysulfides and become deleterious at increasing concentrations. For example, H₂S functions as a gaseous signaling molecule but at elevated levels can poison cytochrome c oxidase of the electron transport chain. The human pathogen *Staphylococcus aureus* contains an apparent complete sulfur oxidation system, termed the *cst* operon, which is under control of the transcriptional regulator CstR (Copper-sensing operon repressor (CsoR)-like sulfurtransferase repressor). In this work, sulfide stress, as exogenous H₂S or RSS, is identified as a strong inducer of the *cst* operon. Failure to express this operon or deletions of enzymes within results in loss cellular viability under sulfide stress conditions. Biophysical investigations into the regulator CstR revealed it does not react with hydrogen sulfide directly but rather reacts with the sulfane sulfur of an inorganic polysulfide or organic persulfide donor to form di-, tri, and tetrasulfide bonds between two conserved cysteine residues, Cys31 and Cys60' on opposite protomers as determined by high-resolution tandem mass spectrometry. These modifications result in negative regulation of *cst* operator DNA binding affinity. Interestingly, CstR displays reaction specificity compared to the structurally similar CsoR

that is also found in *S. aureus*, which controls the expression of genes responsible for copper toxicity resistance. Comparative analysis of CstR and CsoR cysteine reactivity by pulsed-alkylation mass spectrometry reveals a striking difference in Cys31 reactivity (Cys41 in CsoR). These studies provide the framework for better understanding of sulfide homeostasis and stress resistance as well as identification of key differences in CstR and CsoR inducer selectivity.

David, P. Giedroc, Ph.D.

Charles E. Dann III, Ph.D.

Martha Oakley, Ph.D.

James Reilly, Ph.D.

TABLE OF CONTENTS

DEDICATION	iii
ACKNOWLEDGEMENTS	iv
ABSTRACT	v
TABLE OF CONTENTS	vii
ABBREVIATIONS	ix
LIST OF FIGURES	xiii
LIST OF TABLES	xvi
CHAPTER	
I INTRODUCTION	1
The Low Molecular Weight Thiol Pool	3
Cysteine: A Redox-Sensitive Amino Acid in Proteins	6
Oxidative Stress at the Host-Pathogen Interface	9
Reactive Oxygen Species (ROS)	11
Reactive Nitrogen Species (RNS)	13
Reactive Electrophile Species (RES)	15
Reactive Chlorine Species (RCS)	16
Hydrogen Sulfide (H ₂ S) and reactive Sulfur Species (RSS)	16
Sulfur Metabolism in <i>Staphylococcus aureus</i>	20
The CsoR Family of Transcriptional Regulators	22
CstR and the <i>cst</i> Operon	22
Scope of Research	27

II	CHARACTERIZATION OF THE REACTION OF CstR WITH THE CHALCOGEN OXANIONS SELENITE AND TELLURITE	
	Preface.....	29
	Introduction.....	29
	Materials and Methods.....	32
	Results.....	36
	Discussion.....	58
III	CstR IS A PERSULFIDE SENSOR IN <i>Staphylococcus aureus</i>	
	Introduction.....	61
	Materials and Methods.....	65
	Results.....	70
	Discussion.....	96
IV	THE BIOPHYSICAL CHARACTERIZATION OF CstR and CsoR CYSTEINE RESIDUES	
	Introduction.....	102
	Materials and Methods.....	105
	Results.....	109
	Discussion.....	124
V	SUMMARY AND PROSPECTUS	
	Summary.....	128
	Prospective.....	132
	REFERENCES.....	140
	APPENDIX.....	158
	CURRICULUM VITAE	

ABBREVIATIONS

3-MST	3-mercaptopyruvate sulfurtransferase
BigR	Biofilm growth-associated repressor
Blh	β -lactamase-like hydrolase
BSH	Bacillithiol
BSSB	Oxidized bacillithiol
CBS	Cystathionine b-synthase
Cm	Chloramphenicol
CoA	Coenzyme A
CSE	Cystathionine g-synthase
CsoR	Copper-sensitive operon repressor
CstR	CsoR-like sulfurtransferase repressor
Cys	Cysteine
DAO	NADPH oxidase
DUOX	Dual oxidase
FeS	Iron-sulfur clusters
GSH	Glutathione
GSNO	Glutathione S-nitrosothiol
GSSG	Oxidized glutathione
GSSH	Glutathione persulfide
H ₂ O ₂	Hydrogen peroxide
H ₂ S/HS ⁻	Hydrogen sulfide
H ₂ S ₂	Hydrodisulfide

HNO	Nitroxyl
HOCl	Hypochlorite
HS•	Sulfide radical
HSNO	Thionitrous acid
LC-ESI-MS	Liquid chromatography electrospray ionization mass spectrometry
LMW	Low molecular weight
LTQ	Linear triple quadrupole
MG	Methylglyoxal
MMTS	Methylmethanethiolsulfonate
MPO	Myeloperoxidase
MSH	Mycothiols
N ₂ O ₃	Dinitrogen trioxide
Na ₂ S	Sodium sulfide
Na ₂ S ₄	Sodium tetrasulfide
NaHS	Sodium hydrogen sulfide
NF-κB	Nuclear factor kappa B
NmlR	<i>Neisseria merR</i> -like regulator
NO/NO•	Nitric oxide
NO ₂ ⁻	Nitrite
NO ₂ •	Nitrogen dioxide
NOS	Nitric oxide synthase
NOX	NADPH oxidase

$O_2^{\cdot-}$	Superoxide anion
OH^{\cdot}	Hydroxyl radical
OhrR	Organic hydroperoxide reductase repressor
$ONOO^-$	Peroxynitrite
PTM ^{ox}	Oxidative post-translational modification
qRT-PCR	Quantitative real-time polymerase chain reaction
RCS	Reactive chlorine species
RES	Reactive electrophilic species
RNS	Reactive nitrogen species
ROOH	Organic peroxide
ROS	Reactive oxygen species
$RS(S_n)H$	Hydrogen polysulfides
$RS(S_n)SR'$	Polysulfides
RSNO	Nitrosothiol
RSS	Reactive sulfur species
RSSH	Persulfides
$S_2O_3^{2-}$	Thiosulfate
$S_4O_6^{2-}$	Tetrathionate
SDO	Sulfur dioxygenase
SeO_3^{2-}	Selenite
SO_3^{2-}	Sulfite
SOD	Superoxide dismutase
SQR	Sulfide-quinone oxidoreductase

TCA	Trichloroacetic acid
TeO_3^{2-}	Tellurite
TFA	Trifluoroacetic acid
TRPA1	Transient receptor protein channel A1
TS	Thiosulfate
TSB	Tryptic soy broth
TST	Thiosulfate sulfur transferase

LIST OF FIGURES

FIGURE	PAGE
1	Overview of cellular redox potential and LMW thiols2
2	Response to oxidative stress occurs through transcriptional regulators4
3	Oxidative post-translational modifications (PMT ^{ox}) of cysteine residues8
4	Interplay of ROS, RNS, RCS, RES, and RSS10
5	Ribbon representation of selected crystal structure of oxidative stress-sensing transcriptional repressors17
6	Sulfur metabolic pathways in <i>Staphylococcus aureus</i>21
7	Crystal structure of <i>Mycobacterium tuberculosis</i> CsoR23
8	Schematic representation of the <i>cst</i> operon25
9	Sequence alignment of putative CstRs26
10	Mechanism of thiol-mediated selenite reduction31
11	LC-ESI-MS <i>m/z</i> ratios of reduced and oxidized CstR38
12	LC-ESI-MS analysis of CstR following reaction with selenite or tellurite39
13	LC-ESI-MS analysis of CsoR following reaction with selenite or tellurite41
14	Fragmentation patterns of CstR cysteine-containing peptides45
15	Tryptic peptides of selenite-reacted CstR identify a selenotrisulfide46
16	CstR reacted with selenite contains prominent disulfide peaks with oxidized cysteine residues48
17	Fluorescence anisotropy titrations of reduced and cross-linked CstR51
18	LC-ESI-MS analysis of CstR cysteine mutants following reaction sulfite...55
19	LC-ESI-MS analysis of CstR cysteine mutants following reaction with57 tetrathionate

20	Model of sulfide homeostasis	62
21	Model of enzyme-catalyzed detoxification of hydrogen sulfide	64
22	CstR is required for <i>S. aureus</i> defense against sulfide stress.....	72
23	Individual <i>cst</i> genes are required for sulfide stress resistance	74
24	The <i>cst</i> operon is regulated by hydrogen sulfide stress <i>in vivo</i>	77
25	CstR reacts with a sulfane sulfur donor to form a series of mixed di-, tri-, and tetrasulfide crosslinks	81
26	High-resolution tandem mass spectrometry confirms di-, tri-, and tetrasulfide mass shift assignments.....	86
27	Fragmentation data of sulfide-treated CstR samples is not attributed to methionine oxidation of crosslinked CstR tryptic peptides	89
28	Reaction of CstR with sulfide negatively regulates DNA operator binding.	90
29	The <i>cst</i> operon is required for polysulfide and disodium sulfide resistance.	93
30	CsoR is not functionally analogous to CstR	94
31	Abbreviated rendering of sulfur assimilation and hydrogen sulfide metabolism in <i>S. aureus</i> strain Newman	101
32	<i>Mycobacterium tuberculosis</i> CsoR Cu(I) binding pocket	104
33	CstR forms a modest affinity complex with Cu(I) and metal binding does not negatively regulate <i>cst</i> DNA binding.....	110
34	Reaction schematic of the pulse-chase alkylation reaction.....	113
35	Pulsed-alkylation MALDI-TOF results	115
36	Rate analysis of pulsed-alkylation results.....	116
37	Observed pK_a of Cys41 of CsoR is approximately 1 pH unit higher than Cys31 of CstR.....	118
38	CstR lysine mutants impact <i>S. aureus</i> growth under sulfide stress	121
39	K29D CstR does not bind to <i>cst</i> DNA	122

40	Analysis of the electrostatics near the CsoR Cu(I) binding pocket	127
41	Model of sulfide homeostasis in <i>Staphylococcus aureus</i>	131
42	Growth of <i>Staphylococcus aureus</i> under low oxygen conditions and sulfide stress.....	134
43	The <i>cst</i> operon is induced under biofilm growth curve conditions with nitrite stress.....	136
44	The <i>cst</i> operon is required for nitroxyl stress resistance.....	138

LIST OF TABLES

TABLE		PAGE
1	Summary of LC-ESI-MS deconvoluted masses obtained from CstR reaction with selenite, tellurite, or tetrathionate	40
2	Summary of LC-ESI-MS deconvoluted masses obtained from CsoR reaction with selenite, tellurite, or tetrathionate	42
3	Monoisotopic masses for the parent ions of selenite- or tellurite-reacted CstR tryptic peptides.....	44
4	Summary of macroscopic binding constants of WT CstR and CstR cysteine mutants	52
5	Summary of LC-ESI-MS deconvoluted masses obtained for CstR cysteine mutants	56
6	Summary of LC-ESI-MS deconvoluted masses obtained from CstR reaction with LMW sulfur compounds.....	83
7	Monoisotopic masses of di-, tri-, and tetrasulfide cross-linked parent ions in the +4 charge state	85
8	Summary of CstR DNA binding constants following reaction with NaHS or Na ₂ S ₄	91
9	Summary of LC-ESI-MS deconvoluted masses obtained from CsoR reaction with LMW sulfur compounds	95
10	Summary of calculated and observed monoisotopic masses for cysteine-containing peptides	114
11	Summary of pulsed-alkylation rate constants	117
12	Summary of macroscopic binding constants of CstR lysine mutants.....	123

CHAPTER I

INTRODUCTION

All microorganisms continuously monitor their immediate microenvironment and must be capable of responding to changes in cellular redox status irrespective of the specific niche. This is particularly true for bacterial pathogens that colonize the vertebrate host. The bacterial cytoplasm is strongly reducing and is maintained by the ratio of reduced to oxidized low molecular weight (LMW) thiols (Fig. 1). Any small molecule that disrupts the LMW thiol pool or alters the ratio of reduced to oxidized LMW thiols induces an oxidative stress response in the organism. Small molecules that comprise reactive oxygen species (ROS), reactive nitrogen species (RNS), reactive electrophile species (RES), reactive chlorine species (RCS), and reactive sulfur species (RSS)^{1,2} are oxidative stressors as they target both the LMW thiol pool and protein-based thiols.

At superphysiological concentrations oxidative stressors become toxic and can disrupt the electron transport chain, disassemble Fe-S clusters and mononuclear transition metal complexes, induce DNA damage and oxidize membrane lipids and proteins.³⁻⁵ The host attempts to exploit this chemistry as an integral component of host innate immune response against bacterial invaders;⁷ this in turn necessitates a rapid sensing, transcriptional response, detoxification of the oxidative species, and damage repair to restore intracellular redox balance in successful pathogenic bacteria. The regulation of detoxification and repair enzymes used to combat changes in redox state is controlled by redox-sensing DNA-binding transcriptional regulatory proteins.

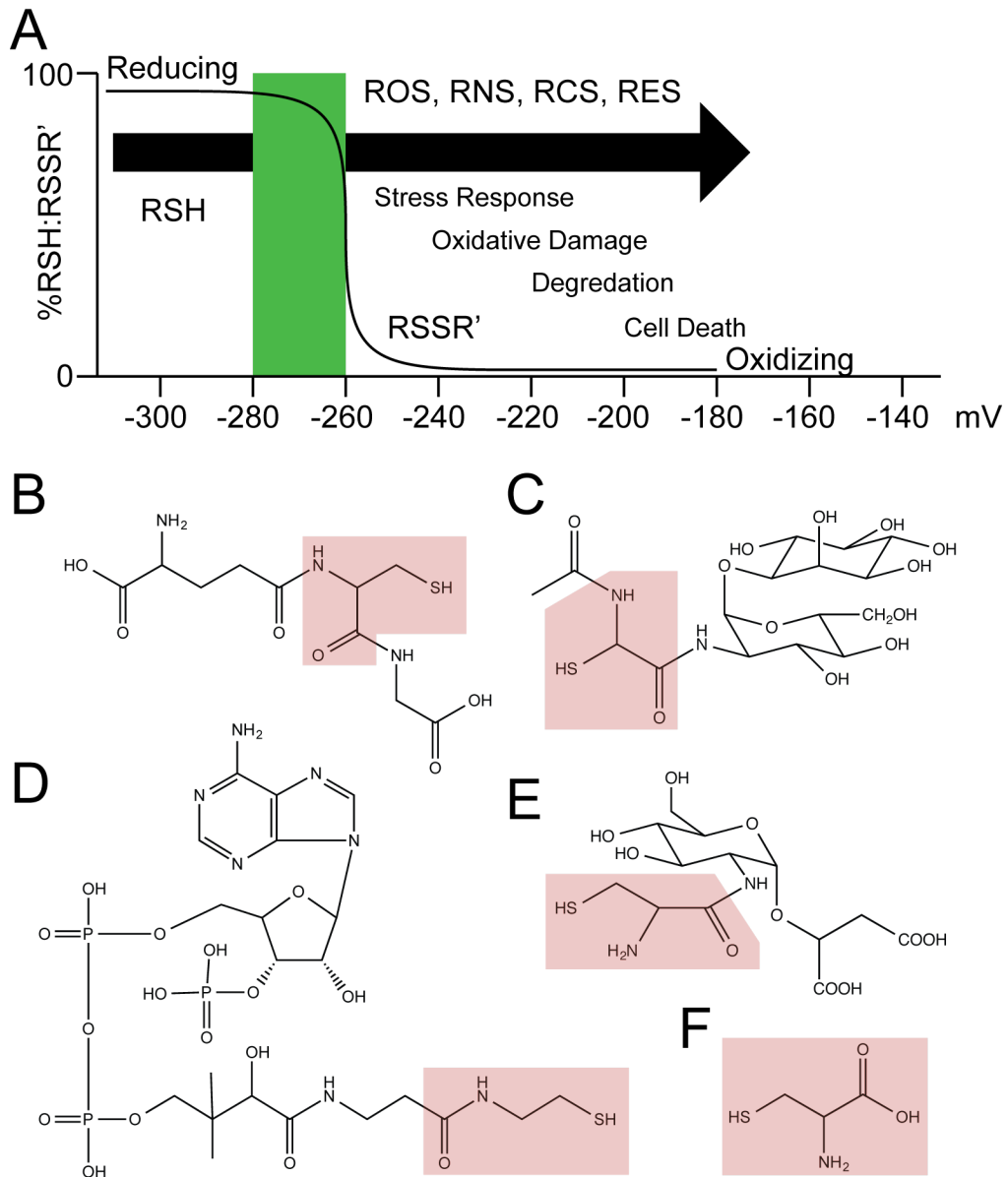


Figure 1. Overview of cellular redox potential and LMW thiols. (A) Cellular redox potential where increasing stress leads to damage of cellular components, degradation, and cell death if the stress surpasses the ability of the cell to adapt. (B-F) Major LMW thiols found in bacteria. Each incorporates the amino acid cysteine, highlighted in red, and therefore a thiol, as part of the primary structure. (B) Glutathione, (C) mycothiol, (D) coenzyme A, (E) bacillithiol, and (F) cysteine.

Two broad types of stress-sensing mechanisms have been described for the vast majority of transcriptional regulatory proteins: those which utilize a prosthetic group and those that detect stress through cysteine post translational modifications. Transcriptional regulators utilizing a prosthetic group include heme-based redox sensors, exemplified by *Mycobacterium tuberculosis* DosS,^{8,9} non-heme Fe-based sensors, *e.g.*, *Bacillus subtilis* PerR;¹⁰ Fe-S-cluster based sensors, including *Escherichia coli* SoxR;¹¹⁻¹³ and *M. tuberculosis* WhiB proteins,¹⁴ or regulators that directly survey the cellular NADH/NAD⁺ ratio, *e.g.*, Rex from Gram-positive pathogens.¹⁵⁻¹⁷

Transcriptional regulators that employ reactive cysteine residues to sense oxidative stress are capable of undergoing a myriad of oxidative post-translational modifications (PTM^{ox}) of the S γ atom (Fig. 2). Several examples include cysteine disulfide bond formation as observed with *Xylella fastidiosa* BigS¹⁸ and *Pseudomonas aeruginosa* MexR,¹⁹ S-thiolations in *Staphylococcus aureus* SarZ,²⁰ and even S-quinonization of QsrR from *S. aureus*,²¹ among others. Less common is the oxidation of the thioether S δ atom of methionine such as hypochlorite sensor HypT from *E. coli*.^{22,23} The exact PTM^{ox} is dependent on the specific regulatory protein but each endows cell with a distinct molecular mechanism to fine-tune the response to a given stressor.

THE LMW THIOL POOL

The reducing potential of the cell (E°) is a function of the ratio of reduced (RSH) to oxidized (RSSR') LMW thiols, where R is a specific organic moiety. Major cellular reductants include glutathione (GSH), mycothiol (MSH), bacillithiol (BSH), cysteine, and coenzyme A (CoA, Fig. 1B-E). GSH is primarily found in Gram-negative bacteria,

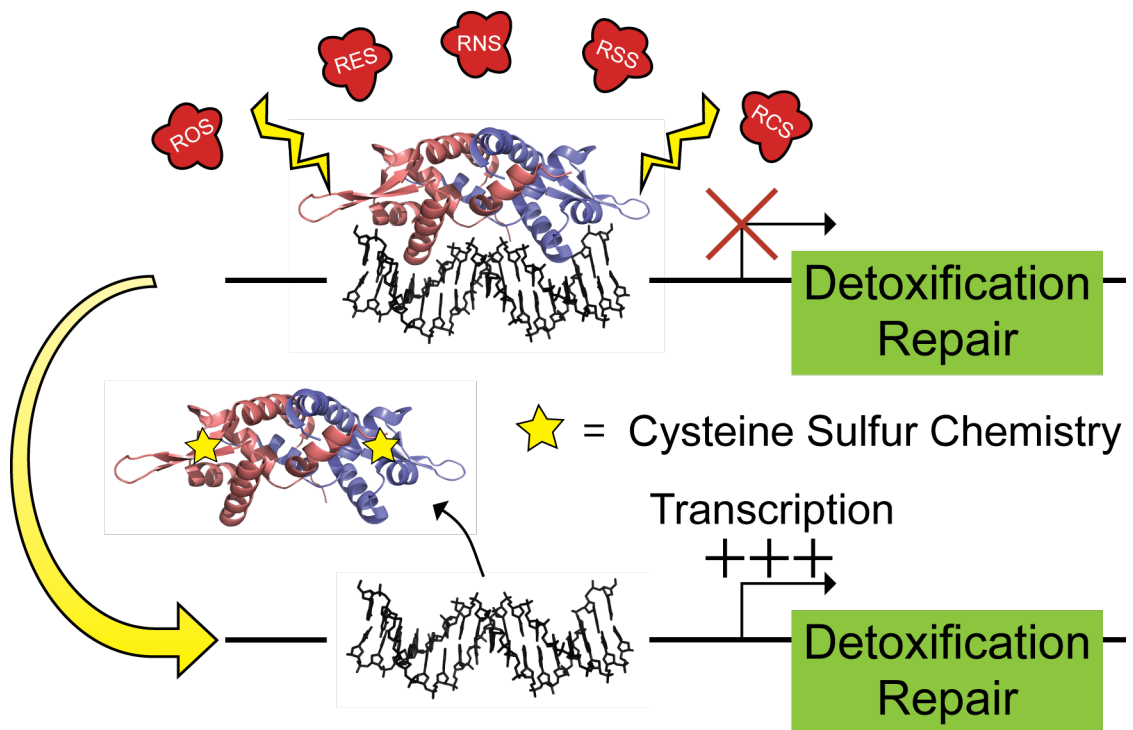


Figure 2. Response to oxidative stress occurs through transcriptional regulators. The mechanism used in many oxidative stress-sensing transcriptional regulators to “sense” stress is often a reactive cysteine that undergoes post-translational modification, leading to derepression of detoxification and/or repair enzymes. Detoxification will target the parent oxidant stressor directly and repair enzymes will reverse the damage caused by the stressor and/or any additional collateral damage caused by the stressor or side reactions that form other reactive species.

MSH in *M. tuberculosis* and other actinomycetes,²⁴ and BSH in many Gram-positive bacteria²⁵ including *Bacillus* spp. and *Staphylococcus* spp. Other bacteria such as *Streptococcus pneumoniae* do not produce GSH but uptake it from their environment.²⁶ For *Escherichia coli* cytoplasm, E° was measured to be ≈ -260 to -280 mV and is characterized with far more RSH than RSSR'.²⁷

The pK_a of a LMW thiol is typically 8.5-9 and thus the reduced form is defined by the equilibrium between protonated and deprotonated species. The intracellular [BSH] is in the 1 mM range for mid-log phase *B. subtilis* cells while the intracellular [GSH] is roughly 10 mM in a typical Gram-negative bacterium.²⁸ The high concentration of reduced LMW thiols in the cell represent an enormous “sink” that is used to protect the cell from oxidative damage. Although thiol-disulfide exchange is facile, LMW thiol-disulfide homeostasis is kinetically facilitated by enzymes that catalyze the reduction of LMW disulfides to free thiols. These enzymes include the well-characterized thioredoxins and glutaredoxins and more recently described mycoredoxins^{29,30} and bacilliredoxins³¹ as well as coenzyme A disulfide reductases.³²

In addition to redox stress, recent work indicates that the LMW thiol pool contributes to the transition metal buffering capacity of the cytoplasm, particularly for more thiophilic metals such as Zn(II)³³ and Cu(I).^{26,34} For example, BSH in *B. subtilis* has been shown to function as a buffer for the labile or free Zn(II) in the cell.³⁵ As the concentration of the reduced bacillithiol decreases, increased “free” zinc is efficiently sensed by the zinc efflux repressor, CzrA,³⁶ which leads to transcriptional derepression of a Zn(II) efflux transporter. This speaks to the strong interconnectedness of the oxidative stress response and metal metabolism in cells where changes in the redox balance are

coincident with perturbations in metal speciation, and can therefore potentially impact enzyme metallation.³⁷

CYSTEINE: A REDOX-SENSITIVE AMINO ACID IN PROTEINS

Cysteine is among the rarest and most functionally diverse of all the amino acids. It is often solvent-accessible, facilitating roles in redox chemistry, regulatory function, enzyme catalysis, structure, and coordination of transition metals.^{38,39} The diverse functionality of cysteine is due to a polarizable sulfur atom that makes reactivity highly tunable through the thiol moiety. Properties that control reactivity are a combination of solvent accessibility, proximity to titratable groups, which contribute to the pK_a of the thiol, and oxidation state.⁴⁰ The intrinsic pK_a of a cysteine in an unstructured peptide region is similar to that of GSH at $\approx 8.5-9.0$. Nearby basic residues such as histidine, lysine, and arginine can stabilize the thiolate anion, RS^- , via electrostatic complementarity and/or hydrogen bonding to the peptide backbone or other sidechains, thereby significantly lowering the pK_a to between 5 and 7 in proteins.⁴¹⁻⁴³ In extreme cases, cysteines have been reported to possess pK_a s as low as 3.5.⁴⁰ RS^- is a potent nucleophile poised to react with electrophilic functional groups. On the other hand, physical proximity to deprotonated acidic residues, *e.g.*, aspartate and glutamate, can raise the pK_a , resulting in stabilization of a protonated thiol at neutral pH. This attenuates the reactivity of the cysteine toward electrophiles. The critical importance of cysteine microenvironment in proteins is highlighted by the observation that thiol reactivity with the oxidant hydrogen peroxide (H_2O_2) can vary over seven orders of magnitude.⁴³

Thiols with low pK_{aS} are far more susceptible to *S*-hydroxylation (sulfenylation, RSOH, Fig. 3, **2**), a major post-translational modification induced by H_2O_2 , which increases electrophilic character and in turn enhances their reactivity toward cellular nucleophiles. Nucleophiles can include other protein cysteine thiolates or LMW thiolate anions that react to form disulfide bonds and *S*-thiolations (Fig. 3, **10-12**).^{42,44} Protein sulfenylation was originally thought to be a transient PTM^{ox} en route to disulfide bond formation but the development of mass spectrometry-based proteomics methods⁴⁵ and *in situ* labeling approaches⁴⁶ has revealed that sulfenylated cysteines can be stable in certain proteins. The crystal structure of sulfenylated SarZ, a global regulator from *S. aureus*, reveals two hydrogen bonds from nearby residues and provides molecular insight into the stabilization of the sulfenic acid.²⁰ A long-lived sulfenylated cysteine is particularly important for inducing a rapid response to changes of redox homeostasis in the cell. Many ROS, RES, and RCS stressors ultimately lead to cysteine sulfenylation as a primary PTM^{ox}.

Further oxidation of sulfenylated cysteines leads to *S*-sulfinic acid to *S*-sulfonic acid formation (Fig. 3, **14** and **15**). The latter two modifications, unlike sulfenylation and disulfide bond formation, are irreversible and cannot be reduced by cellular reductants; however, ATP-dependent sulfiredoxins can enzymatically catalyze the reduction of sulfenylated cysteine.⁴⁷ When sulfenylation of a single, more reactive Cys occurs in the presence of a second Cys, the second Cys can act as a resolving cysteine either *intramolecularly* (Fig. 3, **10**) or *intermolecularly* (Fig. 3, **11**), exactly analogous to the Cys pair in the thioredoxins, peroxiredoxins, glutaredoxins and related dithiol peroxidases that clear ROS and RNS.⁴⁷ Sulfenylated cysteines can also react with LMW

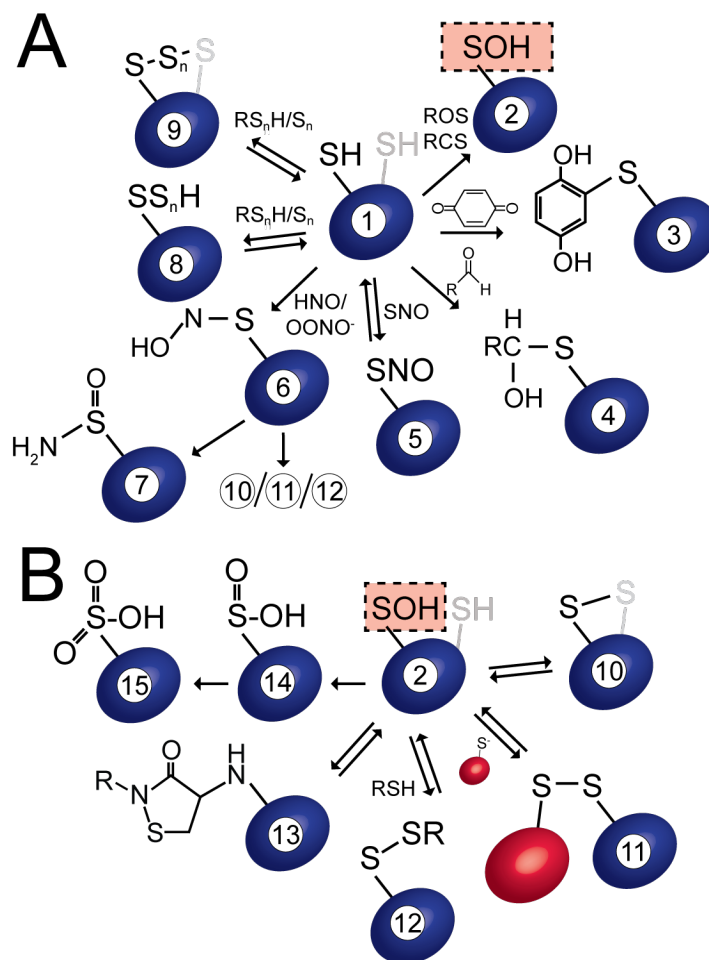


Figure 3. Oxidative post-translational modifications (PTM^{ox}) of cysteine residues. (A) Reactions involving a reduced cysteine thiolate (1, 2-6, 8-9) and (B) reactions that require cysteine sulfenylation (derivative 2) prior to further derivatization (10-15). 1, Cysteine thiol (RS⁻=cysteine thiolate); 2, Cysteine sulfenic acid; 3, S-quinonization; 4, S-alkylation; 5, S-nitrosation; 6, N-hydroxysulfenamide; 7, sulfonamide; 8, S-sulphydration (persulfide, $n=1$; polysulfide, $n>1$); 9, mixed disulfide ($n=0$, disulfide; $n=1$, trisulfide; $n=2$, tetrasulfide), 10, intramolecular disulfide; 11, intermolecular disulfide; 12, S-thiolation; 13, cyclic sulfonamide derived from condensation of a sulfenic acid with a peptide backbone amide group;⁴⁸ 14, sulfinic acid; 15, sulfonic acid. A resolving cysteine is required for some modifications and is shaded gray. This figure was adapted and significantly expanded from refs.^{49,50}

thiols, to create mixed disulfides, known generically as *S*-thiolations (Fig. 3, **12**). The potent cellular oxidant diamide, for example, depletes the reduced LMW thiol pool and induces significant *S*-thiolation in *B. subtilis*, *S. aureus* and *M. tuberculosis*^{51,52} via thiol-disulfide exchange.⁵² There is emerging evidence that *S*-thiolation, e.g., *S*-glutathionation⁵³ functions as a protective barrier to prevent the formation of an irreparable higher oxidation state of cysteine, particularly in enzymes that require an active-site cysteine to function. It was recently shown that *S*-bacillithiolation occurs on the organohydroperoxide regulator, OhrR in *B. subtilis in vivo*^{48,54} and that de-*S*-bacillithiolation is mediated by bacilliredoxins BrxA and BrxB.³¹ *S*-bacillithiolation in Firmicutes⁵⁵ and *S*-mycothiolation in actinomycetes, including *Corynebacterium glutamicum*,⁵⁶ may be a general defense strategy against other forms of oxidative stress, as these modifications are also protective against hypochlorite (HOCl) stress.

OXIDATIVE STRESS AT THE HOST-PATHOGEN INTERFACE

Microorganisms encounter oxidative stress endogenously as a byproduct of normal metabolic processes and exogenously from the environment. A major component of exogenous oxidative stress can be found at the host-pathogen interface. A microbe encounters substantial oxidative stress when it is engulfed by a host immune cell, particularly in an intracellular phagosomal compartment or vacuole in macrophages⁵⁷ or neutrophils.⁵⁸ Here, microorganisms are bombarded with numerous small molecule oxidative stressors. These are derived from NADPH oxidase (NOX), superoxide dismutase (SOD), nitric oxide synthase (NOS), myeloperoxidase (MPO), and other enzymes to form $O_2^{\cdot-}$, H_2O_2 , NO, and HOCl, respectively (Fig. 4).^{59,60} The specific

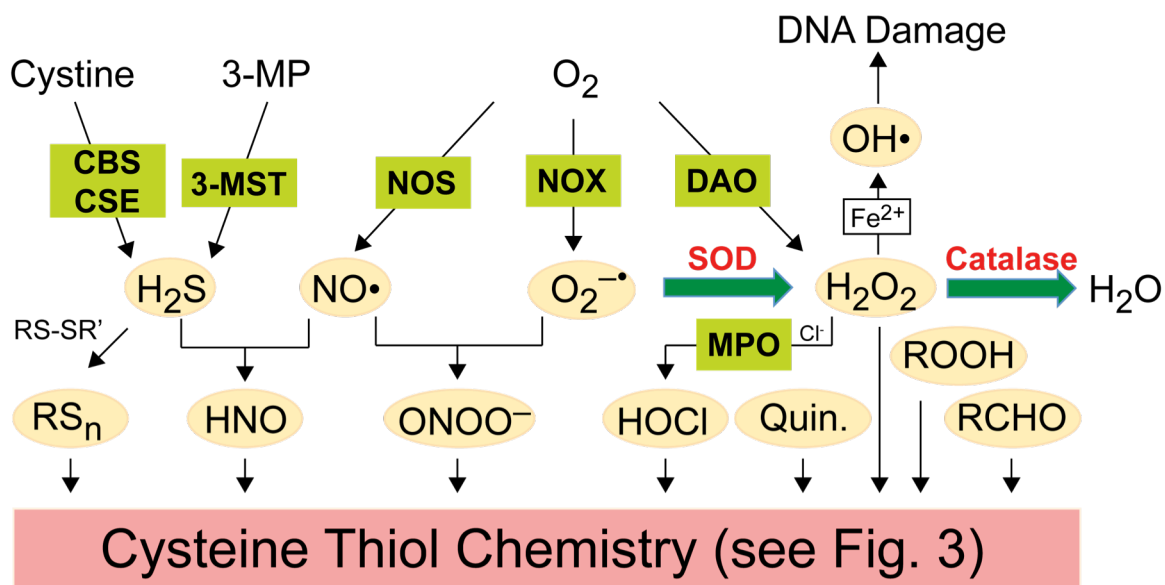


Figure 4. Interplay of ROS, RNS, RCS, RES and RSS. Reaction of oxidative stressors produces byproducts that potentially lead to a reaction with cellular thiols (See Fig. 3). Abbreviations are CBS, cystathionine beta synthase; CSE, cystathionine gamma synthase; 3-MST, 3-mercaptopyruvate sulfurtransferase; 3-MP, 3-mercaptopyruvate; NOS, nitric oxide synthase; NOX, NADPH oxidase; DAO, D-amino acid oxidase; SOD, superoxide dismutase; MPO, myeloperoxidase; H₂S, hydrogen sulfide, RS_n, per/polysulfide; NO, nitric oxide; O₂^{•-}, superoxide; OH[•], hydroxyl radical; H₂O₂, hydrogen peroxide; HOCl, hypochlorite; HNO, nitroxyl; ONOO⁻, peroxynitrite; ROOH, organic peroxide; RCHO, aldehyde/electrophile; Quin, quinone.

stressors and quantities produced are dependent on the host immune cell type. Damage caused by these reactive species is widespread and includes disruption of metal centers and FeS clusters, lipid oxidation, amino acid oxidation, DNA damage, and general disruption of normal cellular physiology.^{3-5,58}

Many oxidative stressors are capable of reacting with one another to form additional toxic species either enzymatically or non-enzymatically (Fig. 4).⁵ For example, MPO, which comprises $\approx 25\%$ of the protein content in the phagocytic vacuole,⁶¹ catalyzes the dismutation of superoxide to H_2O_2 . In the presence of sufficient chloride anion, MPO converts H_2O_2 to HOCl, a potent two-electron oxidant. NOX and MPO thus exploit ROS, RNS and RCS as an integrated oxidative stress-inducing process designed to kill intracellular pathogens through the production of HOCl, chloramines, other RNS, hydroxyl radicals, and singlet oxygen species as recently reviewed.^{60,62} An inducible NOS in neutrophils is chiefly responsible for the production of NO by professional phagocytes and more recently, it has been shown that RCS are generated by the enzyme dual oxidase (DUOX) in gut epithelial cells in *Drosophila* in order to control host-microbe interactions.⁶³ Furthermore, it has long been known that the combination of multiple stressors such as ROS and RNS have synergistic effects on microbial killing.⁶⁴

REACTIVE OXYGEN SPECIES (ROS)

ROS are the most widely recognized form of oxidative stress and are derived from the sequential one-electron reduction of molecular oxygen, from the superoxide anion ($\text{O}_2^{\cdot-}$), to hydrogen peroxide (H_2O_2), hydroxyl radical (OH^{\cdot}) and ultimately H_2O (Fig. 4). Other ROS include organic peroxides (ROOR') and organic hydroperoxides

(ROOH). ROS are capable of oxidizing cysteine, methionine, and tryptophan residues in proteins, as well as the LMW thiol pool. Superoxide itself is a relatively weak oxidant and a modest one-electron reductant, its toxicity may derive from subsequent reaction with the major RNS, nitric oxide, which generates peroxynitrite (ONOO^-) at diffusion-controlled rates (Fig. 3).⁵

Both $\text{O}_2^{\cdot-}$ and H_2O_2 are capable of oxidizing iron-sulfur (Fe-S) clusters at sufficiently fast rates and result in the release of iron,^{65,66} thereby increasing the bioavailable or “free” Fe in the cell. This reduced Fe(II) can then react with H_2O_2 in a classical Fenton reaction to produce the highly oxidative hydroxyl radical (Fig. 4). OH^{\cdot} is short-lived (10^{-9} s) and highly catalytic under the reducing conditions of the cytoplasm. It is generally considered a nonspecific oxidant^{67,68} that induces DNA strand breaks^{69,70} and oxidation of DNA bases, thereby increasing mismatches and mutations.⁷¹ However, H_2O_2 also functions as a second messenger at lower concentrations in mammals.⁷²

The detection mechanism of ROS by transcriptional regulators is stressor and organism specific. Superoxide has long been thought to be sensed directly in *E. coli* by the MerR family protein SoxR through the oxidation of a 2Fe-2S cluster containing regulator.^{12,73} However, recent work suggests that this may not be the case, and instead it is responsive to the intracellular NADPH/NADP⁺ ratio.⁷⁴⁻⁷⁶ Hydrogen peroxide on the other hand, is directly sensed by OxyR, found largely in Gram-negative bacteria, *e.g.*, *E. coli*, or PerR in Gram-positive bacteria, best characterized in *B. subtilis*.⁷⁷ Remarkably, each senses H_2O_2 through completely different structural mechanisms. OxyR employs reactive cysteine residues while PerR utilizes an iron atom capable of binding peroxide through an open coordination site, which ultimately leads to the oxidation of two Fe-

coordinating histidine residues to 2-oxo-His *in vivo*.¹⁰ PerR ligand oxidation results in Fe release and dissociation from the DNA operator-promoter region, leading to transcriptional derepression of the PerR regulon.⁷⁸ In contrast, organic hydroperoxides are sensed by the regulator OhrR in *B. subtilis* through a reactive cysteine residue (Fig. 5).^{79,80} In OhrR, a sulfenic acid is initially formed followed by a subsequent reaction to form *S*-thiolations with coenzyme A, cysteine and bacillithiol, and also condensation of the sulfenic acid to form a sulfenamide with the peptide backbone.⁴⁸ The condensation reaction is known as transnitrosation (Fig 3B, **13**) .

REACTIVE NITROGEN SPECIES (RNS)

The most well studied RNS is NO^{*}, a gasotransmitter that has long been known for its role in smooth muscle relaxation and neurotransmission in mammals.⁸¹ However, NO stress can lead to the formation of other nitrogen-containing oxidants including nitrogen dioxide (NO₂^{*}), peroxyxynitrite, and dinitrogen trioxide (N₂O₃, Fig. 4). At elevated concentrations, RNS disrupt Fe-S clusters and Fe metabolism, induce *S*-nitrosation of cysteine residues, forms metal-nitrosyl complexes and catalyzes protein nitration, e.g. 3-nitrotyrosine formation. It should be noted, however, that the direct reaction of NO with thiols does not occur at a physiologically relevant rate, in contrast to the transnitrosation reaction (Fig. 3B, **13**).^{82,83} Many of these concepts were recently and comprehensively reviewed.⁵

More recently, nitroxyl (HNO), the one-electron reduced form of NO, has emerged as a candidate gasotransmitter. HNO is characterized by a signaling pathway that is distinct from that of nitric oxide.⁸⁴⁻⁸⁶ In mammalian systems, HNO has been

suggested to mediate vasodilation through HNO-mediated disulfide bond formation in the transient receptor protein channel A1 (TRPA1), resulting in calcium influx.⁸⁷ In contrast to mammalian systems, the microbial stress response to nitroxyl is completely uncharacterized. However, HNO is clearly capable of reacting with cysteine thiolates to form a (hydroxyamino)sulfanyl derivative (Fig. 3B, *II*) that is subsequently resolved by a second thiolate (derived from a second cysteine or a LMW thiol) to form a disulfide bond with the liberation of hydroxylamine (Fig. 3B, *6, 7*).^{87,88}

HNO can be derived from a two-step reaction where H₂S and NO or *S*-nitrosothiols (RSNO) react to form thionitrous acid (HSNO). HSNO subsequently reacts with a second equivalent of HS⁻ to form H₂S₂ (hydrodisulfide) and HNO.^{87,89} Following formation HNO can also react with molecular oxygen to generate OONO⁻ at diffusion-controlled rates,⁹⁰ again suggesting significant interplay among multiple RNS, ROS, RCS, and RSS species (Fig. 4). HNO exemplifies the complexity of interacting oxidative small molecule stressors at the host-pathogen interface and further connects this oxidative chemistry with hydrogen sulfide homeostasis and cysteine catabolism.

All NO sensors that have been described to date harbor heme or 4Fe-4S cluster prosthetic groups^{91,92} in which NO reacts rapidly with redox-sensitive transition metal complexes, *e.g.*, Fe(III)-porphyrin complexes, under physiological conditions.⁵ This is likely due to the low reactivity NO exhibits toward cysteine thiolates. A *bona fide* cysteine thiol-dependent NO-sensing transcriptional regulator has not yet been described but would likely undergo a transnitrosation reaction with a LMW *S*-nitrosothiol, *e.g.* GSNO or cysteine nitrosothiol (Fig. 3, *5*).⁹³ *In vitro* work has established that *S. pneumoniae* NmlR (*Neisseria merR*-like regulator) and *B. subtilis* AdhR (aldehyde

dehydrogenase regulator) are each capable of undergoing the transnitrosation reaction.⁹³ However, the most recent work suggests that NmlR-type regulators may function in formaldehyde sensing or in other types of carbonyl or electrophile stress.⁹⁴⁻⁹⁶

REACTIVE ELECTROPHILE SPECIES (RES)

RES are electron-poor small molecules that are generated as part of normal cellular metabolism, as well as from lipid peroxidation and nitration of nucleic acids and lipids. They are capable of reacting with the side chains of cysteine, histidine, and lysine in addition to DNA bases. Proteins containing a cysteine thiol with a low pK_a are particularly susceptible to electrophile stress. RES are not considered specific to the host-pathogen interface some forms of ROS can lead to their generation. For example, hypochlorite stress leads to an increase in the production of the RES stressor methylglyoxal (MG)⁴ and thus bacteria must be capable of clearing toxic carbonyl compounds that include the electrophiles formaldehyde and related short chain aldehydes. A number of recent reviews discuss RES in detail,⁹⁷⁻⁹⁹ including mechanisms of toxicity¹⁰⁰ and RES-based cellular signaling.¹⁰¹

Quinones are another class of carbon-based electrophiles and are involved in electron transport, quorum sensing, and are the major redox component of soils.¹⁰² Ubiquinone and menaquinone are produced endogenously and function in electron transport^{97,103} and sulfide oxidation and detoxification.¹⁰⁴ Quinone derivatives are also found in a number of cytotoxic molecules including anthracycline and cercosporin. Electrophilic quinones can undergo Michael addition with thiols, termed *S*-alkylation (Fig. 3, 4).^{105,106} Several RES-sensing transcriptional repressors have recently been

characterized, including YodB, MhqR, and QsrR (Fig. 5).^{21,107,108} The regulation and homeostasis of quinones is generally poorly understood.

REACTIVE CHLORINE SPECIES (RCS)

Reactive chlorine species (RCS), notably hypochlorite, have long been known as potent killers of pathogens sequestered within phagosomes.^{4,109} HOCl is also the active ingredient in many disinfectants used ubiquitously in households and hospitals. The effectiveness of RCS lies in its broad-spectrum chemical reactivity, resulting in the oxidation of virtually every cellular component. This includes metal centers, lipids, DNA, amino acids (including cysteines), the LMW thiol pool, and small molecule metabolites. Reaction with proteins leads to unfolding followed by degradation or aggregation which leads to cell death. These concepts were recently and comprehensively reviewed.⁴ Several microbial RCS-sensing regulators have been identified to date and include HypR¹¹⁰ from *B. subtilis* (Fig. 5), and NemR¹¹¹, and RclR¹¹², each found in *E. coli*.

HYDROGEN SULFIDE (H₂S) AND REACTIVE SULFUR SPECIES (RSS)

Hydrogen sulfide (H₂S) is a recently classified “gasotransmitter” or signaling molecule that plays important roles in many (patho)physiological processes, including vasorelaxation, cardioprotection, and neurotransmission in mammals.¹¹³⁻¹¹⁵ H₂S is freely membrane permeable and once inside the cell is readily deprotonated and the more nucleophilic HS⁻ anion predominates. HS⁻ is then either assimilated, or in some organisms, effluxed via active transport.¹¹⁶ It has also been the subject of numerous recent reviews.^{114,115,117,118} At increased concentrations, H₂S poisons cytochrome c of the

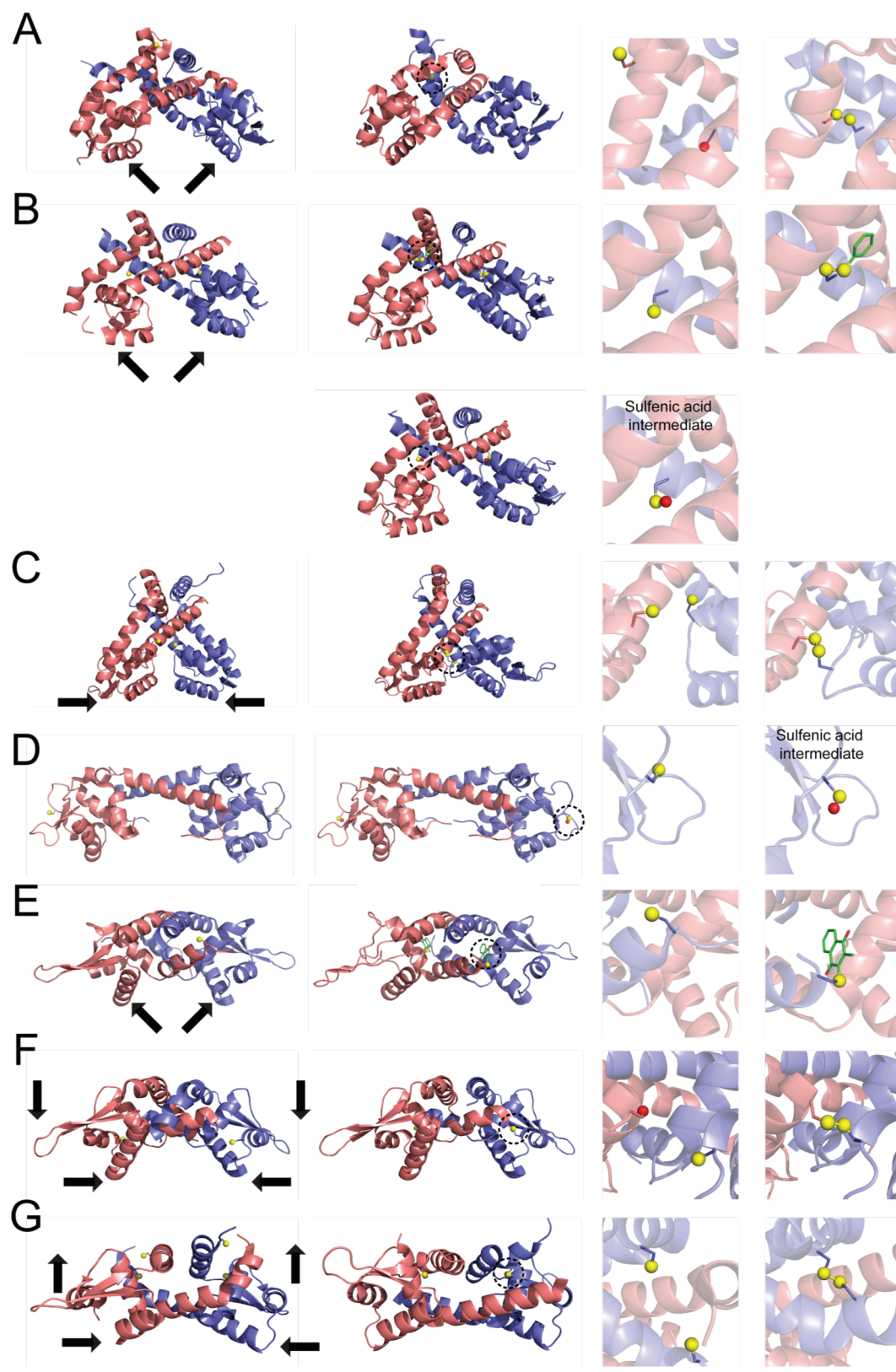


Figure 5. Ribbon representations of selected crystal structures of oxidative stress-sensing transcriptional repressors. (A-C) MarR, (D) Rrf2, and (E-G) ArsR/SmtB families in the reduced (*first, third* columns) and oxidized (*second, fourth* columns) states. Global structures are shown (*first, second* columns), with the region highlighted by the *black* dashed-circle expanded to the immediate *right* (*third, fourth* columns). All proteins shown are homodimers (protomers shaded *salmon, slate*) and use cysteine as a regulatory switch to induce a quaternary structural change that results in dissociation from the DNA operator in the oxidized state. Arrows (*first* column) schematize secondary structure movement(s) upon transit from the reduced to the oxidized states, with thiol chemistry highlighted on the *right* (sulfurs, *yellow spheres*; oxygens, *red spheres*; S-thiolation and S-quinonizations, *green sticks*). (A) *X. campestris* OhrR [pdb codes 2PEX, reduced; 2PFB, oxidized]¹¹⁹ with reduced form (*third* column) modeled by a Cys-to-Ser substitution. (B) *S. aureus* SarZ (3HSE, reduced; 3HRM, sulfenylated; 3HSR, S-thiolated with benzenethiol).²⁰ (C) *P. aeruginosa* MexR (LNW¹²⁰, reduced; 3MEX¹²¹, oxidized). (D) *S. aureus* CymR (3T8R, reduced; 3T8T, oxidized)¹²² illustrating little observable structural change upon sulfenylation with S-thiolation known to negatively regulate DNA binding. (E) *S. aureus* QsrR (4HQE, reduced; 4HQM, S-quinonized).²¹ (F) *B. subtilis* HypR (4A5N, reduced; 4A5M, oxidized),¹¹⁰ with the reduced (*third* column) modeled by a Cys-to-Ser substitution. (G) *X. fastidiosa* BigR (3PQJ, reduced; 3PQK, oxidized)¹⁸ forms an intramolecular disulfide bond *in vitro* and is regulated by sulfide stress *in vivo*.¹⁸

electron transport chain. H₂S is produced endogenously via the trans-sulfuration pathway involving cysteine or cystine¹ and 3-mercaptopyruvate (3-MP) and the action of cystathionine β-synthase (CBS),¹²³ cystathionine γ-synthase (CSE)¹¹³ and 3-mercaptopyruvate sulfurtransferase (3-MST)¹²⁴ (Fig. 2, see Fig. 20 Chapter 3).

The relationship between mammalian-derived H₂S on bacterial pathogens is completely unknown. However, H₂S appears to play a protective role in resistance to generalized oxidative stress in several human microbial pathogens, including *S. aureus*, *E. coli*, *P. aeruginosa*, and *B. anthracis*. The protection may be due to increased sulfide coordination of released Fe(II), thus minimizing a potential source of damage caused by bactericidal ROS.¹²⁵

Reactive sulfur species (RSS) is a general term given to sulfite, bisulfite, and sulfane sulfur-containing species, including persulfides (RSSH), polysulfides (RS(S_n)SR', $n \geq 1$) and hydrogen polysulfides (RS(S_n)H, $n > 1$). Hydrogen polysulfides are estimated to be present in mammalian cells at micromolar concentrations. This is consistent with an emerging picture where sulfane sulfur species are the primary source of “free” sulfur in the cell rather than H₂S.¹ Cysteine S-sulfhydration is becoming an increasingly recognized cysteine posttranslational modification.^{1,126-129} Protein thiols do not react directly with hydrogen sulfide¹²⁷ but rather S-sulfhydration is either catalyzed by oxidized metal ion complexes, e.g., Fe(III) porphyrin complexes, that catalyze the one-electron oxidation of H₂S to the HS[•] radical. Another alternative is via reaction of the more electrophilic cysteine species, notably cysteine sulfenic acid or other more oxidized sulfur species.¹³⁰ These more oxidized sulfur species include organic and

inorganic persulfides and polysulfides, which lead to cysteine *S*-sulphydration in *in vitro* reactions.^{115,130} Several specific *S*-sulphydration targets have been identified in mammalian cells including protein tyrosine phosphatases and nuclear factor kappa B (NF- κ B).^{131,132} Two bacterial sulfide stress sensing transcriptional regulators have been characterized to date: *A. tumefaciens* BigR (Fig. 5)¹⁸ and *S. aureus* CstR.¹³

SULFUR METABOLISM IN *Staphylococcus aureus*

S. aureus is an opportunistic Gram-positive non-motile cocci that is the causative agent of numerous illnesses ranging from minor skin infections to life-threatening diseases.^{133,134} In contrast to other human pathogens, *S. aureus* lacks a functional sulfate assimilation pathway and must use other mechanisms to obtain sulfur from organic and inorganic sources (Fig. 6).¹³⁵ Sulfur acquisition is essential for the biosynthesis of cysteine, iron-sulfur clusters, and other low molecular weight sulfur-containing compounds and for maintenance of cellular redox balance.^{136,137} Recent work has shown that perturbation of cysteine metabolism in *S. aureus* increases susceptibility to oxidative stress and decreases the ability of this microorganism to form biofilms, which are essential for survival both inside and outside of a host.^{137,138} Components of sulfur metabolic pathways, including cysteine biosynthesis, may be suitable antimicrobial and vaccine targets in *S. aureus* as they have been shown in *M. tuberculosis*.¹³⁹⁻¹⁴¹

Although *S. aureus* lacks the sulfate assimilation pathway, it is capable of growing on inorganic thiosulfate as a sole sulfur source^{6,135} presumably by assimilating the sulfane sulfur and effluxing sulfite (SO_3^{2-}). Thiosulfate can be generated by the mammalian host from mitochondrial hydrogen sulfide (H_2S) detoxification¹⁴² via sulfur

dioxygenase and sulfide quinone reductase (SQR) activities.¹⁴³ In any case, *S. aureus* sulfur metabolism and regulation in response to stress remains relatively underexplored.

THE CsoR FAMILY OF TRANSCRIPTIONAL REGULATORS

Members of the CsoR (copper-sensitive operon repressor) family of transcriptional regulators form a homotetrameric bundle ($\alpha 1, \alpha 1', \alpha 2, \alpha 2'$) consisting of an all α -helical dimer of dimers structural arrangement that lacks a canonical DNA binding motif (Fig. 7).¹⁴⁴⁻¹⁴⁶ Proteins in this family operate by a derepression mechanism in which binding of the cognate metal results in release of operator DNA. CsoRs bind one Cu(I) per protomer with high affinity in an S_2N trigonal geometry between the $S\gamma$ of two cysteine residues (Cys41 and Cys 70 in *S. aureus*) and the $N\delta 1$ nitrogen of a histidine residue (His66, Fig. 7)^{144,145} and control the expression of the copper resistance genes *copA* and *copZ*.^{6,144} CopA is a membrane-bound Cu(I)-translocating P-type ATPase that effluxes copper from the cell^{147,148} and CopZ is a copper chaperone.¹⁴⁹ In some CsoRs, e.g. *M. tuberculosis* CsoR, the allosteric switching mechanism occurs in the second coordination shell and involves a hydrogen bonding interaction between Tyr40, $N\epsilon 2$ of His66, and Glu86 that links Cu(I) binding to release from DNA.¹⁵⁰ Perturbation of this network results in failure to respond to Cu(I)-binding.¹⁵⁰ Some organisms, including *S. aureus*, encode more than one CsoR-like protein of high similarity that fundamental differences in the primary sequence and control the expression of genes unrelated to copper toxicity and homeostasis.⁶

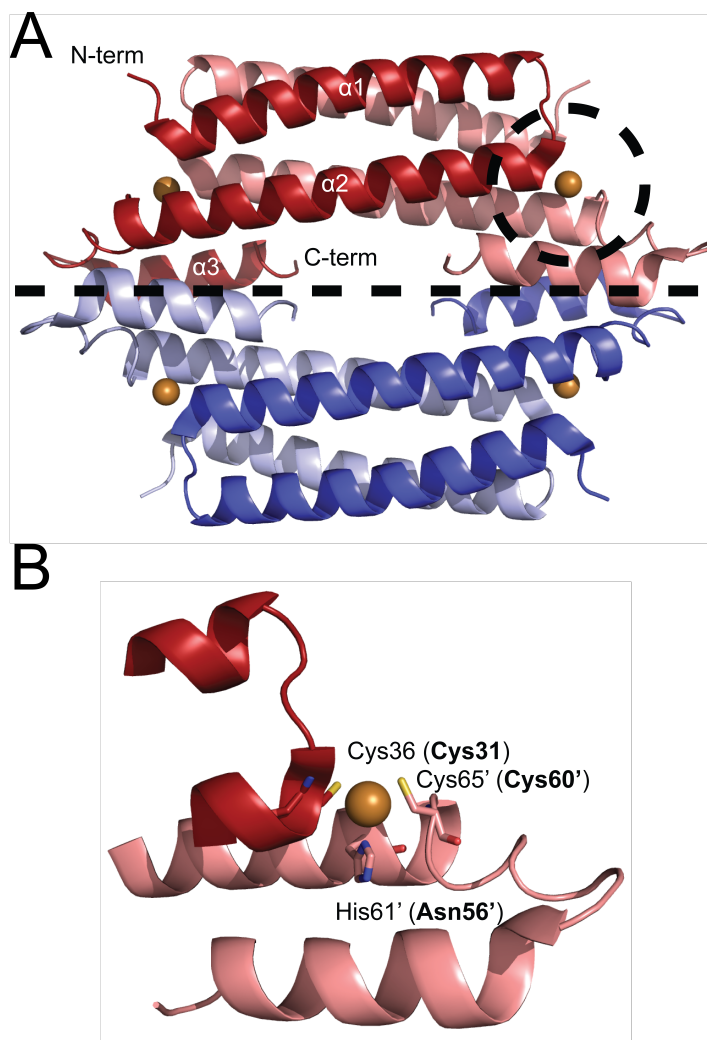


Figure 7. Crystal structure of *M. tuberculosis* CsoR¹⁴⁴ (A) and the Cu(I) binding site (B). CsoRs feature an all alpha-helical tetrameric bundle as a “dimer of dimers” which is displayed either blue or red and separated by the dashed line. There are four individual Cu(I) binding sites, two per dimer. Labeled residues are those of *M. tuberculosis* and those in parentheses are the analogous residues in *S. aureus* CstR. PDB: 2HH7

CstR AND THE *cst* OPERON

S. aureus strain Newman contains one *bona fide* Cu(I)-sensing CsoR and a second CsoR-like protein of unknown function, termed CstR (CsoR-like sulfur transferase repressor). CstR is 35% identical and 65% similar to CsoR. CstR retains both cysteine residues but lacks the Cu(I)-binding histidine residue (Fig. 7) and fails to respond to copper toxicity *in vivo*. Early studies established that CstR operates through a derepression mechanism, analogous to CsoR and tightly controls the expression of the divergently transcribed *cst* operon (Fig 8). These early studies, however, did not yield an inducer for the *cst* operon.⁶

Five genes are encoded in the *cst* operon, NWMN_0026-NMWN_0029. These include a putative sulfite/sulfonate efflux pump (TauE, NWMN_0026), the regulator CstR (NWMN_0026.5), two multi-domain sulfurtransferases, termed CstA and CstB (NWMN_0027 and NWMN_0028, respectively), and a sulfide quinone oxidoreductase (SQR, NWMN_0029, Fig. 8). CstA contains three domains, the first of which bears a high degree of similarity to rhodanese thiosulfate sulfur transferases (TST) which have historically been characterized to cleave the sulfur-sulfur bond of thiosulfate ($S_2O_3^{2-}$) to form an enzyme cysteine-bound persulfide, RSSH, and liberate sulfite (SO_3^{2-}).¹⁵¹ More recently rhodanases have been shown to act in shuttling persulfides in molybdopterin^{152,153} and 2-thiouridine¹⁵⁴ biosynthesis as well as in the detoxification of hydrogen sulfide.¹⁴² The middle domain shares homology with the sulfurtransferase TusA which is involved in persulfide shuttling in 2-thiouridine¹⁵⁵ and molybdopterin^{153,156,157} biosynthesis, depending on the organism. The final domain, TusD/DsrE, shares homology with the each of the proteins from the heterotrimeric sulfur

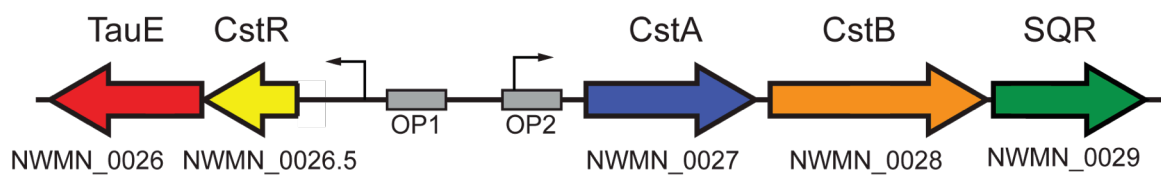


Figure 8. Schematic representation of the *cst* operon, NWMN_0026-NWMN_0029, and operator binding sites OP1 and OP2.

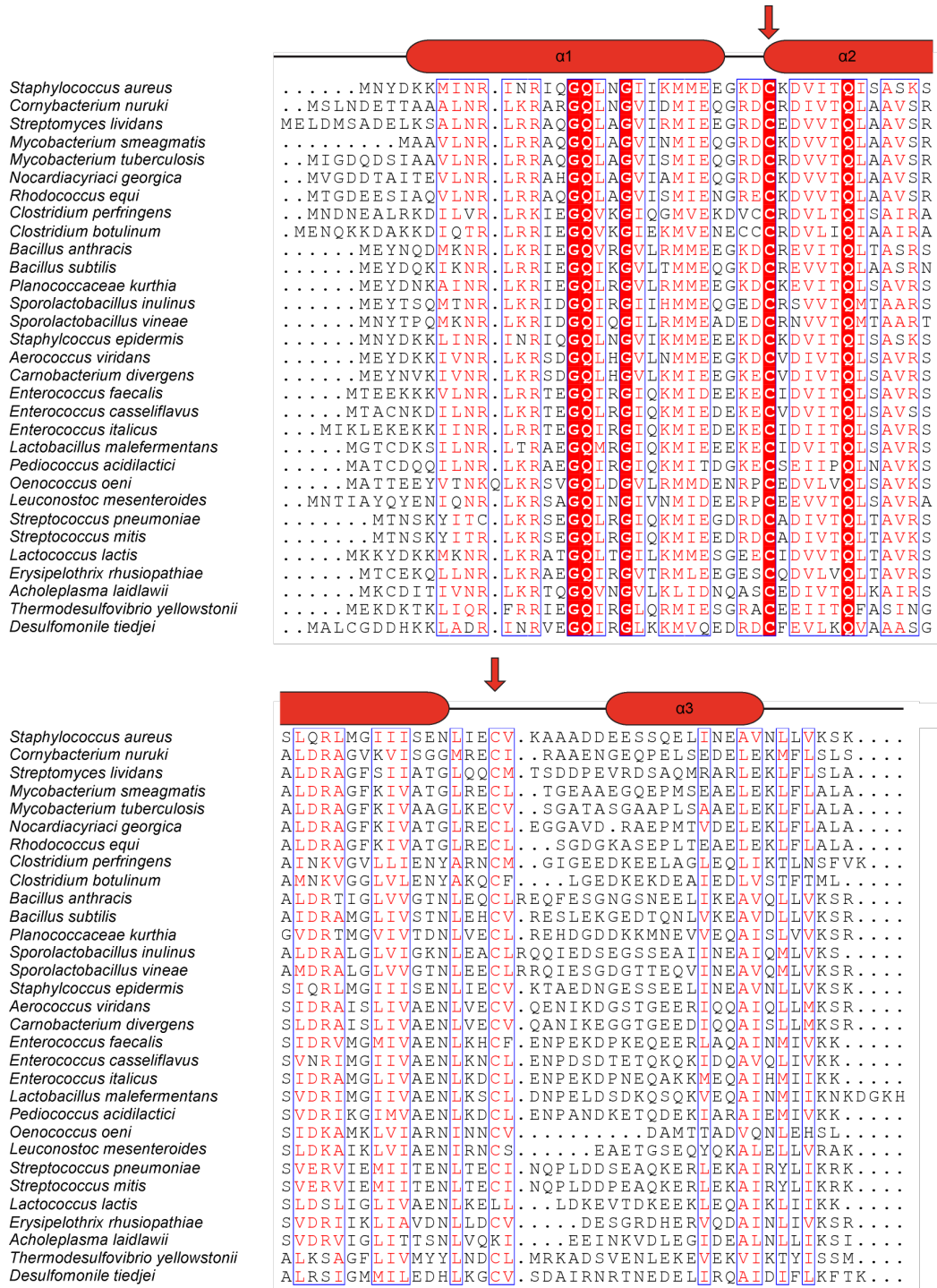


Figure 9. Sequence alignment of putative CstRs. Arrows indicate location of conserved cysteine residues. Secondary structure is based on CsoR structures deposited in the PDB (2HH7¹⁴⁴ and 4M1P¹⁴⁵). Alignment was prepared using Endscript 2.¹⁵⁸

transferases in the TusBCD complex involved in 2-thiouridine biosynthesis¹⁵⁹ and the hexameric sulfur transferases DsrEFH involved in dissimilatory sulfite reduction.¹⁶⁰ The second sulfur transferase, CstB, is a two domain protein that consists of a glyoxalase II-like domain that bears similarity to the sulfur dioxygenases (SDO) ETHE1 from humans¹⁶¹ and Blh (β -lactamase-like hydrolase) from *Xylella fastidiosa* and *Agrobacterium tumefaciens*,¹⁸ both of which are involved in sulfide detoxification.¹¹⁸ Both ETHE1 and Blh are required. Chromosomal deletion of the ETHE1 leads to embryonic lethality in mice as a result of sulfide toxicity-induced ethylmalonic encephalopathy¹⁶¹ and *A. tumefaciens* Blh is required for growth under hypoxic conditions.¹⁸ The more C-terminal domain of CstB contains an additional TST.

Lastly, the *cst* operon encodes a sulfide quinone oxidoreductase, NWMN_0029, a class of membrane-bound proteins characterized to be responsible for the first step of the hydrogen sulfide oxidation pathway.¹¹⁸ The *cst* operon appears to encode a complete sulfur oxidation system contained within a single operon (Fig. 21, Chapter 3). At the start of the work presented in this dissertation, the physiological function of the *cst* operon was unknown, but is now proposed to oxidize S^{2-} to thiosulfate ($S_2O_3^{2-}$, see Chapter 3).

SCOPE OF RESEARCH

Hydrogen sulfide and RSS are highly reactive and are toxic at increasing concentrations. To maintain homeostasis and avoid toxicity, these species require rapid sensing and detoxification. This dissertation focuses on the characterization of CstR as a sulfide stress-sensing transcriptional regulator in *S. aureus*. Discussed in Chapter II are the follow-up studies to the initial CstR characterization identified CstR as a sulfite-

sensing transcriptional regulator.⁶ This work utilized the more reactive chalcogen oxyanions selenite (SeO_3^{2-}) and tellurite (TeO_3^{2-}) as SO_3^{2-} surrogates. We show that CstR reacts with SeO_3^{2-} and TeO_3^{2-} to form seleno- and tellurotrisulfides between Cys31 and Cys60' of CstR by LC-ESI-MS and tandem high-resolution mass spectrometry and that these PTMs negatively regulate DNA binding *in vitro*. Additionally, the Cu(I)-sensing transcriptional regulator CsoR does not react with SeO_3^{2-} and only weakly reacts with TeO_3^{2-} , indicating fundamental differences in cysteine reactivity in these paralogous repressors.¹⁶² In Chapter III, we identify RSS as the *in vivo* inducer of the *cst* operon by qRT-PCR and investigate the effect of mutation of CstR cysteine residues on *S. aureus* viability in response to H_2S and other RSS stress. In addition, we extensively characterize the reaction of CstR with $\text{H}_2\text{S}/\text{HS}^-$, polysulfides, and the sulfane sulfur donor GSSH by mass spectrometry.¹³ Finally in Chapter IV, we address and probe the differential reactivity and selectivity of CstR vs CsoR toward RSS stress and Cu(I), respectively. We also explore factors contributing to differences in cysteine reactivity. Lastly, we test low oxygen growth conditions and the induction of the *cst* operon with nitroxyl. Collectively, these studies provide the basis for H_2S /RSS detoxification and homeostasis in *S. aureus* while expanding the functional role of the CsoR/RcnR family of transcriptional regulators.

CHAPTER II

CHARACTERIZATION OF THE REACTION OF CstR WITH THE CHALCOGEN OXYANIONS SELENITE AND TELLURITE

PREFACE

At the time in which I first joined the Giedroc lab, the working model for CstR involved directly sensing sulfite (SO_3^{2-}). We have since learned that other sulfur species are the main inducers for transcriptional derepression of the *cst* operon *in vivo* (see Chapter 3). Chapter 2 primarily focuses on probing the old working model but provides several important findings for differences in cysteine reactivity for CstR vs CsoR.

INTRODUCTION

CstR is a member of the CsoR family of transcriptional regulators.^{145,146} CsoRs regulate the expression of genes that are responsible for mitigating copper toxicity.^{144,145} CstR controls the expression a divergently-transcribed operon, termed *cst*, of unknown function.⁶ *S. aureus* encodes both CstR and CsoR. In this organism, CsoR functions as a *bona fide* Cu(I)-sensing transcriptional regulator and CstR was proposed to respond to sulfite toxicity.⁶ This hypothesis was developed from data indicating that CstR reacts directly with the chalcogen oxyanion SO_3^{2-} through two conserved cysteine residues, Cys31 and Cys60.⁶ The source of sulfite was thought to derive from catabolism of thiosulfate (TS, $\text{S}_2\text{O}_3^{2-}$), the first step which is likely catalyzed by a rhodanese or thiosulfate sulfurtransferases (TSTs). TSTs cleave the S—S bond of TS to form a cysteine-bound persulfide, liberating sulfite. The persulfide could then be shuttled into an

as of yet unknown acceptor. Leading ultimately to the biosynthesis of cysteine, bacillithiol, or other low molecular weight (LMW) sulfur-containing species¹⁶³ (Fig. 6, Chapter 1). The *cst* operon contains two rhodanese-like domains and could provide *S. aureus* with the ability to utilize an alternative inorganic sulfur source, e.g., thiosulfate. The liberated sulfite would then undergo a multi-electron reduction catalyzed by Cys31 and Cys60' of CstR to form a mixture of di- and trisulfide cross-linked species, resulting in induction of the *cst* operon.⁶

The sulfur in SO_3^{2-} is in the +4 oxidation state and it typically reduced by sulfite reductases that use cofactors or metal centers as prosthetic groups to reduce SO_3^{2-} to S^0 or S^{2-} . These cofactors include NADPH, flavins, siroheme, and ferredoxin.^{164,165} The reduction of sulfite by CstR therefore represents a potentially novel mechanism for the stoichiometric reduction of sulfite to S^0 through trisulfide bond formation. It was postulated that CstR may react with the related chalcogen oxyanions, selenite (SeO_3^{2-}) and tellurite (TeO_3^{2-}), both of which are biologically available and toxic to many microorganisms and could act as a surrogate in place of the less reactive SO_3^{2-} .¹⁶⁶ Chalcogen oxyanions display increasing reactivity as one moves down the periodic table and are generally more reactive than sulfite.^{136,167} Toxicity from these compounds is presumed to result from disruption of the low molecular weight thiol pool,¹⁶⁸ e.g., glutathione, cysteine, or coenzyme A (Fig 1, Chapter 1). Thiols undergo redox reactions with SeO_3^{2-} and TeO_3^{2-} to form a mixture of disulfides and seleno- or tellurotrisulfides, respectively (Fig. 10);¹⁶⁹ analogous chemistry can also occur at enzyme active sites or with metal-chelating cysteine residues.¹⁷⁰ Many firmicutes and related Gram-positive bacteria, including *S. aureus*, exhibit strong resistance to these compounds through

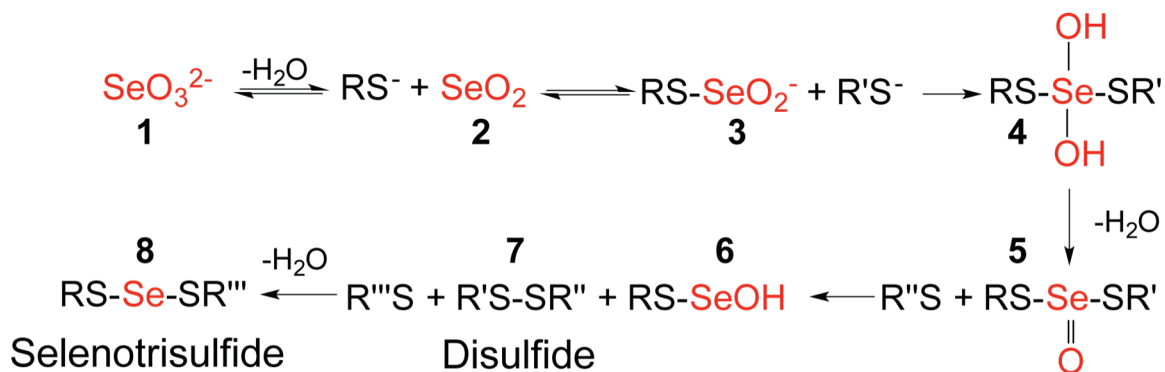


Figure 10: Mechanism of thiol-mediated selenite reduction. Selenite (SeO_3^{2-} , **1**) freely exchanges with water between selenite and selenium dioxide (SeO_2 , **2**), the later of which can react with a free thiolate (RS^-) to form thioselenic acid (RS-SeO_2^- , **3**). Thioselenic acid can then be attacked by a second thiolate ($\text{R}'\text{S}^-$) to form thioselenate ($\text{RS-Se(OH)}_2\text{-SR}'$, **4**) and after condensing to thioselenate ($\text{RS-SeO-SR}'$, **5**), is capable of reacting with a third thiolate ($\text{R}''\text{S}^-$) to form thioselenic acid (RS-SeOH , **6**) and a disulfide ($\text{RS}'\text{S-SR}''$, **7**). Finally, thioselenic acid can be attacked by a fourth thiolate equivalent ($\text{R}'''\text{S}^-$) to form a selenotrisulfide ($\text{RS-Se-SR}'''$, **8**).

unknown mechanisms,¹⁷¹ but likely through direct reduction by the LMW thiol pool and will form pink or black colonies from the reduction of SeO_3^{2-} or TeO_3^{2-} to Se^0 or Te^0 , respectively.¹⁶⁶

In this chapter, the products of *S. aureus* CstR reacted with the chalcogen oxyanions SeO_3^{2-} and TeO_3^{2-} are characterized by mass spectrometry with emphasis on the observed post-translational modifications. In each case it is established that the cross linking of the cysteine pair negatively regulates DNA binding *in vitro*. In addition, the functional importance of individual CstR cysteine residues in driving negative regulation of CstR operator DNA binding is explored.

MATERIALS AND METHODS

CstR protein expression and purification. An overexpression plasmid for *S. aureus* CstR carried on a pET-3a vector was previously obtained.⁶ CstR was expressed in Rosetta™ (DE3)pLysS *E. coli* competent cells. Briefly, cell pellets containing expressed CstR were resuspended in Buffer A (25 mM Tris, 5 mM DTT, 1 mM EDTA, pH 8.0) and 500 mM NaCl at 30 mL lysis buffer per 1 L of culture and lysed via sonication. Lysate debris was removed by centrifugation. Nucleic acids were precipitated by dropwise addition of 10% polyethylenimine solution (PEI), pH 7.0, to a final concentration of 0.015% v/v, stirred at 4° C for 1 h, and removed by centrifugation. Ammonium sulfate was added to the PEI supernatant at 57% saturation (0.35 g/mL), stirred for 1 hour and pelleted by centrifugation. This pellet was resuspended and buffer exchanged by dialysis into Buffer A containing 90 mM NaCl. During the buffer exchange, the majority of CstR precipitated and was collected by centrifugation. The CstR pellet was washed twice with dialysis

buffer and resuspended in Buffer A with 500 mM NaCl. Insoluble protein was pelleted and the supernatant was concentrated with an Amicon Ultra centrifugal concentrator filter tube with a 3000 Da cut-off weight prior to loading on a Superdex G200 16/60 gel filtration prep-grade column (GE Healthcare) equilibrated with Buffer A and 500 mM NaCl. Fractions containing CstR, as determined by 18% SDS-PAGE, were pooled and concentrated to 1-2 mL and dialyzed into Buffer B (10 mM Tris, 500 mM NaCl, pH 8.0) in an anaerobic glovebox (Vacuum Atmospheres). All buffers used in the glovebox were passed over a Chelex 100 resin (Biorad) to remove trace metals and degassed and backfilled with argon three times on a Schlenk line. All glassware used anaerobically was soaked in a 2% nitric acid bath overnight and extensively washed with Milli-Q water. The reduced state of the thiols was confirmed by LC-ESI-MS and quantified by DTNB assay¹⁷² following dialysis. Mutant CstR plasmids were prepared using standard site-directed mutagenesis techniques with appropriate primers and purified as described for wild type CstR.

Reaction with chalcogen oxyanions. 15 μ M samples of CstR (protomer) were reacted anaerobically in Buffer C (10 mM HEPES, 200 mM NaCl, pH 7.0) with a 5-fold thiol excess of sulfite (SO_3^{2-}), selenite (SeO_3^{2-}), tellurite (TeO_3^{2-}), or tetrathionate ($\text{S}_4\text{O}_6^{2-}$) overnight (~17 h) at room temperature (~22 °C). Following the reaction, samples were sealed in septa cap vials for immediate LC-ESI-MS analysis. Samples for fluorescence anisotropy or tryptic digest and subsequent high-resolution tandem mass spectrometry analysis were reacted for 36 h to ensure reaction completion.

LC-ESI-MS analysis of intact CstR and CsoR. LC-ESI-MS analysis was performed at the Indiana University Mass Spectrometry Facility using a Waters/Micromass LCT Classic time of flight (TOF) mass spectrometer with a CapLC inlet. Proteins were loaded onto a 50 mm Agilent BioBasic C8 reverse-phase column with a 5 mm particle size and 300 Å pore size in Solvent A (5% acetonitrile, 95% water, 0.1% formic acid) and eluted with a 20 min linear gradient from 10% Solvent A to 90% Solvent B (95% acetonitrile, 5% water, 0.1% formic acid). Elution was monitored at 215 nm. Data were collected and analyzed using MassLynx Software (Waters).

High-Resolution Linear Triple Quadrupole (LTQ)-Orbitrap Tandem Mass Spectrometry Analysis of Tryptic Peptides. Reacted and unreacted CstR samples were solution digested anaerobically with proteomics-grade trypsin from porcine pancreas (Sigma-Aldrich) at 37 °C overnight (~17 h) with a 1:50 ratio of trypsin to CstR. Following digestion, samples were desalted using a C18 Zip-Tip column (Millipore), air-dried, and resuspended in degassed Milli-Q water immediately prior to analysis. All preparation steps were performed anaerobically. Parameters used for LTQ-orbitrap tandem mass spectral analysis are similar to those previously described.¹⁵⁰ Briefly, 5 µL of protein digest were loaded onto a 15 mm x 100 mm i.d. C18 reversed-phase trapping column. Peptides were eluted through a 150 mm x 75 mm i.d. analytical column packed with 5 mm, 100 Å Magic C18AQ packing material (Michrom BioResources Inc.) using a 60 min gradient from 97% to 60% Solvent A (97:3:0.1 water–acetonitrile–formic acid, Solvent B is 0.1% formic acid in acetonitrile) at 250 nL min⁻¹ on a Dionex UltiMate 3000 nanoLC. Eluent from the column was ionized and electrosprayed directly into a LTQ-Orbitrap XL mass

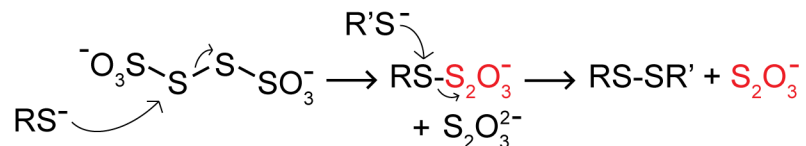
spectrometer (Thermo-Finnigan) which recorded mass spectra and “top five” data-dependent tandem mass spectra of the peptide ions. Data were interpreted by manual investigation to identify candidate MS/MS spectra and assign identifications of the fragment ions for confirmation of the modified CstR. In some cases, cross-linked peptides eluted within the exclusion window of a previous peak and were not selected for fragmentation. To obtain fragmentation spectra of these species, multiple reaction monitoring¹⁷³ (MRM) was employed to ensure collection of fragmentation data.

Fluorescence anisotropy titrations. Double-stranded fluorescein-labeled *cst* OP1 DNA constructs were purified and prepared as previously described.¹⁵⁰ Briefly, the double-stranded DNA was prepared by mixing 1.1 mol equivalents of complementary unlabeled DNA (ATGTGTCAAATACCCCTAGAGGTATTTG) to fluorescently labeled DNA (F-CAAATACCTCTAGGGGTATTTGACACAT, where F = fluorescein), heated to 95 °C for 10 min, and slowly cooled to room temperature. To confirm formation of the double stranded DNA, native TBE polyacrylamide gel electrophoresis was performed. Fluorescence anisotropy titrations were performed essentially as described^{13,162} where 10 nM *cst* OP1 dsDNA was titrated with the indicated CstR under strictly anaerobic conditions. Injections of 1-5 μ L were equilibrated for three minutes and then anisotropy was monitored using an ISS PC1 Spectrofluorometer. Fluorescein was excited at 490 nm and polarization monitored with a 515 nm cut-off filter in the L-format. Each data point collected was an average and standard deviation of five measurements. Normalized r values for the fractional saturation of *cst* OP1 was calculated as $(r_{\text{obs}} - r_0)/(r_{\text{complex}} - r_0)$ from 0 to 1 where r_{complex} represents the maximum anisotropy obtained and r_0 represents

free *cst* OP1 DNA. For titrations not reaching saturation, r_{complex} was calculated from the addition of the anisotropy change of reduced CstR to r_0 of the corresponding non-saturating CstR. Collected data were fit to a sequential non-dissociable tetramer (CstR₄) binding model^{6,13,162} using DynaFit¹⁷⁴ (Appendix Fig. 1) assuming a linear relationship between r_{obs} and v_i and the binding density at the i th addition of titrant.⁶ The macroscopic binding constant, K_{tet} , is reported and was determined as $K_{\text{tet}} = (K_1 \cdot K_2)$ due to high uncertainty in extracting unique K_i values, K_1 and K_2 , as there is a strong inverse correlation and little sigmoidal behavior in the binding isotherms as previously described.^{6,13,162} Reported affinities (K_{tet}) are the average of three independent experiments.

RESULTS

CstR reacts with selenite and tellurite to form di- and trisulfide-like species. To better understand the di- and trisulfide cross-linking of CstR when reacted with sulfite,⁶ the heavier chalcogen oxyanions, SeO_3^{2-} and TeO_3^{2-} , were employed as surrogates. To establish the differentiation by charge state distribution, the m/z ratios of reduced and oxidized CstR were compared by LC-ESI-MS. CstR was oxidized with tetrathionate ($\text{S}_4\text{O}_6^{2-}$) which undergoes a double displacement reaction to form disulfide bonds (Scheme 1).¹⁷⁵ Here, fully reduced CstR and cross-linked CstR dimers are readily distinguishable based on charge state distribution from +8-13 to +11-20, respectively (Fig. 11). The observed shift in the distribution of charge states is due to an effective doubling of the possible protonation sites from the formation of a disulfide bond between



Scheme 1. Thiols react with tetrathionate in a double displacement reaction to form disulfide bonds. A thiolate (RS⁻) attacks a central sulfur atom in tetrathionate to form a cysteine S-thiosulfonate and liberating a thiosulfate anion (S₂O₃²⁻). A subsequent thiol attacks the cysteine sulfur atom to liberate a second equivalent of thiosulfate and form a disulfide bond (RS-SR') between the two thiols.¹⁷⁵

Cys31 and Cys60' of two CstR protomers and provides the basis for distinguishing reduced from cross-linked CstR by LC-ESI-MS.

Using the now-established straightforward reporter on CstR cross-linking, we then monitored CstR reactions with SeO₃²⁻ and TeO₃²⁻ by LC-ESI-MS. In both cases, the cross-linked form of CstR is observed and closer inspection of individual charge states reveals a +32 Da mass shift followed by +79 or +128 Da mass shifts, consistent with selenium and tellurium, respectively (Fig. 12). These are annotated as RS-Se-SR' and RS-Te-SR' cross-links between Cys31 and Cys60' for seleno- and tellurotrisulfides, respectively. In addition to the seleno- and tellurotrisulfides, a doubly oxygen adducted cross-linked species is also observed. A complete mass list of observed species is available in Table 1.

The Cu(I) sensor CsoR does not react with selenite and only partially reacts with tellurite. The *S. aureus* copper sensor CsoR does not undergo reaction with SO₃²⁻ and the *cst* operon is not induced under conditions of copper stress.⁶ To better understand the differences in CstR and CsoR reactivities, CsoR was reacted with the same 5-fold thiol excess of selenite and tellurite and analyzed by LC-ESI-MS. A shift in the mass to charge range was observed for CsoR where reduced CsoR was +7 to +15 and CsoR oxidized by

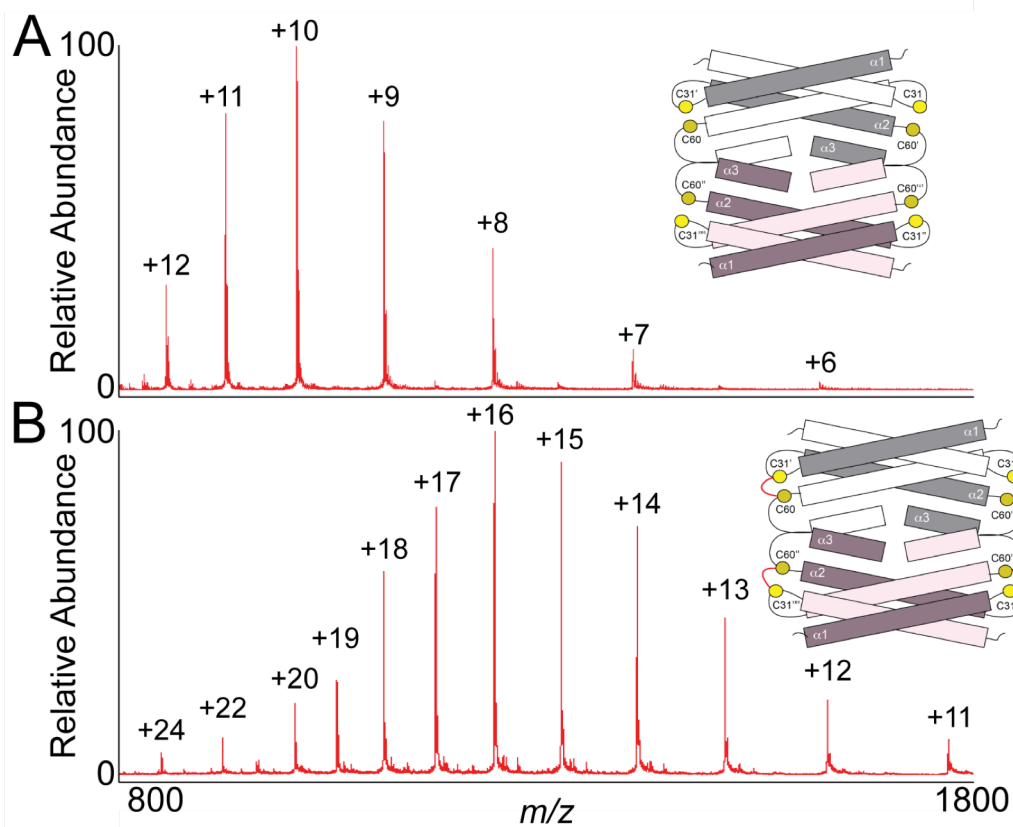


Figure 11. LC-ESI-MS m/z ratios of reduced and oxidized CstR. Unreacted or reduced CstR displays a m/z range of +6 to +13 (A) and cross-linked or oxidized CstR ranges from +11 to +24 (B). Inset: cartoon representation of cysteine locations in CstR. Formation of a disulfide bond between Cys31 and Cys60' results in the covalent cross-linking of the 'white' and 'grey' protomers, red lines.

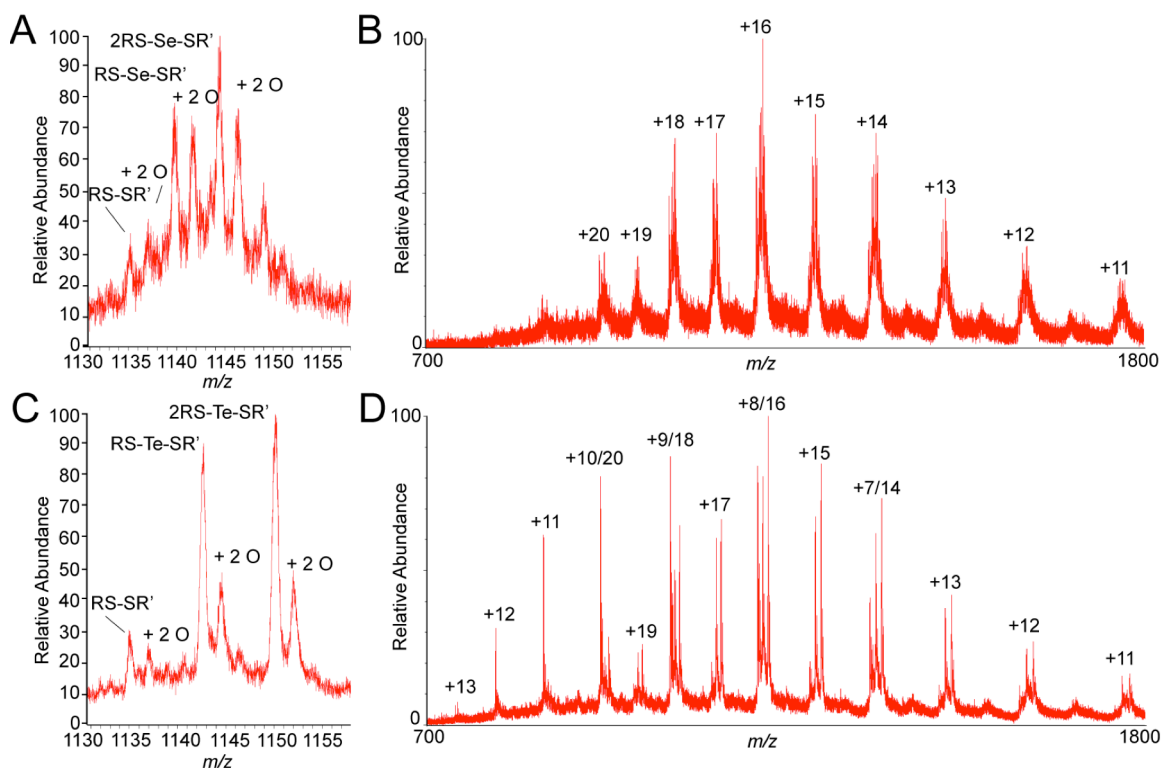


Figure 12: LC-ESI-MS analysis of CstR following reaction with selenite or tellurite. CstR was reacted with a 5-fold thiol excess of selenite (A-B) or tellurite (C-D) for 17 h. (A) The +16 charge state of SeO_3^{2-} -reacted CstR with a (B) charge state distribution of +11 to +20. (C) The +8 or +16 charge state distribution of TeO_3^{2-} -reacted CstR with a (D) charge state distribution of +7 to +13 for the reduced protein and +11 to +20 for cross-linked CstR. Masses corresponding to disulfide formation between Cys31 and Cys60' are denoted RS-SR' and seleno- and tellurotrisulfide formation have been denoted RS-X-SR' where X = Se or Te.

Table 1. Summary of deconvoluted masses obtained from CstR reaction with selenite, tellurite, or tetrathionate. Mass shifts are relative to either reduced ($\text{CstR}^{\text{RS-H}}$) or disulfide cross-linked CstR ($\text{CstR}_2^{\text{RS-SR}'}$) as indicated by (-).

Modifier	M_r Expected	M_r Observed	Mass Shift	Assignment
None	9641.2	9641.3	-	$\text{CstR}^{\text{RS-H}}$
	9663.2	6443.4	22.1	$\text{CstR}^{\text{RS-H}} + \text{Na}$
	19280.4	19282.3	-	$\text{CstR}_2^{\text{RS-SR}'}$
SeO_3^{2-}	9641.2	9638.2	-	$\text{CstR}^{\text{RS-H}}$
	9663.2	9660.4	22.2	$\text{CstR}^{\text{RS-H}} + \text{Na}$
	19280.4	19277.5	-	$\text{CstR}_2^{\text{RS-SR}'}$
	19312.4	19309.7	32.2	$\text{CstR}_2^{\text{RS-SR}'} + 2 \text{O}$
	19359.4	19357.4	79.9	$\text{CstR}_2^{\text{RS-Se-SR}'}$
	19391.4	19389.6	112.1	$\text{CstR}_2^{\text{RS-Se-SR}'} + 2 \text{O}$
	19425.4	19422.5	145	$\text{CstR}_2^{\text{RS-Se-SR}'} + 3 \text{Na}$
	19438.3	19437.1	159.6	$\text{CstR}_2^{(\text{RS-Se-SR}')2}$
	19470.3	19468.8	191.3	$\text{CstR}_2^{(\text{RS-Se-SR}')2} + 2 \text{O}$
	19503.4	19500.3	222.8	$\text{CstR}_2^{(\text{RS-Se-SR}')2} + 3 \text{Na}$
19517.3	19515.8	238.3	$\text{CstR}_2^{(\text{RS-Se-SR}')2} + \text{Se}$	
TeO_3^{2-}	9641.2	9640.2	-	$\text{CstR}^{\text{RS-H}}$
	9657.2	9656.2	16	$\text{CstR}^{\text{RS-H}} + \text{O}$
	9673.2	9671.6	31.4	$\text{CstR}^{\text{RS-H}} + 2 \text{O}$
	9768.8	9767.5	127.3	$\text{CstR}^{\text{RS-H}} + \text{Te}$
	19280.4	19279.7	-	$\text{CstR}_2^{\text{RS-SR}'}$
	19312.4	19311.4	31.7	$\text{CstR}_2^{\text{RS-SR}'} + 2 \text{O}$
	19408	19407.3	127.6	$\text{CstR}_2^{\text{RS-Te-SR}'}$
	19440	19439.1	159.4	$\text{CstR}_2^{\text{RS-Te-SR}'} + 2 \text{O}$
	19535.6	19534.6	254.9	$\text{CstR}_2^{(\text{RS-Te-SR}')2}$
	19567.6	19567.6	287.9	$\text{CstR}_2^{(\text{RS-Te-SR}')2} + 2 \text{O}$
$\text{S}_4\text{O}_6^{2-}$	9641.2	-	-	$\text{CstR}^{\text{RS-H}}$
	19280.4	19279.4	-	$\text{CstR}_2^{\text{RS-SR}'}$
	19302.4	19300.6	21.2	$\text{CstR}_2^{\text{RS-SR}'} + \text{Na}$
	19312.4	19311.6	32.2	$\text{CstR}_2^{\text{RS-S-SR}'}$
	19324.4	19322.4	43	$\text{CstR}_2^{\text{RS-SR}'} + 2 \text{Na}$

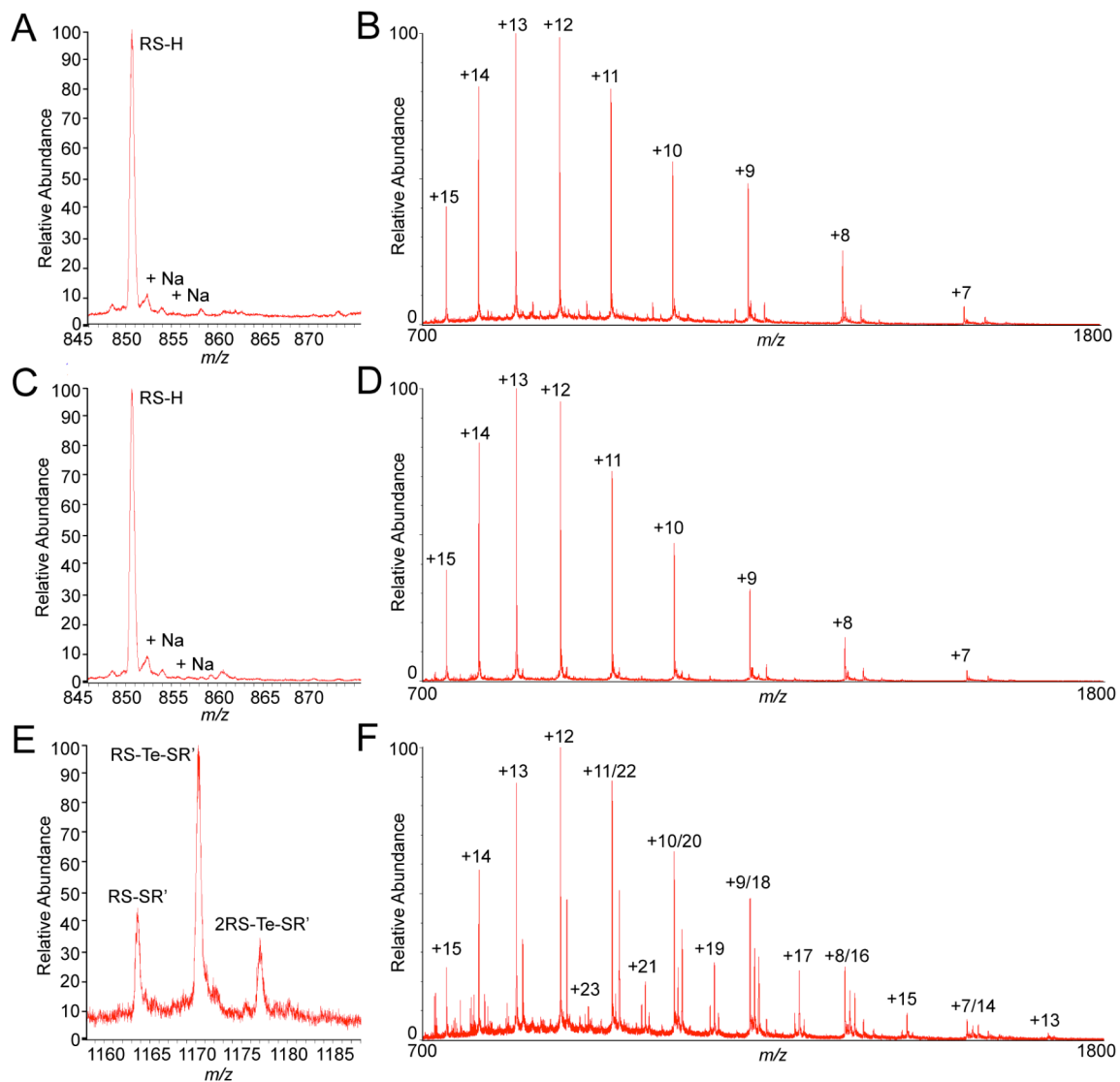


Figure 13. LC-ESI-MS analysis of CsoR following reaction with selenite or tellurite. CsoR (A-B) was reacted with a 5-fold thiol excess of selenite (C-D) or tellurite (E-F) for 17 h. *Left:* The +13 charge state for reduced CsoR (A and C) and +19 charge state for cross-linked CsoR. *Right:* the m/z ratios of reduced CsoR (B) or CsoR following reaction with SeO_3^{2-} (D) or TeO_3^{2-} (F).

Table 2. Summary of deconvoluted masses obtained from CsoR following reaction with selenite, tellurite, or tetrathionate. Mass shifts are relative to either reduced (CsoR^{RSH}) or disulfide cross-linked CstR ($\text{CsoR}_2^{\text{RS-SR}'}$) as indicated by (-).

Modifier	M_r Expected	M_r Observed	Mass Shift	Assignment
None	11036.6	11034.9	-	$\text{CsoR}^{\text{RS-H}}$
	11058.6	11057.0	22.1	$\text{CsoR}^{\text{RS-H}} + \text{Na}$
SeO_3^{2-}	11036.6	11035.4	-	$\text{CsoR}^{\text{RS-H}}$
	11058.6	11057.5	22.1	$\text{CsoR}^{\text{RS-H}} + \text{Na}$
TeO_3^{2-}	11036.6	11033.2	-	$\text{CsoR}^{\text{RS-H}}$
	21069.2	22065.4	-	$\text{CsoR}^{\text{RS-SR}'}$
	21196.8	22192.2	126.8	$\text{CsoR}^{\text{RS-Te-SR}'}$
	21324.4	22318.1	252.7	$\text{CsoR}^{(\text{RS-Te-SR}')_2}$

tetrathionate from +13 to +23. Here, CsoR was shown to be unreactive toward SeO_3^{2-} and no change in charge state distribution was observed. However, when reacted with the more reactive TeO_3^{2-} chalcogen oxyanion, a small portion of CsoR is cross-linked and a mass shift +128 Da is observed, consistent with the formation of a tellurotrisulfide (Fig. 13, Table 2). The lower reactivity of CsoR with chalcogen oxyanions suggests a fundamental difference in cysteine reactivity compared to CstR.

CstR cross-linking by selenite contains a selenotrisulfide. To determine the nature of the cross-linking in SeO_3^{2-} -reacted CstR, the protein was digested with trypsin. The resulting peptides were desalted using a C18 ZipTipTM (Millipore). All steps leading to LTQ-orbitrap tandem mass spectrometry analysis were performed anaerobically. Cross-linked peptides were initially identified in the +4 charge state by accurate mass (Table 3) and the most abundant peptides contained two missed cleavages near Cys31, $^{24}\text{MMEEGKDCKDVITQISASK}^{42}$ (denoted peptide “A”), and the Cys60 peptide $^{48}\text{LMGIIISENLIECVK}^{62}$ (denoted peptide “B”). Comparison of the accurate masses of the disulfide and selenotrisulfide cross-linked peptides, 946.980 and 966.960 Da, respectively, reveals a mass shift of 79.920 Da, a mass fully consistent with the ^{80}Se isotope, 79.91652 Da (Table 3). Additionally, the isotopic distribution of the LTQ data matches the predicted distribution of peptide A and B with the addition of a selenium atom.

Next, the location of the selenium atom was determined by inspection of the fragmentation pattern of Se-containing peptides. As controls, the Cys31 and Cys60-containing peptides were mapped individually (Fig. 14) and used as templates for the

Table 3. Monoisotopic masses for the parent ions of selenite- or tellurite-reacted CstR tryptic peptides. Data was obtained from tandem high-resolution mass spectrometry. n.d. denotes no data.

Sample	Assignment	Charge State	<i>m/z</i> Ratio	
			Calculated	Observed
Control	Cys31, RS-H	+ 3	705.004	705.003
	Cys60, RS-H	+ 2	704.361	704.352
SeO ₃ ²⁻	RS-SR'	+ 4	946.978	946.980
	+ O	+ 4	950.977	950.978
	+ 2 O	+ 4	954.976	954.972
	+ 3 O	+ 4	958.974	958.972
	RS-Se-SR'	+ 4	966.958	966.960
	RS-SR'	+ 4	946.978	946.790
TeO ₃ ²⁻	RS-Te-SR'	+ 4	979.455	-

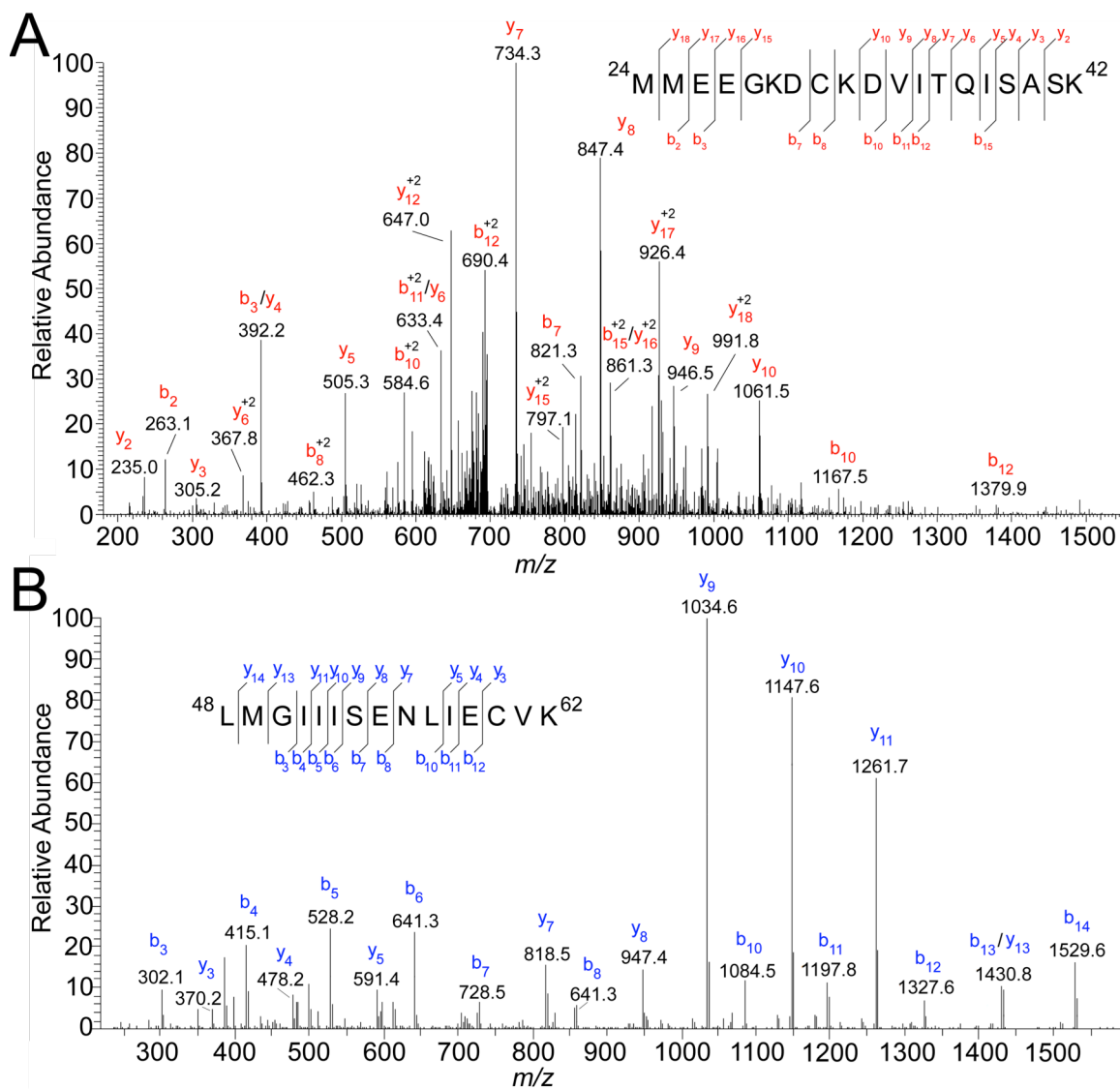


Figure 14. Fragmentation patterns of CstR cysteine-containing peptides. (A) Cys31-containing peptide, MMEEGKDCKDVITQISASK and (B) Cys60-containing peptide LMGIISENLIIECVK obtained following tryptic digest of reduced CstR. Both peptides readily fragment and most b and y ions are observed. These spectra were used to help identify cross-linked CstR peptides (see Fig. 15C-D).

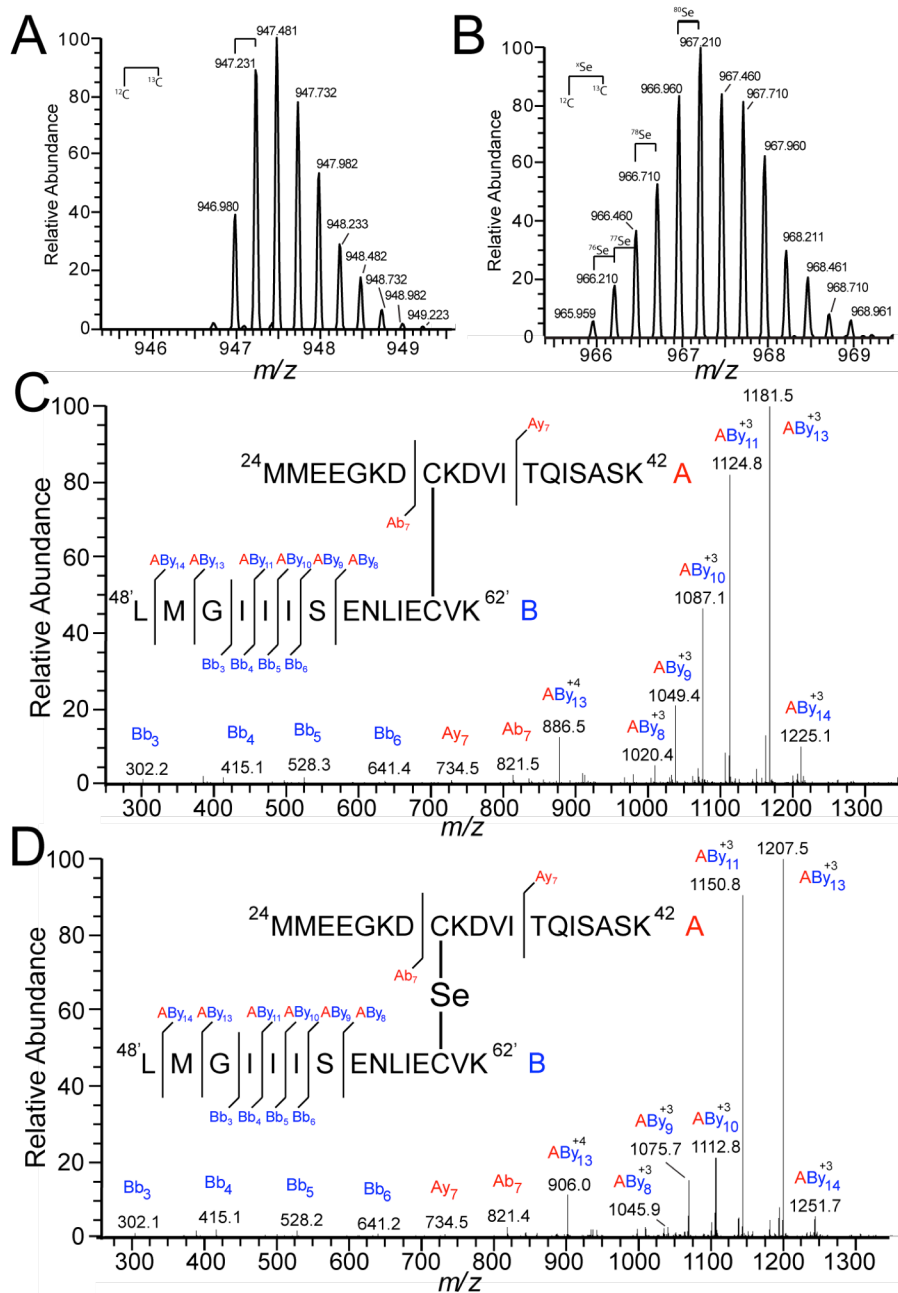


Figure 15. Tryptic peptides of selenite⁻-reacted CstR identify a selenotrisulfide. (A-B) Monoisotopic masses and distribution for (A) disulfide cross-linked CstR (946.980 Da observed) and (B) addition of a selenium atom (966.710 Da observed for ⁸⁰Se). Among the preceding peaks are lighter Se isotopes, including ⁷⁶Se, ⁷⁷Se, and ⁷⁸Se. (C-D) Fragmentation pattern of the di- and selenotrisulfide cross-linked peptides. Peptide “A” (red) corresponds to the Cys31-containing peptide, ²⁴MMEEGKDCKDVI TQISASK⁴² and peptide “B” (blue) is the Cys60'-containing peptide, ⁴⁸LMGIIISENLIECVK⁶². Fragmentation ions, b and y, are assigned relative to the respective peptide “A” or “B”, and cross-linked peptides are denoted as “AB_{yn}”.

fragmentation pattern of the cross-linked species. In all cross-linked spectra, peptide A fragmented to yield exclusively Ab_7^+ and Ay_7^+ ions as the major fragmentation products and remained intact for all ions containing cross-linked peptides. Peptide B fragmented more readily to yield a series of Bb ions. Numerous Cys31-Cys60' cross-linked fragments (denoted peptide "AB") were identified with +78 to +80 Da mass shifts relative to the disulfide cross-linked peptide ions (Fig. 15). Analogous samples were prepared to verify the tellurotrisulfide assignment but these efforts were ultimately unsuccessful (Table 3). This is likely due to rapid hydrolysis of $RS-Te-SR'$ to $RS-H$ or $RS-SR'$ and elemental tellurium, Te^0 .¹⁷⁶

SeO₃²⁻ and TeO₃²⁻ reacted with CstR contain reduction intermediates. In both the selenium and tellurium cross-linked CstR spectra, a +32 Da mass shift was observed relative to the disulfide, selenotrisulfide, and tellurotrisulfide (Fig. 12, Table 1). Further examination of the LTQ data reveals the existence of peaks corresponding to disulfide cross-linked CstR with singly, doubly, and triply oxygen adducted AB peptides with high mass accuracy (Fig. 16A, Table 3). The most abundant oxygen adduct contains two oxygen atoms and is consistent with the LC-ESI-MS data (Fig. 12A) but it was unclear if these were associated with methionine residues or the sulfur atoms involved in the disulfide. Inspection of the fragmentation pattern indicates that the oxygen atoms are not due to methionine oxidation. This indicates that the +32 Da mass shifts are likely present on the cysteine S γ atoms and are assigned as either a thiosulfonate or α -disulfoxide (Fig. 16B, Scheme 2). At the time of publication,¹⁶² neither a protein-derived thiosulfonate nor

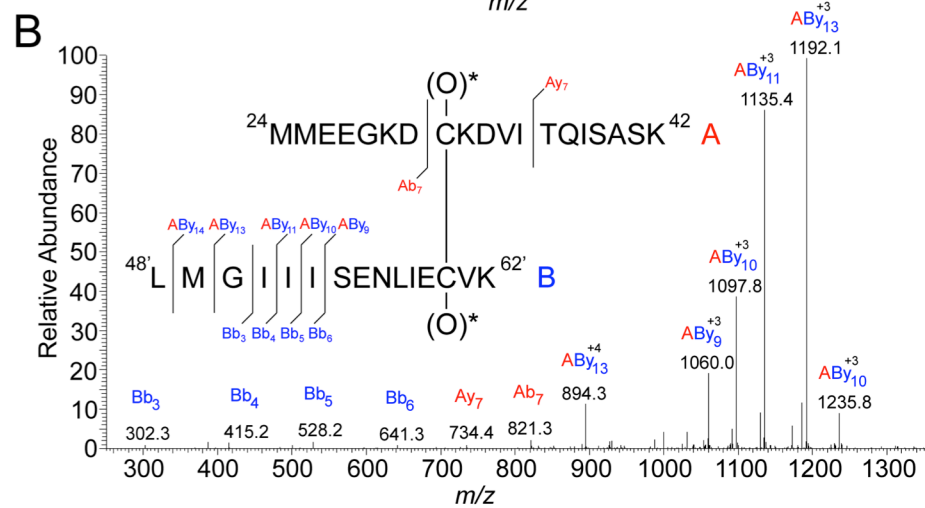
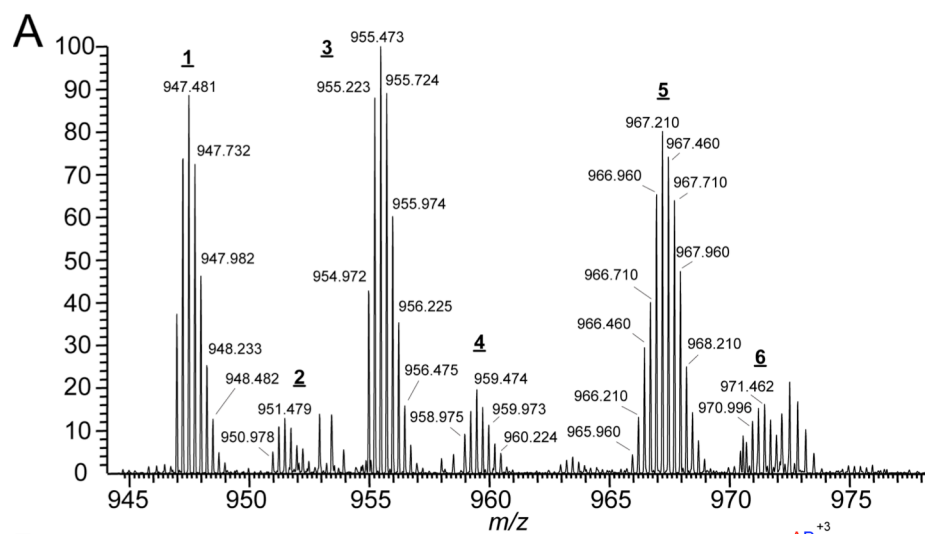
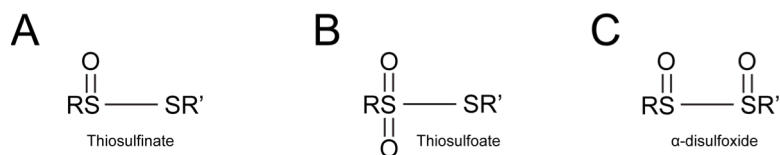


Figure 16. CstR reacted with selenite contains prominent disulfide peaks with oxidized cysteine residues. (A) Distribution of +4 ions detected over the elution range of CstR cross-linked species. The labeled cross-linked peptides are; **1**, disulfide cross-linked CstR (see Fig. 15); **2**, disulfide cross-linked CstR with one oxidized methionine; **3**, disulfide cross-linked CstR with two oxygen atoms distributed between the cysteine residues (fragmentation shown in panel B); **4**, Same as **3** with an oxidized methionine; **5**, selenotrisulfide cross-linked CstR (see Fig. 15); **6**, selenotrisulfide cross-linked CstR with one oxidized methionine (fragmentation data not shown). (B) Fragmentation pattern of disulfide cross-linked CstR with two cysteine oxidations (peak **3** from panel A). Cross-linked AB_y_n ions contain a mass shift of +32 Da and correspond to two total oxygen atom adductions on one or both cysteine S_γ atom. An oxidation of either Met residue on peptide “A” yields an Ab_7 ion with a mass of approximately 837 or 853 Da for one or two oxygen atoms, respectively. The observed Ab_7 ion has a mass consistent with the reduced state, 821 Da. Similarly, a Met residue oxidation on peptide “B” would yield Bb_n ions with a mass shift of +16 or +32 Da, *e.g.*, the observed Bb_3 ion would shift to approximately 318 or 334 Da with one or two oxygen atoms, respectively. As a result, we conclude that the oxygen adducts here (*) are assignable as either a mixture of thiosulfonates or α -disulfoxide.

α -disulfoxide had been observed but had been described in the organic literature for thiol-containing compounds.¹⁷⁷



Scheme 2: Depiction of thiosulfinate (A), thiosulfonate (B), and α -disulfoxide (C) oxygen adducts.

Formation of disulfides, selenotrisulfides, or tellurotrisulfides negatively regulates cst OP1 DNA binding in vitro. To test if the formation of disulfides, selenotrisulfides, or tellurotrisulfides on CstR lead to the negative regulation of *cst* operator DNA binding, fluorescence anisotropy titrations were performed. Fully reduced CstR or CstR reacted with tetrathionate ($S_4O_6^{2-}$), SeO_3^{2-} , or TeO_3^{2-} was titrated into a solution containing fluorescently-labeled *cst* OP1 under strictly anaerobic conditions (Fig. 17). Data from these experiments were fit to a sequential tetramer binding model (Scheme 3).^{6,13,162} Each



Scheme 3. CstR DNA sequential tetramer binding model.

of the modified CstRs bound *cst* operator DNA with a reduced affinity of ~30-60 fold relative to fully reduced CstR (Table 4). These results suggest that regulation of CstR DNA binding is indiscriminate with respect to the nature of the cross-linking in the formation of di-, tri-, seleno-, or tellurotrisulfides negatively regulate *cst* DNA binding.

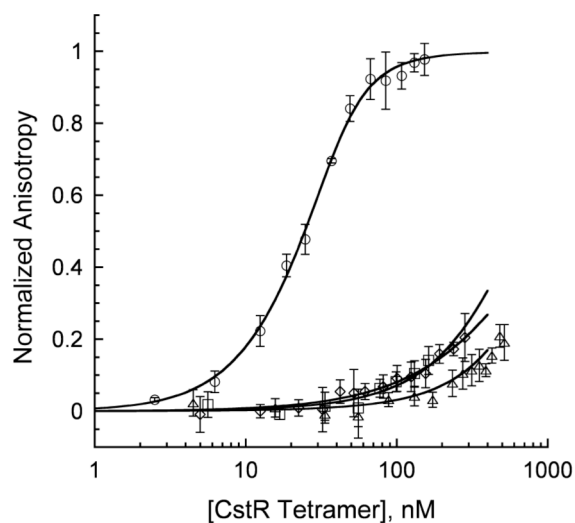


Figure 17. Fluorescence anisotropy titrations of reduced and cross-linked CstR. Fluorescence anisotropy titrations of reduced CstR (circles) and CstR following reaction with SeO_3^{2-} (squares), TeO_3^{2-} (diamonds), or tetrathionate ($\text{S}_4\text{O}_6^{2-}$, triangles) with fluorescently-labeled *cst* OP1. All data were fit to a sequential tetramer binding model where two tetramers bind one operator DNA in a step-wise fashion defined by K_1 and K_2 . K_{tet} describes the average macroscopic binding constant where $K_{\text{tet}} = (K_1 \cdot K_2)^{1/2}$. Tetrameric bundles were assumed to be non-dissociable.

Table 4. Summary of macroscopic binding constants of WT CstR and CstR cysteine mutants. Data was obtained from fluorescence anisotropy experiments of WT CstR or CstR cysteine mutants with *cst* OPI.

Protein	r_0	r_{complex}	$K_{\text{tet}} (\text{M}^{-1})$ $\times 10^{-7}$
WT CstR	0.133	0.155	6.3 (\pm 0.5)
+ SeO_3^{2-}	0.132	0.154*	0.20 (\pm 0.03)
+ TeO_3^{2-}	0.133	0.155*	0.13 (\pm 0.14)
+ $\text{S}_4\text{O}_6^{2-}$	0.132	0.154*	0.11 (\pm 0.11)
C31A CstR	0.135	0.161	3.3 (\pm 0.7)
+ MMTS	0.135	0.159	2.0 (\pm 0.5)
C60A CstR	0.135	0.159	4.2 (\pm 1.0)
+ MMTS	0.136	0.158*	0.31 (\pm 0.03)
C31A/C60A CstR	0.134	0.157	12 (\pm 5)

*Fit to Δ anisotropy of corresponding non-derivatized CstR

Cys31 of CstR initiates the reaction with chalcogen oxyanions. To better understand the reduction reaction of CstR with chalcogen oxyanions, single and double cysteine substitution mutants were prepared, specifically C31A, C60A, and C31A/C60A CstR. Here, the C31A CstR mutant reports on the reactivity of Cys60 while C60A CstR reports on Cys31. Each mutant was reacted with a 5-fold thiol excess of sulfite to test the importance of individual cysteine residues. LC-ESI-MS analysis of sulfite-reacted C31A or C60A CstR revealed that only the C60A mutant reacted with SO_3^{2-} to form *S*-sulfocysteine (RS-SO_3^{2-} , Fig. 18, Table 5). This result indicates that Cys31 of CstR initiates the chalcogen oxyanion reduction while Cys60' is required to continue the reaction toward cross-linked products.

These results reveal that reduction of chalcogen oxyanions is ordered and is not a random multi-thiol mechanism. This suggests that the local microenvironment near the two thiols directs these compounds to Cys31 first or that the intrinsic reactivity of Cys31 is greater than that of Cys60. Similar findings characterize the reactions of C31A and C60A CstRs with SeO_3^{2-} except that both reactions form $\text{RS-SR}'$ and $\text{RS-Se-SR}'$ crosslinks, likely involving the same cysteine residues reaching across the tetramer interface. C60A CstR gives a number of oxidation products including the anticipated *S*-selenocysteine on Cys31 (Table 5) and in both cases, these modifications are also inhibitory to operator DNA binding. These features perhaps make CstR ideally suited to react with a wide range of cellular thiol oxidants and it coincides with the observation that the formaldehyde-sensing FrmR is a CsoR-family protein that retains a single cysteine corresponding to Cys31 in CstR that is thought to react with carbon electrophiles via Michael addition.¹⁷⁸

Perturbation of Cys31 is both necessary and sufficient to negatively regulate DNA binding in vitro. Given the importance of Cys31 in the order of reduction, it was hypothesized that modification of Cys31 may be both necessary and sufficient to negatively regulate DNA binding by CstR. To test this, C31A or C60A CstR was reacted with the cysteine-modifying reagent, methylmethanethiolsulfonate (MMTS) to form a cysteine *S*-thiomethyl (RS-SCH₃, Table 5). Although both C31A and C60A CstR mutants bind DNA with an affinity that is similar to WT CstR in their reduced form, the derivatized mutants differ significantly. Derivatization of Cys31 (C60A CstR) diminishes DNA binding affinity while the same modification of Cys60 (C31A CstR) has little impact on DNA binding affinity and is similar to the reduced WT CstR. (Fig. 18C, Table 4).

By sequence alignment and homology modeling, CstR cysteine residues are likely located in positions similar to those of CsoR (Fig. 19A) and as such, the distances between the corresponding Cys31 and Cys60' across the dimer interface likely range between 8-9 Å. In addition, the distances between Cys60' and Cys60'' across the tetramer interface range between 4-11 Å, depending on the rotational orientation of the cysteine side chains when measured for several CsoR proteins. For comparison, Cys31 and Cys31''' are separated by approximately 22.5 Å (Fig. 19A).^{144,145,179} To begin probing the potential interaction between cysteine residues across the tetramer interface, C31A and C60A CstR were reacted with tetrathionate. The reaction of C60A CstR with tetrathionate leads to the formation of a cysteine *S*-thiosulfonate on Cys31 (RS-S₂O₃) while the same reaction with C31A CstR leads to the formation of a disulfide bond between Cys60' and Cys60'' across the tetramer interface (Fig. 19B-C). The formation of

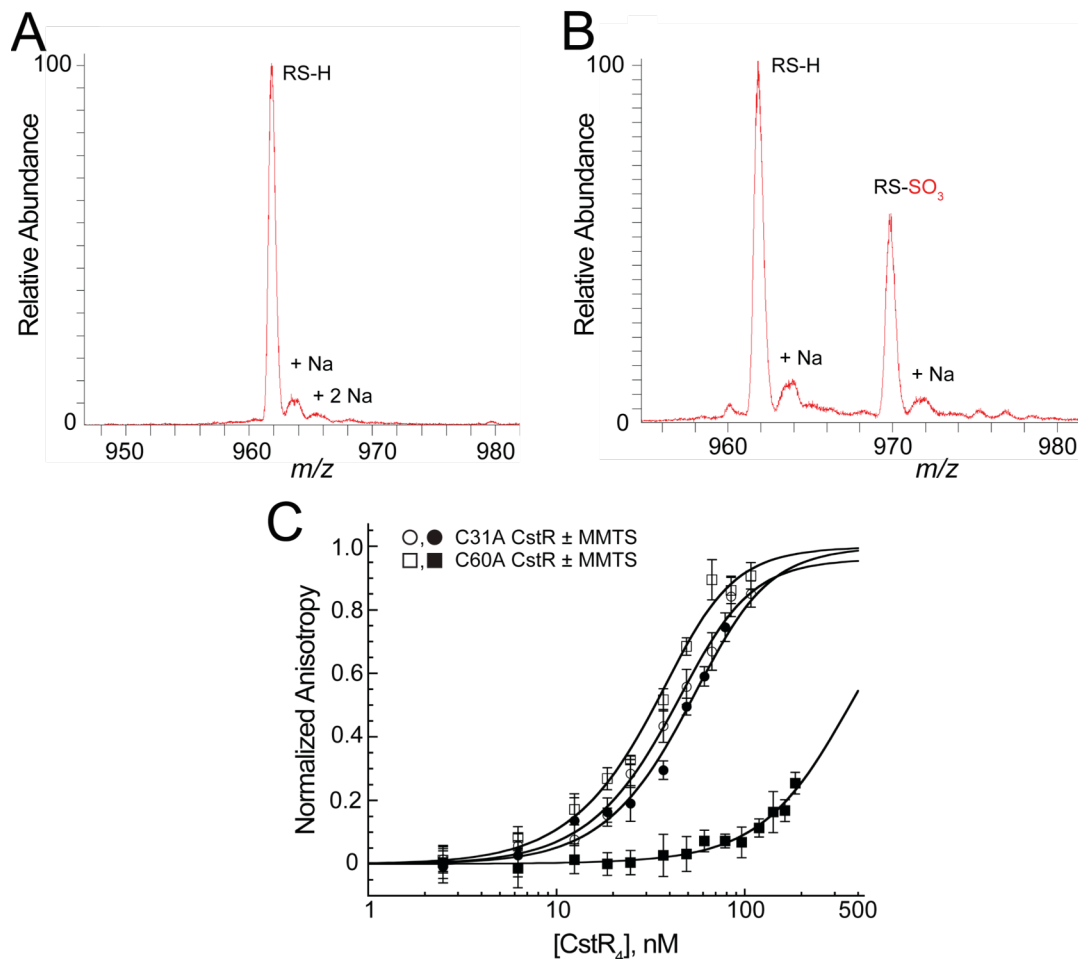


Figure 18. LC-ESI-MS analysis of CstR cysteine mutants following reaction with sulfite. C31A CstR (A) remains fully reduced while C60A CstR reacts with SO₃²⁻ to form an *S*-sulfocysteine on Cys31 as indicated by a +80 Da mass shift (Table 5). Both peaks shown are in the +11 charge state. (C) Fluorescence anisotropy titrations of reduced (open symbols) C31A or C60A CstR cysteine mutants or following derivatization with MMTS (closed symbols). A summary of binding constants is available in Table 4.

Table 5: Summary of deconvoluted masses obtained for CstR cysteine mutants. Data was collected by LC-ESI-MS and all masses are relative to CstR^{RS-H} or CstR₂^{RS-SR'} as indicated by (-).

Protein	Modifier	M _r Expected	M _r Observed	Mass Shift	Assignment
C31A CstR	None	9609.1	9607.2	-	CstR ^{RS-H}
	MMTS	9656.2	9653.3	46.1	CstR ^{RS-SCH3}
	SO ₃ ²⁻	9609.1	9606.5	-	CstR ^{RS-H}
		9631.1	9627.9	21.4	CstR ^{RS-H} + Na
		9653.1	9648.6	42.1	CstR ^{RS-H} + 2 Na
	SeO ₃ ²⁻	9609.1	9606.0	-	CstR ^{RS-H}
		9625.1	9622.3	16.3	CstR ^{RS-H} + O
		19216.2	19211.6	-	CstR ₂ ^{RS-SR'}
		19295.2	19290.2	78.6	CstR ₂ ^{RS-Se-SR'}
		19327.2	19326.4	114.8	CstR ₂ ^{RS-Se-SR'} + 2 O
	S ₄ O ₆ ²⁻	9609.1	9606.2	-	CstR ^{RS-H}
		19216.2	19211.5	-	CstR ₂ ^{RS-SR'}
		19232.2	19227.5	16.0	CstR ₂ ^{RS-SR'} + O
		19238.2	19232.6	21.1	CstR ₂ ^{RS-SR'} + 2 Na
		19260.2	19254.8	43.3	CstR ₂ ^{RS-SR'} + 2 Na
	C60A CstR	None	9609.1	9607.0	-
MMTS		9656.2	9653.5	46.5	CstR ^{RS-SCH3}
SO ₃ ²⁻		9609.1	9607.3	-	CstR ^{RS-H}
		9631.1	9628.3	21.0	CstR ^{RS-H} + Na
		9689.2	9687.4	80.1	CstR ^{RS-SO3}
SeO ₃ ²⁻		9711.2	9708.3	101.0	CstR ^{RS-SO3} + Na
		9609.1	9606	-	CstR ^{RS-H}
		9625.1	9622.5	16.5	CstR ^{RS-H} + O
		9641.1	9638.3	32.3	CstR ^{RS-H} + 2O
		9688.1	9684.5	78.5	CstR ^{RS-H} + Se
		9720.1	9717.7	111.7	CstR ^{RS-SeO2}
		9736.1	9738.8	132.8	CstR ^{RS-SeO3}
		19216.2	19211.6	-	CstR ₂ ^{RS-SR'}
		19248.2	19245.4	33.8	CstR ₂ ^{RS-SR'} + 2 O
19295.2		19290.3	78.7	CstR ₂ ^{RS-Se-SR'}	
19327.2		19323.3	111.7	CstR ₂ ^{RS-Se-SR'} + 2 O	
S ₄ O ₆ ²⁻	9609.1	-	-	CstR ^{RS-H}	
	9721.1	9718.1	112.1	CstR ^{RS-S2O3}	
	9753.1	9750.7	144.7	CstR ^{RS-S3O3}	
C31/60A CstR	None	9577.0	9575.3	-	No Thiol

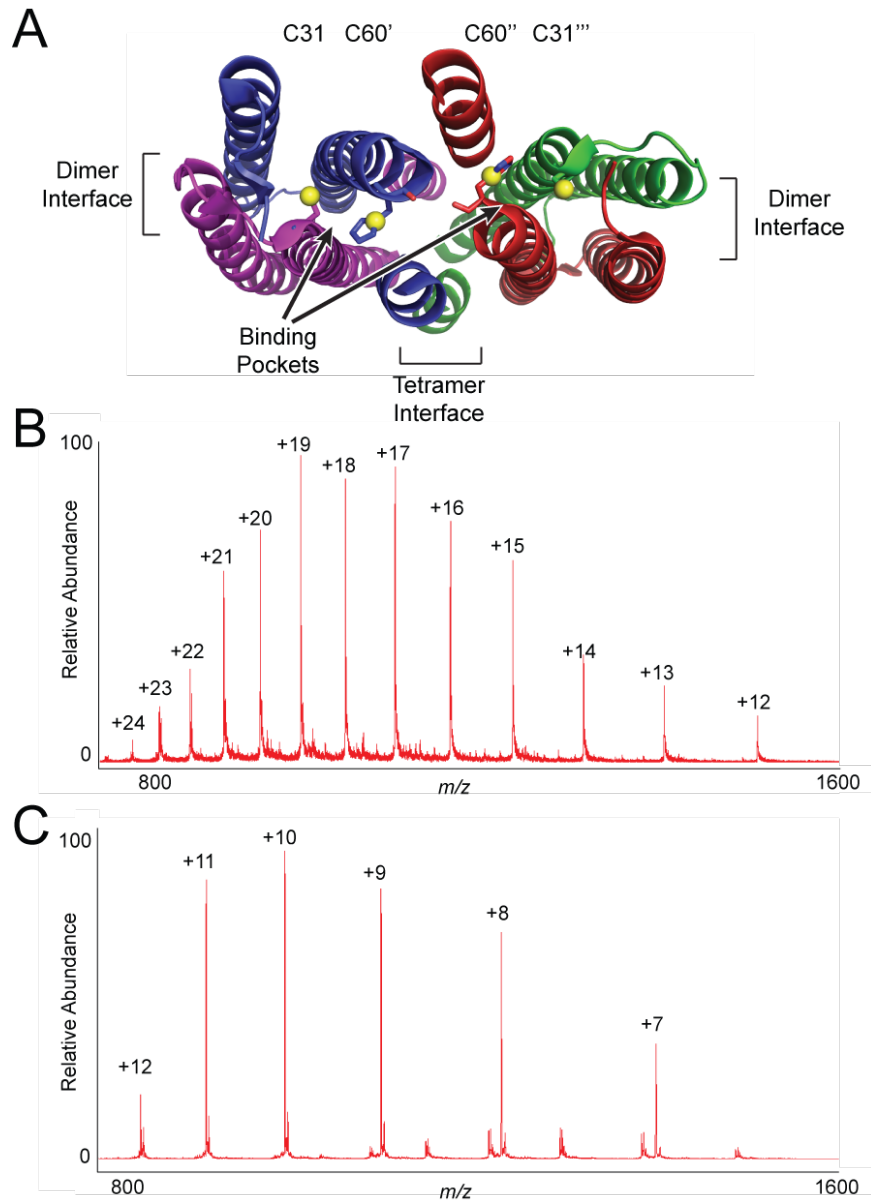


Figure 19. LC-ESI-MS analysis of CstR cysteine mutants following reaction with tetrathionate. (A) Model of *Thermus thermophilis* CsoR (PDB; 3AAI)¹⁷⁹ illustrating probable positions of CstR cysteine sulfur atoms (yellow spheres). Each protomer is differentially colored. Reaction of tetrathionate with C31A CstR (B) leads to the formation of a disulfide bond between C60A' and C60A'' across the dimer interface. The analogous reaction with C60A CstR (C) results in the formation of a cysteine S-thiosulfonate.

an *S*-thiosulfonate on Cys31 is therefore likely due to the relatively larger distance between the two thiols. Likewise, the formation of a disulfide bond in the C31A CstR mutant is indicative of the close proximity of Cys60' and Cys60'' across the tetramer interface.^{144,145,179} In the CstR double cysteine mutant, C31A/C60A CstR, no reaction is observed (Table 5).

DISCUSSION

In this chapter, the reaction of CstR with the chalcogen oxyanions SeO_3^{2-} and TeO_3^{2-} was explored. This work was prompted by previous observations where CstR reacts with the related chalcogen oxyanion SO_3^{2-} to form a series of mixed disulfides, including putatively assigned di- and trisulfides. The use of selenite and tellurite allowed unambiguous exploration of the nature of the cross-links previously observed.⁶ The LC-ESI-MS results indicate that CstR reacts with both SeO_3^{2-} and TeO_3^{2-} to form adducts similar to those previously reported for the lighter chalcogen oxyanion SO_3^{2-} .⁶ The modification of CstR by these oxyanions takes the form of a mixed disulfide, $\text{CstR}_2^{(\text{RS-SR}')}$ and $\text{CstR}_2^{(\text{RS-X-SR}')n, n=1 \text{ or } 2}$ where X is Se or Te. Despite the greater intrinsic reactivity of TeO_3^{2-} ,¹⁶⁷ CstR reacts more readily with the smaller and less reactive SeO_3^{2-} chalcogen oxyanion and, surprisingly, much more readily than with SO_3^{2-} itself. This suggests that the reactive site of CstR is somehow tuned to selenite specificity, whether by optimal distance between cysteine sidechains, or by some other factor influencing cysteine reactivity.

Although CstR is reactive toward biologically available chalcogen oxyanions, the paralogous transcriptional regulator CsoR is weakly reactive or unreactive under the

same experimental conditions. The crystal structure of apo-CsoR from *Streptomyces lividans*¹⁸⁰ shows an ~8 Å separation between S γ atoms of the regulatory cysteine residues. *S. aureus* CsoR and CstR are likely to exhibit similar distances between S γ atoms, yet only CstR appears to be readily susceptible to cross-linking, suggesting another mechanism besides size discrimination may be involved.

Several reports have begun to explore the mechanisms by which other regulatory proteins are capable of forming reversible disulfide bonds to influence DNA binding in response to oxidative stress. Several examples include HypR,¹¹⁰ SarZ,²⁰ MexR,¹⁹ and BigR,¹⁸ which sense hypochlorite, global changes in cellular redox state, antibiotic stress, and hydrogen sulfide, respectively. The distance between S γ atoms of the regulatory cysteine residues in these proteins typically ranges from 7-10 Å, similar to that of apo-CsoR (~8 Å). Like the CsoR family, these proteins appear to use a common structural motif to sense a wide variety of stimuli. Nearby residues may be influencing the pK_a of the cysteine residues or the electrostatics in CstR vs CsoR. Additional studies are needed to understand the basis for discriminating among these diverse signals and are the subject of Chapter 4.

We have also shown that the selenite and tellurite modifications negatively regulate *cst* OP1 operator DNA binding. These experiments lead to the prediction that CstR reacts with selenite in cells thereby inducing the *cst* operon, which we investigate further in Chapter 3. The metabolic significance of selenite toxicity remains largely unexplored and it is unclear how the *cst* operon would be involved in chalcogen oxyanion resistance.

Finally, we established that Cys31 of CstR is required to initiate the reaction with sulfite. Furthermore, derivatization of only this thiol is necessary and sufficient to negatively regulate DNA binding. Furthermore, modification of Cys60 does not impact DNA binding affinity. The differences between Cys31 and Cys60 and the corresponding cysteine residues in CsoR are explored further in Chapter 4.

CHAPTER III

CstR IS A PERSULFIDE SENSOR IN *Staphylococcus aureus*

INTRODUCTION

Sulfur is an essential component of many cellular components and is involved in catalysis, protein structure, metal binding, and signaling. Cells have evolved mechanisms for acquiring or assimilating sulfur for the production of cysteine, methionine, glutathione and related low molecular weight (LMW) thiols, biotin, molybdopterin, lipoic acid, and others.¹⁶³ It is generally accepted that the major forms of sulfur trafficked in the cell are LMW per- and polysulfides. These are comprised of hydrodisulfides or persulfides (RSSH) hydropolysulfides (RS(S_n)SH), and polysulfides, (RS(S_n)SR) that are derived from organic LMW thiols, RSH, *e.g.*, glutathione.¹²⁹ Collectively, these species are known as reactive sulfur species (RSS) and also include hydrogen sulfide (H₂S).

Recent studies in mammalian cells suggest that LMW per- and polysulfides accumulate to levels greater than 100 μM.¹ The production of LMW per- and polysulfides has been linked to the enzymes cystathionine β-synthase (CBS) and cystathionine γ-lyase (CSE, Fig. 20).¹ The LMW per- and polysulfide pool is in free exchange with proteins that can also undergo reversible *S*-sulfhydration at cysteine residues.^{127,181} Notable examples of *S*-sulfhydration of proteins include cysteine desulfurases, rhodanases and sulfide:quinone oxidoreductases, but may include many additional targets.¹ Protein *S*-sulfhydration may represent an important oxidative posttranslational cysteine modification for sulfur trafficking in the cell.

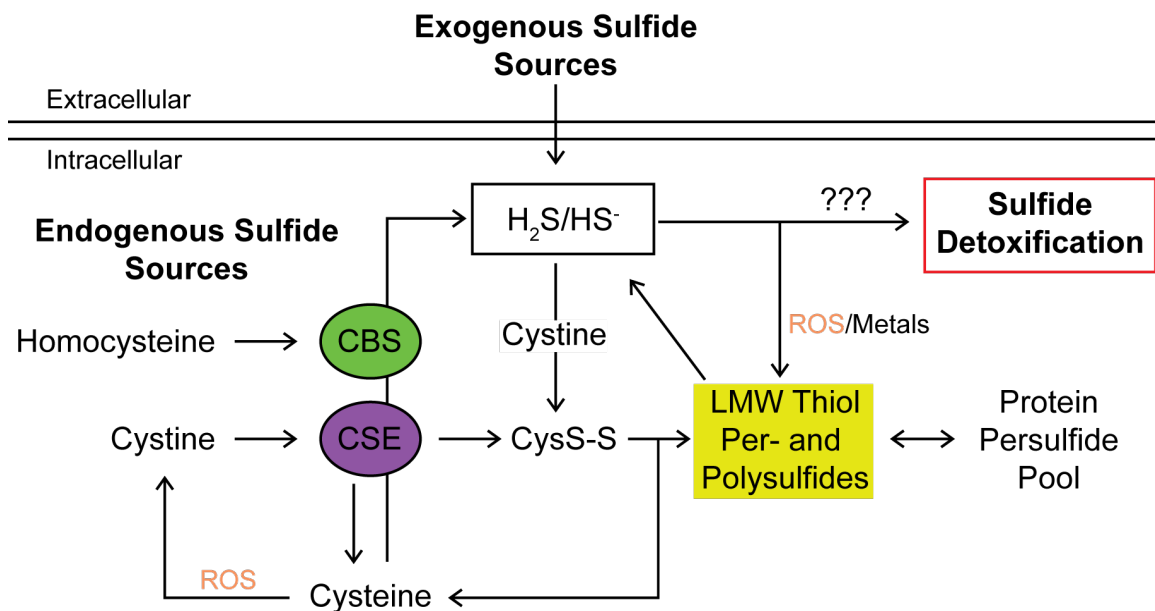


Figure 20. Model of sulfide homeostasis. Hydrogen sulfide can be encountered exogenously from the environment or produced endogenously by the action of the enzymes CBS or CSE. These enzymes are also capable of converting cystine to cysteine persulfide¹ that can exchange the persulfide with the LMW thiol pool via *trans*-persulfuration and contribute to the LMW per- and polysulfide pool. LMW per- and polysulfides can exchange with the protein persulfide pool.¹ Increased levels of hydrogen sulfide and therefore LMW per- and polysulfides leads to a sulfide detoxification response. Adapted from Miranda and Wink (2014).¹⁸³

Bacteria, including *S. aureus*, that harbor deletions of the genes CBS and CSE produce significantly less HS⁻ and are more susceptible to oxidative and antibiotic stress.¹²⁵ The protective effect of CBS and CSE might be traced to LMW per- and polysulfides that are capable of rapidly reacting with ROS.^{1,130} Interestingly, bacterial cells in culture are known to produce increased amounts of hydrogen sulfide under conditions of oxidative stress.¹²⁵ However, sulfur species become toxic at increasing concentrations through disruption of cytochrome c oxidase of the electron transport chain¹⁸² and likely perturbation of other metal centers.¹¹³ This requires detoxification of excess RSS to maintain homeostasis. The exact speciation of RSS under sulfide stress conditions is unknown but thought to be primarily hydrodisulfides, hydropolysulfides, and polysulfides.¹ It is therefore important to control the bioavailability of sulfur in the cell to shuttle sulfur into biosynthetic pathways, signaling, and provide oxidative stress resistance while mitigating the toxic effects experienced at higher concentrations.

The detoxification of the RSS H₂S has been well characterized in mammalian mitochondria and results in the oxidation of sulfur from S²⁻ to S⁶⁺ (Fig. 21A).^{113,118,123} The initial step of H₂S oxidation is the reaction of H₂S with a sulfide quinone oxidoreductase to form a cysteine-bound persulfide which is then transferred either directly or indirectly by way of a LMW thiol to a sulfur dioxygenase. At the sulfur dioxygenase, the sulfur is oxidized to an *S*-sulfonate and transferred to either a sulfite oxidase or a thiosulfate sulfur transferase (TST) for further oxidation to either sulfate (SO₄²⁻) or thiosulfate (S₂O₃²⁻), respectively (Fig. 21A).^{113,118,123} Interestingly, the proteins encoded in the *cst* operon bear a striking resemblance by sequence alignment to those

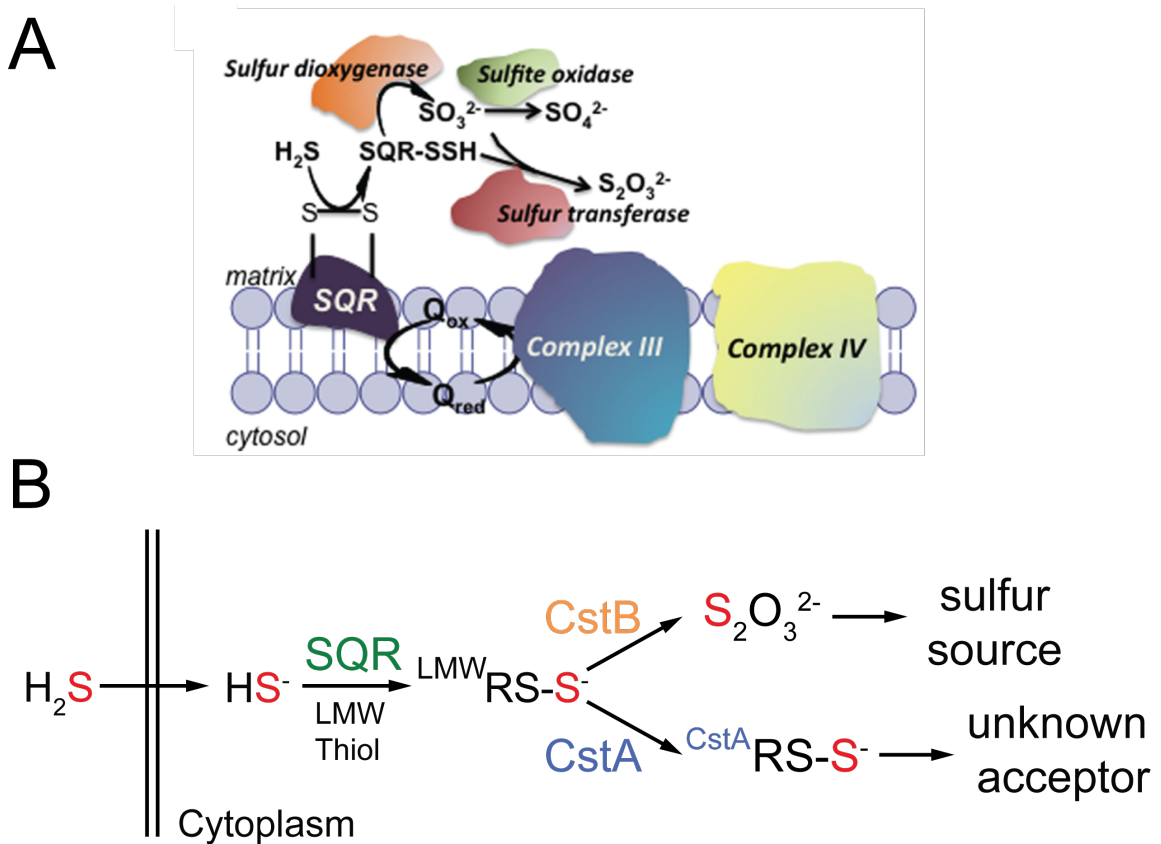


Figure 21. Model of enzyme-catalyzed detoxification of hydrogen sulfide. (A) Human mitochondrial hydrogen sulfide detoxification pathway. Adapted from Kabil and Banerjee (2010).¹¹³ (B) Putative functions for proteins encoded in the *cst* operon in bacteria. CstB has been shown to catalyze the conversion of a LMW persulfide, e.g., CoA-SSH or BSSH, to thiosulfate in the presence of oxygen (Shen, J., unpublished results). TS ($S_2O_3^{2-}$) is a known sulfur source for *S. aureus*.⁶ The CstA rhodanese domain has been shown to accept a persulfide to form an *S*-sulphydration (see Fig. 3, Chapter 1) and subsequently transfer the persulfide to the TusA domain. The sulfur donor in these experiments was either a LMW thiol or cysteine desulfurase (Higgins, K., *et al.* submitted).

characterized in mammalian mitochondria. NWMN_0029 encodes an SQR, NWMN_0028 contains an SDO domain, and both NMWN_0028 and NMWN_0027 exhibit TST domains (Fig. 21B), all of which may be involved in sulfide detoxification.

In this chapter, we test the prediction that the *cst* operon endows *S. aureus* with a defense mechanism against sulfide stress and establish that CstR is a sulfane sulfur-sensing transcriptional repressor. Acute sodium hydrogen sulfide (NaHS), disodium sulfide (Na₂S) or sodium tetrasulfide (Na₂S₄) stress introduced into cultures at mid-log growth phase in a variety of growth media induces the *cst* operon in a manner that requires both cysteine residues in CstR, Cys31 and Cys60. To gain insight on the nature of the post-translational modifications driving *cst* induction, recombinant CstR was reacted with sodium sulfide (Na₂S), glutathione persulfide (GSSH), and sodium tetrasulfide (Na₂S₄) under strictly anaerobic conditions. Although Na₂S is an inducer of the *cst* operon *in vivo*, the cysteine thiols on CstR do not react directly with S²⁻ *in vitro*. In contrast, CstR readily reacts with a sulfane sulfur (S⁰) donor, such as organic glutathione persulfide (GSSH) or inorganic tetrasulfide (S₄²⁻), under anaerobic conditions. This reaction forms a mixture of di-, tri-, and tetrasulfide crosslinks as determined by high-resolution tandem mass spectrometry. These modifications lead to dissociation of CstR from the DNA operator *in vitro*. Taken together, these results are consistent with a model in which CstR governs sulfide homeostasis in *S. aureus* by sensing sulfane sulfur from per- or polysulfides, leading to transcriptional derepression of the *cst* operon. The potential connection between these findings and those previously reported for the *cst* operon and nitrite stress in biofilms is discussed.

MATERIALS AND METHODS

Chemicals and Reagents. Sodium hydrogen sulfide ($\text{NaHS}\cdot x\text{H}_2\text{O}$; Sigma-Aldrich, 161527; CAS# 207683-19-0), sodium thiosulfate ($\text{Na}_2\text{S}_2\text{O}_3$; Sigma-Aldrich 217263; CAS# 7772-98-7; $\geq 99\%$ reagent-plus grade), sodium sulfite (Na_2SO_3 , Sigma-Aldrich S0505; CAS#7757-83-7; $\geq 98\%$ ACS-certified grade) and sodium tetrasulfide (Na_2S_4 , Alfa Aesar 88697; CAS# 12034-39-8; $\geq 90\%$) were obtained as crystalline solids, and used as freshly dissolved stock solutions in degassed, deionized metal-free water, without purification. Freshly prepared NaHS solutions were compared with freshly prepared stock solutions of authentic Na_2S_4 and estimated to contain 0.3% sulfur as polysulfide (expressed as tetrasulfide sulfur equivalents) by UV-Vis absorption spectroscopy quantified at 372 nm using a standard curve (Appendix Fig. 2).¹³⁰ All reagents used in the preparation of the chemically defined growth medium (HHWm) were obtained from Fisher or Sigma-Aldrich as tissue culture grade and were used without purification.

Fluorescent Anisotropy Titrations. All titrations were performed as described in Chapter 2.

In vitro Reactions with NaHS, Na_2S , and Na_2S_4 with CstR. 15 μM samples of CstR (protomer) were reacted anaerobically in a Vacuum Atmospheres (Amesbury, MA) glovebox ($\leq 0.5\%$ O_2) in fully degassed 10 mM PO_4^{3-} , 200 mM NaCl, 1 mM EDTA at pH 7.0 with a 5-fold thiol excess of NaHS, Na_2S , or Na_2S_4 for 17 h at 22° C unless otherwise noted. After 17 h, samples were sealed in septa cap vials for immediate LC-ESI-MS analysis or prepared for tryptic digest. Samples for digest were precipitated with a 12.5%

final concentration of trichloroacetic acid (TCA) and placed on ice for 1 h. Precipitated samples were sealed in septa cap vials and centrifuged at 4 °C for 20 min. The resulting pellets were washed twice with ice-cold acetone and resuspended in 10 mM ammonium bicarbonate at pH 8.2 and 10% acetonitrile. Proteomics-grade trypsin from porcine pancreas (Sigma) was added at a 1:50 ratio and digested for 1 h at 37 °C. A final concentration of 0.25% trifluoroacetic acid (TFA) was added to quench the digests. Finally, samples were desalted using a C18-packed ZipTip™ column (Millipore), dried, and resuspended in Milli-Q water. All preparative steps were performed anaerobically to avoid oxidation of cysteine and methionine residues. An additional CstR sample was digested and prepared aerobically following reaction with NaHS as a control to demonstrate methionine oxidation.

Glutathione Persulfide Preparation and CstR reactions. Glutathione persulfide (GSSH) was prepared by reacting a 5-fold excess of sodium sulfide (Na₂S) with oxidized glutathione (GSSG).¹⁸¹ This reaction was performed anaerobically at 30° C for 30 min in fully degassed 10 mM phosphate buffer, 200 mM NaCl, and 1 mM EDTA. To confirm and quantify the formation of persulfide, a cyanolysis assay¹⁸⁴ was performed showing that 98.9% of GSSG was converted to GSSH and GSH (Appendix Fig. 3). This ≈1:1 mixture of GSH/GSSH was reacted anaerobically with reduced CstR and control reactions were performed with GSSG and GSH as described for other sulfur compounds.

Preparation of S. aureus Deletion Strains. All *S. aureus* strains were a generous gift from Professors Eric Skaar (Vanderbilt University) and Thomas E. Kehl-Fie (University of

Illinois at Urbana-Champaign).¹³

Preparation of S. aureus Complementation Strains. Individual *S. aureus* genes were subcloned into the pOS1 vector harboring the constitutive P_{lgt} promoter¹⁸⁵ between the *NdeI* and *BamHI* restriction sites. For *CstB*, a short sequence was looped into the multiple cloning site of pOS1, GTCTAGA, to utilize the *XhoI* restriction site of pOS1 because the *cstB* gene sequence contains an *NdeI* restriction site. Each construct was electroporated into *S. aureus* RN4220 to obtain a properly methylated plasmid prior to electroporation into *S. aureus* strain Newman. WT and deletion strains were also transformed with empty vectors as controls. Plasmid DNA was maintained by addition of 10 $\mu\text{g}/\text{mL}$ chloramphenicol (Cm) to plates and growth media.

S. aureus Growth Curves. 5 mL of fresh TSB broth was inoculated with *S. aureus* from frozen glycerol cell stocks and grown to saturation overnight (~14 h). A 1 mL aliquot was pelleted by centrifugation and resuspended in an equal volume TSB or HHWm minimal media^{6,186,187} and then diluted in 15 mL TSB or HHWm supplemented with either 0.50 mM thiosulfate or 0.25 mM cystine and the indicated stressor. All strains carried the pOS1 empty vector (WT) or the indicated allele and were grown in the presence of 10 $\mu\text{g}/\text{mL}$ Cm with the exception of ΔtauE strain, which did not carry pOS1 and was grown in the absence of Cm. All cultures were grown aerobically at 37 °C in duplicate with shaking (200 rpm) in loosely-capped 50 mL Falcon tubes. Cell density was monitored by measuring OD₆₀₀ with a Spectronic® 20 Genesys® spectrophotometer (Thermo Scientific). The starting OD₆₀₀ of each culture was ≈ 0.007 .

S. aureus *Quantitative Real Time (qRT-PCR) Growth Conditions.* For preparation of samples for RNA extraction, 15 mL cultures were grown in TSB or HHWm with the indicated sulfur source to an OD₆₀₀ of 0.2, at which point the indicated stressor was added to the growth media. The stressors used in these experiments were 0.2 mM NaHS, 2.4 mM sodium hypochlorite¹⁸⁸ (ClO⁻), 10 mM sodium sulfite (SO₃²⁻), 0.2 mM sodium selenite (SeO₃²⁻), 0.5 μM nitric oxide¹⁸⁹ (NO) presented as the NO donor MAHMA NONOate¹⁸⁹ ([6-(2-hydroxy-1-methyl-2-nitrosohydrazino)-*N*-methyl-1-hexanamine]; Sigma Aldrich), 5 mM sodium nitrite¹⁹⁰ (NO₂⁻), 0.025 μM paraquat,¹⁹¹ or 1 mM diamide.¹⁹¹ At 10 or 30 min following addition of stressor to the culture, a 5 mL aliquot was removed and placed on ice until centrifugation at 4 °C (~2 min). After centrifugation, the cell pellet was washed with PBS, centrifuged, and stored at -80 °C.

RNA Extraction (Performed by Kevin Bruce). Pellets were thawed on ice and resuspended in 1 mL TriReagent (Cat. #TR-118, Molecular Research Center, Inc.). Cells were placed in tubes containing 0.1 mm silica beads (Lysing matrix B tubes, Cat. #6911-100, MP Biomedicals) and lysed in a bead beater (FastPrep®-24, MP Biomedicals). RNA was extracted by adding 200 μL of chloroform, mixing and centrifuging for 15 minutes at 16,100 x g. The aqueous layer was extracted and added to one volume of 70% ethanol. RNA purification was completed using the RNeasy minikit (Cat. #74104, Qiagen), including the on-column DNase I treatment (Cat. #79254, Qiagen). 5 μg total RNA was subsequently digested with the DNA-freeTM kit (Cat. #AM1906, Ambion) and diluted five-fold. First-strand cDNA was synthesized using random hexamers (Quanta

Biosciences) and the qScript Flex cDNA synthesis kit (Cat. #95049-100, Quanta Biosciences). Reactions without reverse transcriptase were also prepared to check for possible DNA contamination.

qRT-PCR (Performed by Kevin Bruce). Reactions contained 10 μ L 2x Brilliant III Ultra-Fast SYBR Green QPCR Master Mix (Cat. #600882, Agilent), 2 μ L each of 2 μ M QPCR primers (Table S5), 0.3 μ L of 2 μ M ROX reference dye and 6 μ L diluted cDNA. Relative transcript amounts were measured using the MX3000P thermocycler (Stratagene) and normalized to 16S rRNA. The thermal profile contained 1 cycle at 95°C for 3 min, 40 cycles at 95°C for 20 s to 59°C for 20 s. Subsequently, a dissociation curve starting at 55°C going to 95°C in 0.5°C increments with a dwell time of 30 s was performed to assess the specificity of the reactions. At least two, and typically three biologically independent samples were measured for each treatment, and the mean (\pm SD) values are reported. Transcript amounts were compared using two-way ANOVA with Bonferroni tests (GraphPad Prism, ver 5.0).

RESULTS

The cst operon is essential for normal growth under sulfide stress. To test the hypothesis that the *cst* operon is involved in sulfide detoxification, *S. aureus* was grown in a variety of media with various sulfur sources in the presence and absence of 0.2 mM NaHS (Fig. 22). These media included a rich growth medium, TSB, and chemically defined HHWm.¹⁸⁷ HHWm was supplemented with either 0.5 mM thiosulfate (TS, HHWm+TS) or 0.25 mM cystine (Cys, HHWm+Cys) as the sole sulfur source.⁶ Growth in

HHWm+TS in the presence of NaHS results in a significant growth defect while cultures grown in HHWm+Cys or TSB are comparatively less negatively impacted by sulfide stress (Fig. 22A-C). Wild-type *S. aureus* was next compared to a $\Delta cstR$ deletion strain where the expression of the *cst* operon is derepressed, leading to massive overexpression of those genes regulated by OP1 (*tauE*) or OP2 (*cstA*, *cstB*, *sqr*).⁶ When the $\Delta cstR$ strain is grown in the presence of NaHS, it fails to recover (Fig. 22A). We next tested a $\Delta cstR$ complemented with a wild type *cstR* allele carried on the pOS1-P_{lgt} complementation vector ($\Delta cstR$:CstR). When the $\Delta cstR$:CstR strain was grown in the presence of NaHS, we observe a growth phenotype identical to that of the WT *S. aureus* strains (Fig 22A). In contrast, the $\Delta cstR$ strain transformed with a double cysteine mutant allele of *cstR* ($\Delta cstR$:CstR^{C31A/C60A}) exhibits a severe growth defect and therefore fails to complement the $\Delta cstR$ strain (Fig. 22A). These results collectively suggest that the regulation of the *cst* operon is required for normal growth under sulfide stress. In addition, the two cysteine residues in CstR are essential for sensing sulfide stress.

We next tested wild-type and $\Delta cstR$:CstR^{C31A/C60A} *S. aureus* strains grown in HHWm+Cys (Fig. 22B) or in rich TSB media (Fig. 22C) in the presence or absence of NaHS. When grown in HHWm+Cys under NaHS stress, WT *S. aureus* does not exhibit a significant growth defect whereas the $\Delta cstR$:CstR^{C31A/C60A} strain is clearly impaired (Fig. 22B). When grown in TSB medium, there is a small but measurable growth defect in the presence of HS⁻ stress for both strains (Fig. 22C). The results of each growth condition collectively suggest that limitation of nutrients or sulfur availability increases the susceptibility of *S. aureus* to sulfide stress. The requirement to synthesize cysteine from TS may significantly impair the ability of the organism to acclimate to sulfide

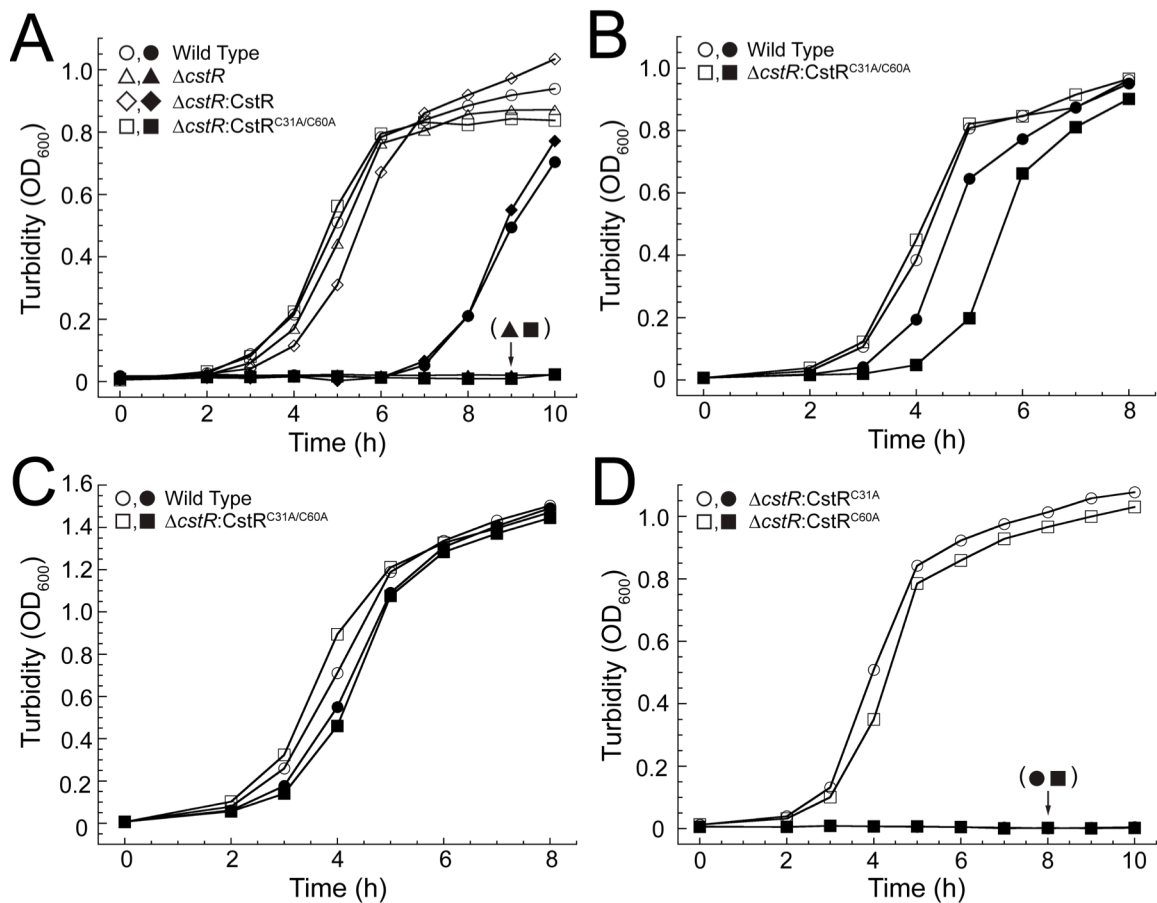


Figure 22. CstR is required for *S. aureus* defense against sulfide stress. Growth curves of wild-type (WT) and $\Delta cstR$ *S. aureus* mutant strains transformed with the indicated CstR allele carried on pOS1 complementation vector under aerobic conditions at 37 °C with shaking in the absence (open symbols) or presence (filled symbols) of 0.2 mM NaHS. (A) WT (circles), $\Delta cstR:pOS1$ (triangles), $\Delta cstR:CstR$ (diamonds), and $\Delta cstR:CstR^{C31A/C60A}$ (squares) *S. aureus* grown in HHWm minimal media supplemented with 0.5 mM thiosulfate (HHWm+TS). (B) WT and $\Delta cstR:CstR^{C31A/C60A}$ *S. aureus* strains grown in HHWm supplemented with 0.25 mM cysteine. (C) WT and $\Delta cstR:CstR^{C31A/C60A}$ grown on rich TSB media. (D) $\Delta cstR:CstR^{C31A}$ (circles) and $\Delta cstR:CstR^{C60A}$ (squares) *S. aureus* strains grown in HHWm + 0.5 mM TS in the absence and presence of 0.2 mM NaHS. The data points correspond to a single representative growth curve.

toxicity in the minimal HHWm+TS medium; however, an inducible *cst* operon (in either the WT or $\Delta cstR$:CstR strain) is clearly required for assimilation of organic sulfur (cystine) in the presence of NaHS as well. High cellular TS may also inhibit *cst* enzymes because TS is a common byproduct of HS⁻ detoxification.¹¹⁸

Previous results indicated that perturbation of Cys31 of CstR was necessary and sufficient to regulate DNA binding *in vitro* (Fig. 18, Chapter 2)¹⁶² and we hypothesized that Cys31 in CstR alone could confer resistance to sulfide stress *in vivo*. The $\Delta cstR$ strain was transformed with plasmids encoding individual cysteine mutants of CstR, $\Delta cstR$:CstR^{C31A} and $\Delta cstR$:CstR^{C60A} and grown in HHWm+TS in the presence and absence of NaHS. Both $\Delta cstR$:CstR^{C31A} and $\Delta cstR$:CstR^{C60A} strains fail to grow (Fig. 22D), indicating that both CstR cysteine residues are required for mitigating sulfide stress *in vivo*.

cstA, *cstB*, and *SQR* are each essential for mitigating sulfide stress. To test the hypothesis that the genes encoded within the *cst* operon are involved in sulfide stress detoxification, individual *S. aureus* deletion strains were grown in the presence or absence of sulfide stress in HHWm+TS medium. The individual deletion strains included $\Delta tauE$, $\Delta cstA$, $\Delta cstB$, and Δsqr . No growth defect was observed for the $\Delta tauE$ strain under sulfide stress and thus the physiological function of TauE remains unclear (Fig. 23A). In strong contrast, the $\Delta cstA$, $\Delta cstB$, and Δsqr *S. aureus* strains each exhibited a severe growth phenotype when grown under sulfide stress (Fig. 23B-D). We next complemented the $\Delta cstA$, $\Delta cstB$, and Δsqr strains with the corresponding wild-type allele carried on the pOS1-P_{lgt} vector and repeated the growth curves. These experiments reveal that wild-type

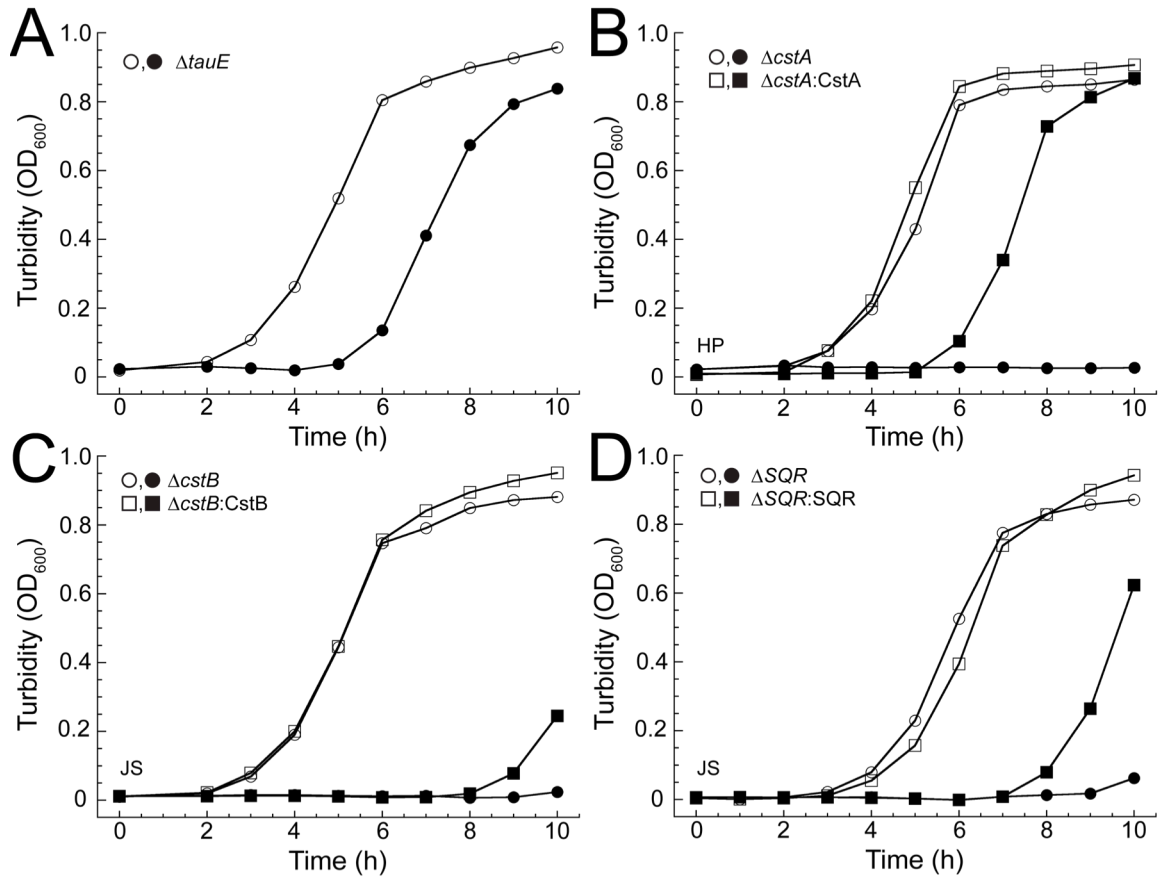


Figure 23. Individual *cst* genes are required for sulfide stress resistance. Representative growth curves of individual *cst* operon gene deletion strains (circles) and corresponding complementation strain (squares) grown in the absence (*open* symbols) or presence of 0.2 mM NaHS (*closed* symbols) in HHWm+TS at 37 °C with shaking. (A) $\Delta\tau E$ (no complementation strain shown) (B) $\Delta cstA$ and $\Delta cstA:CstA$. (C) $\Delta cstB$ and $\Delta cstB:CstB$. (D) Δsqr and $\Delta sqr:SQR$. HP: Experiment performed by Hui Peng. JS: Experiment performed by Jiangchuan Shen.

cstA provides full complementation (Fig. 23B) while the wild-type *cstB* and *sqr* complemented strains appear to give an intermediate growth phenotype (Fig. 23C-D). These data provide strong evidence in support of the proposal that *S. aureus* requires CstR-dependent transcriptional derepression of each of the downstream *cst* genes, *cstA*, *cstB*, and *sqr*, to mitigate the cellular effects of sulfide toxicity.

Acute exogenous (poly)sulfide stress induces the cst operon. Expression levels of the *tauE*, *cstR*, *cstA*, *cstB*, and *sqr* genes were monitored following acute NaHS toxicity in HHWm+TS at OD₆₀₀ of ≈ 0.2 by qRT-PCR. A 15-30-fold induction of the OP2-regulated downstream *cst* genes, *cstA*, *cstB*, and *sqr*, was observed at 10 min post stress, with comparatively little induction of the *cstR* and *tauE* genes in this divergently transcribed operon (Fig. 24A). The relative induction of each side of the operon qualitatively matches that previously observed in a Δ *cstR* strain⁶ (see also Fig. 24C). Strikingly, by 30 min, the mRNA levels of all induced genes return nearly to pre-induction levels, consistent with an acute phase response to sulfide toxicity.¹⁹² Induction experiments were repeated for cells grown in TSB and HHWm+Cys as slight growth defects were also observed in these growth mediums. *tauE* and *cstA* were used as reports as they inform on the induction of the upstream and downstream regions of the divergently transcribed *cst* operon, respectively. When the experiment was performed in TSB, an induction profile similar to that obtained for cells grown in HHWm+TS was observed where there is stronger upregulation for the downstream *cstA* than the upstream *tauE* gene. Additionally, mRNA levels return to baseline by 30 min (Fig. 24B). When this experiment was performed for cultures grown in HHWm+Cys, both *tauE* and *cstA* are

induced at 10 min and both genes remained induced at 30 min post-addition of NaHS (Fig. 24B).

We next determined induction profiles for $\Delta cstR$ mutant strains complemented with CstR cysteine mutants in the presence and absence of sulfide stress. The *cst* operon was massively upregulated in the $\Delta cstR$ strain (Fig. 24C), consistent with previous observations.⁶ When the $\Delta cstR$ strain is complemented with either wild-type *cstR* ($\Delta cstR:CstR$) or C31A/C60A *cstR* ($\Delta cstR:CstR^{C31A/C60A}$) alleles, repression of the operon is restored. Upon addition of NaHS to the $\Delta cstR:CstR$ culture, the *cst* operon is induced at 10 min post addition and returns to baseline by 30 min (Fig. 24C), albeit to a lesser extent than with the WT strain. The induction level may be lower here as a result of the constitutive expression of CstR, which might function as a partial sink for (poly)sulfide toxicity leading to an attenuated induction upon sulfide stress. In the case of the WT strain under the same conditions, *cstR* is not significantly upregulated (Fig. 24A). In any case, this finding recapitulates the wild-type strain, and is consistent with restoration of the growth curve in the $\Delta cstR:CstR$ strain (Fig. 22A). When the same experiment is performed with the $\Delta cstR:CstR^{C31A/C60A}$ strain, no induction of the operon is observed in response to addition of NaHS stress (Fig. 24C). This experiment was repeated for the individual CstR cysteine mutants, $\Delta cstR:CstR^{C31A}$ and $\Delta cstR:CstR^{C60A}$ strains. Here, both mutant strains fail to respond to NaHS stress *in vivo* and the operon remains repressed through the duration of the experiment (Fig. 24D). The combination of these induction experiments support a homeostasis model in which lack of regulation of the *cst* operon results in failure to mitigate sulfide toxicity.

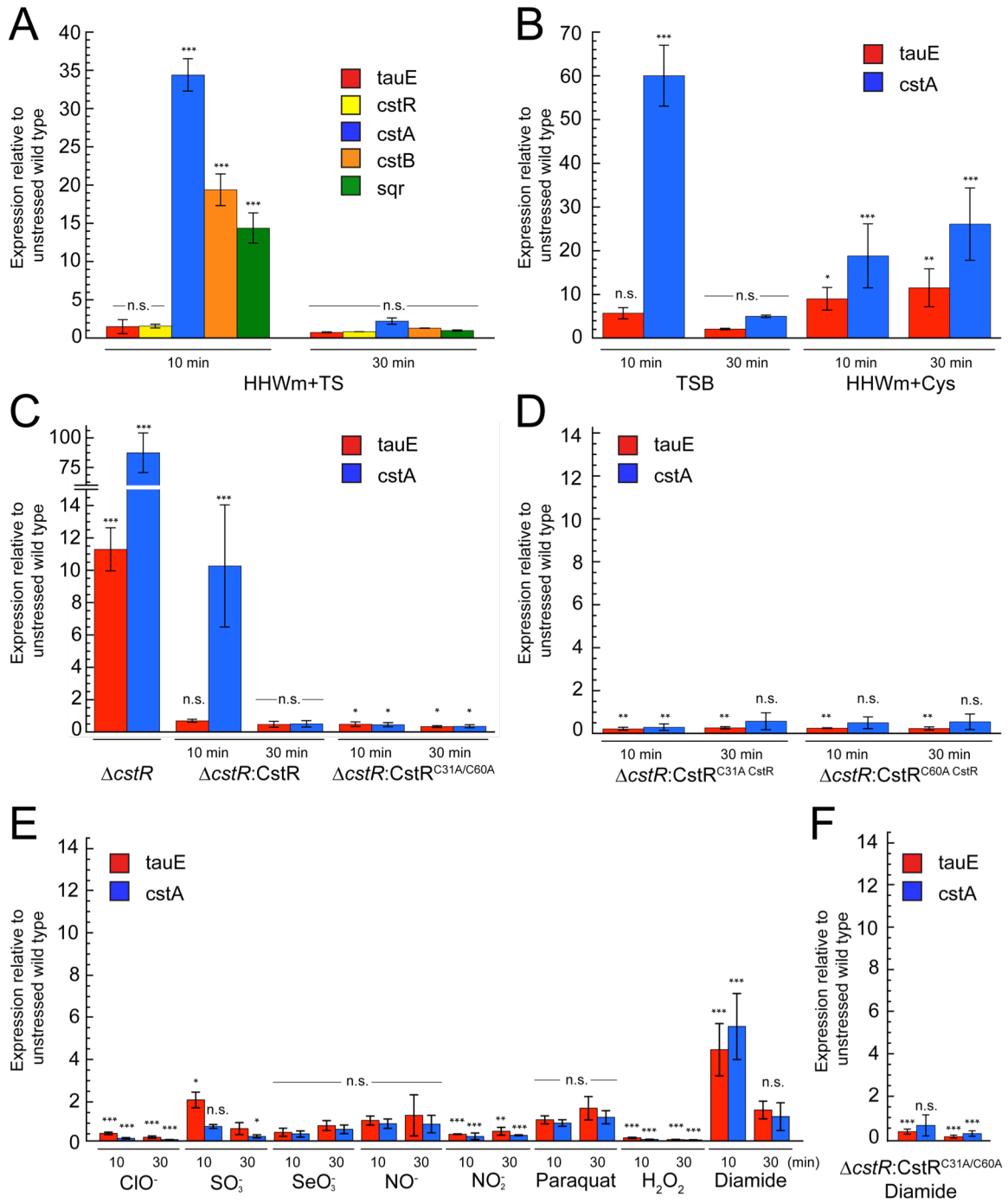


Figure 24. The *cst* operon is regulated by hydrogen sulfide *in vivo*. Quantitative RT-PCR experiments for WT and mutant *S. aureus* cultures grown to an OD₆₀₀ of 0.2 and challenged with 0.2 mM NaHS added to the growth medium at *t*=0. Aliquots for analysis were collected at 10 and 30 min post addition. All cultures were grown in HHWm+TS unless otherwise noted. (A) Relative expression levels for individual *cst* operon genes post addition of NaHS. (B) Levels of *tauE* and *cstA* expression in TSB (left) or HHWm+Cys (right). (C) $\Delta cstR$ (left), $\Delta cstR:CstR$ (middle), and $\Delta cstR:CstR^{C31A/C60A}$ (right). (D) $\Delta cstR:CstR^{C31A}$ (left) and $\Delta cstR:CstR^{C60A}$ (right) individual cysteine mutants of CstR. (E) RT-PCR analysis for WT *S. aureus* exposed to acute toxicity of 2.4 mM hypochlorite (ClO⁻), 10 mM sulfite (SO₃²⁻), 0.2 mM selenite (SeO₃²⁻), 0.5 mM nitric oxide (NO) as MAHMA NONOate, 5 mM nitrite (NO₂⁻), 25 nM paraquat, 10 mM hydrogen peroxide (H₂O₂), or 1 mM diamide. (F) $\Delta cstR:CstR^{C31A/C60A}$ *S. aureus* exposed to 1 mM diamide stress. *N* = 3 error bars represent one s.d. from the mean, with fold-expression relative to wild-type, unstressed cells. Two-way ANOVA analysis was performed relative to 16S RNA at the indicated time point (*** = *p* < 0.001, ** = *p* < 0.005, * = *p* < 0.050, and n.s. = not statistically significant).

Induction of the cst operon is specific to sulfide stress. It was next of interest to assess the specificity of *cst* operon induction to sulfide stress. To do this, induction of the *tauE* and *cstA* genes was determined upon addition of a range of biologically relevant oxidative and nitrosative stressors by qRT-PCR. These include hypochlorite (HOCl), sulfite (SO₃²⁻), selenite (SeO₃²⁻), nitric oxide (NO•), nitrite (NO₂⁻), paraquat (1,1'-dimethyl-4,4'-bipyridinium dichloride), hydrogen peroxide (H₂O₂) and diamide (3-(dimethylcarbamoylimino)-1,1-dimethylurea). Of these, only diamide strongly induces both *tauE* and *cstA* at 10 min post addition of the reagent, with the expression returning to baseline by 30 min (Fig. 24E). In the Δ *cstR*:CstR^{C31A/C60A} strain, diamide fails to induce the operon, revealing that the induction by diamide is CstR-dependent and not through some alternative pathway (Fig. 24F). These experiments were carried out such that there was no noticeable growth phenotype upon addition of the inducer to the growth medium (Appendix Fig. 4). Sulfite was capable of inducing *tauE* but not *cstA* at 10 min post addition (Fig. 24E), consistent with the previous findings that sulfite reacts with CstR *in vitro*^{6,162}. However, sulfite is clearly not a primary inducer *in vivo* as the induction of *tauE* increased only two-fold. Finally, SeO₃²⁻, NO•, H₂O₂ and paraquat stress do not significantly induce *cst* operon expression; however, the relative expression of *tauE* and *cstA* appears to decrease with ClO⁻, NO₂⁻ and H₂O₂ stress (Fig. 24E).

CstR reacts with a per- and polysulfide donors to form di-, tri-, and tetrasulfides in vitro. *S. aureus* viability and induction of the *cst* operon by sulfide stress requires CstR cysteine residues (Fig. 22 and 23). This suggests that CstR cysteine residue(s) react directly with sulfide and/or polysulfide, which in turn, drives DNA operator dissociation and

transcriptional derepression of the *cst* operon. However, the reaction of a protein thiolate with S^{2-} is not chemically possible.^{127,130} Indeed, when CstR was reacted with NaHS or Na_2S under strictly aerobic conditions in the presence of a metal chelator, no reaction was observed by LC-ESI-MS (Fig. 25A-C). This suggests that CstR likely does not directly sense NaHS *in vivo*. Recent work indicates that the major form of RSS in the cell exists as per- and polysulfides¹ which are oxidation products of S^{2-} . Per- and polysulfides can be formed rapidly and non-enzymatically in the presence of oxygen with a sulfenic acid intermediate or metal-catalyzed HS^{\bullet} formation.^{44,127,130} The sulfane sulfur of a per- or polysulfide is capable of reacting directly with cysteines^{127,130} and were investigated for reactivity with CstR. In these experiments, inorganic polysulfide Na_2S_4 and organic persulfide, GSSH, were tested as model sulfane sulfur donors. Reaction with Na_2S_4 polysulfide yields a series of mixed disulfides, including an interprotomer disulfide bond and a series of peaks corresponding to the incorporation of 0-4 sulfur atoms (Fig. 25D). These were putatively assigned as di- (+0 S), tri- (+1 S), and tetrasulfide (+2 S) cross-links (Table 6); the +3 S and +4 S species are predicted to correspond to CstR dimers that possess mixed interprotomer tri- and tetrasulfide linkages (+3 S) and a pair of tetrasulfide linkages (+4 S), respectively. We next reacted with CstR with an organic persulfide, GSSH, and observe a mixture of crosslinked species that incorporate 0, 1, 2 or 3 S atoms (Fig. 25E). This result is qualitatively similar to the products formed with polysulfides (Fig. 25D). As controls, CstR was reacted with the starting material GSSG used to produce GSSH and reaction byproduct GSH (See Materials and Methods) and the reaction products characterized by LC-ESI-MS (Fig. 25F-G). As expected, reduced GSH does not react with CstR (Fig. 25F) and in contrast, disulfide-crosslinked CstR is the only

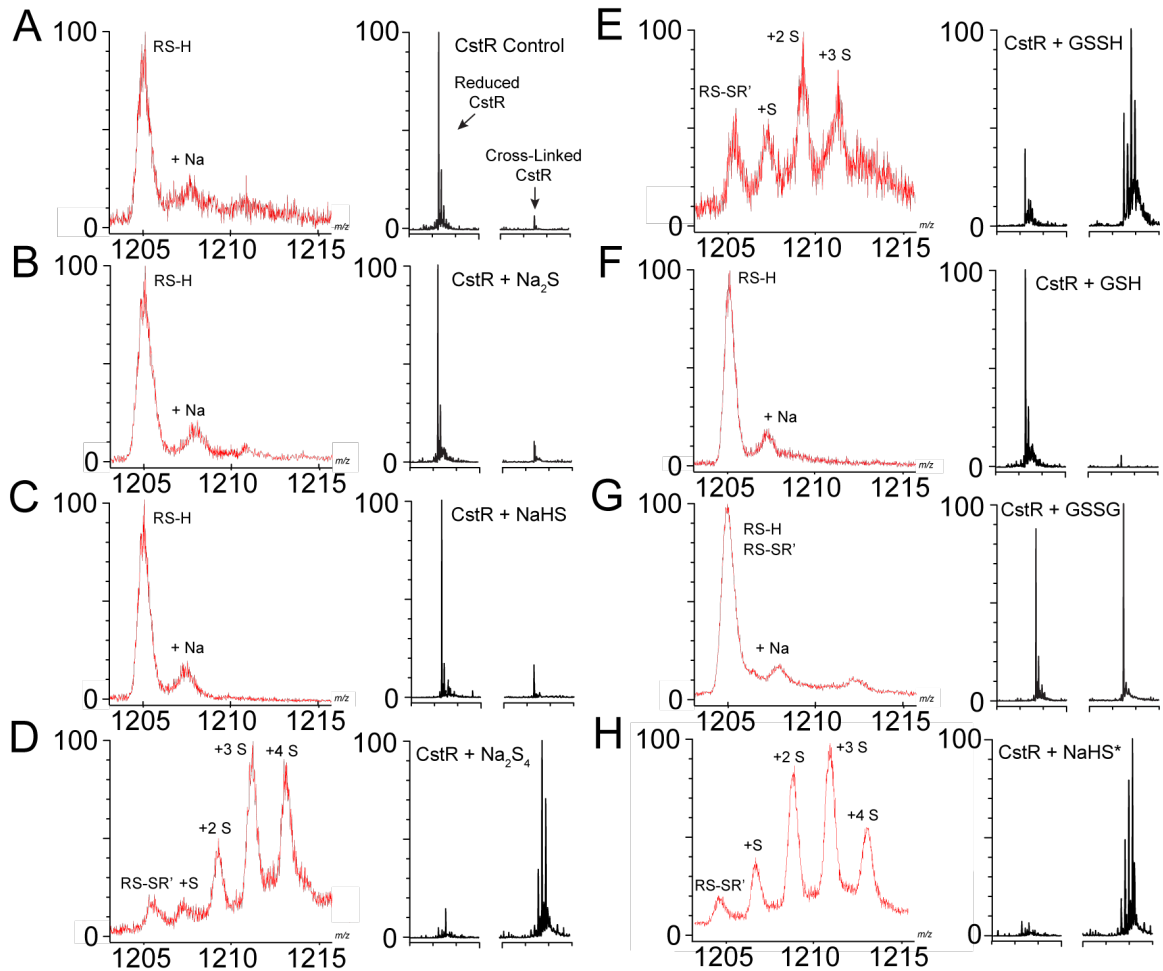


Figure 25. CstR reacts with NaHS, Na₂S₄, and GSSH to form a series of mixed di-, tri-, and tetrasulfide crosslinks. LC-ESI-MS spectra of intact reduced CstR (A), CstR following reaction with (B) Na₂S, (C) NaHS* (D) Na₂S₄, (E) NaHS, (F) GSH, (G) GSSG, and (H) GSSH. *Black* traces represent the ratio of reduced (*left*) or cross-linked (*right*) CstR in the deconvoluted mass spectra. *Red* traces represent *m/z* ratios of the +8 or +16 charge states of reduced or cross-linked dimeric CstR species, respectively, with corresponding post-translational modification assignments shown. RS-H indicates reduced CstR and RS-SR' represents an interprotomer disulfide bond between Cys31 and Cys60'. Each 'S' represents a mass shift of +32 Da relative to the RS-SR' disulfide in the deconvoluted spectra. For a sample like GSSG (panel G), the +8 and +16 *m/z* overlap but can be deconvoluted based on the *m/z* distribution of the reduced vs. oxidized forms.¹⁶² For a summary of the observed masses, refer to Supplemental Table S2. (*) indicates a reaction performed with NaHS in 10 mM HEPES, 200 mM NaCl, pH 7.0. All other reactions were performed in 10 mM PO₄³⁻, 200 mM NaCl, 1 mM EDTA, pH 7.0.

Table 6. Summary of LC-ESI-MS deconvoluted masses obtained from CstR reaction with LMW sulfur compounds. All mass shifts are relative to either the reduced or disulfide form of CstR as indicated by (-). Observed masses in italics represent masses observed in controls and are starting masses.

Protein	M _r Observed (Da)	Mass Shift	Assignment	M _r Expected (Da)	
CstR Control	9640.2	-	<i>CstR</i> ^{RS-H}	9641.2	
	9661.3	21.1	<i>CstR</i> ^{RS-H} + Na	9663.2	
	19279.3	-	<i>CstR</i> ₂ ^{RS-SR'}	19280.4	
CstR + 5x NaHS	9640.0	-	<i>CstR</i> ^{RS-H}	9641.2	
	9662.5	22.5	<i>CstR</i> ^{RS-H} + Na	9663.2	
	19279.7	-	<i>CstR</i> ₂ ^{RS-SR'}	19280.4	
	19311.7	32.0	<i>CstR</i> ₂ ^{RS-S-SR', R''S-SR'''}	19312.5	
	19342.8	63.1	<i>CstR</i> ₂ ^{RS-S-SR', R''S-S-SR''''}	19344.5	
	19372.5	92.8	<i>CstR</i> ₂ ^{RS-S-S-SR', R'S-S-SR''''}	19376.6	
CstR + 5x Na ₂ S ₄	19403.7	124.0	<i>CstR</i> ₂ ^{RS-S-S-SR', R''S-S-S-SR''''}	19408.7	
	9642.5	-	<i>CstR</i> ^{RS-H}	9641.2	
	19282.0	-	<i>CstR</i> ₂ ^{RS-SR'}	19280.4	
	19313.9	31.9	<i>CstR</i> ₂ ^{RS-S-SR', R''S-SR'''}	19312.5	
	19346.5	64.5	<i>CstR</i> ₂ ^{RS-S-SR', R''S-S-SR''''}	19344.5	
	19378.9	96.9	<i>CstR</i> ₂ ^{RS-S-S-SR', R'S-S-SR''''}	19376.6	
CstR + 5x NaHS (PO ₄ ³⁻ + EDTA)	19410.0	128.0	<i>CstR</i> ₂ ^{RS-S-S-SR', R''S-S-S-SR''''}	19408.7	
	9640.1	-	<i>CstR</i> ^{RS-H}	9641.2	
	9662.4	22.3	<i>CstR</i> ^{RS-H} + Na	9663.2	
	19279.0	-	<i>CstR</i> ₂ ^{RS-SR'}	19280.4	
	CstR + 5x Na ₂ S	9640.0	-	<i>CstR</i> ^{RS-H}	9641.2
		9662.4	22.4	<i>CstR</i> ^{RS-H} + Na	9663.2
9684.5		44.5	<i>CstR</i> ^{RS-H} + 2Na	9665.2	
19279.8		-	<i>CstR</i> ₂ ^{RS-SR'}	19280.4	
CstR + 5x GSSG	9640	-	<i>CstR</i> ^{RS-H}	9641.2	
	9662.2	22.2	<i>CstR</i> ^{RS-H} + Na	9663.2	
	9683.5	43.5	<i>CstR</i> ^{RS-H} + 2Na	9665.2	
	19280	-	<i>CstR</i> ₂ ^{RS-SR'}	19280.4	
	19302	22	<i>CstR</i> ₂ ^{RS-SR'} + Na	19302.4	
CstR + 5x GSH	9640	-	<i>CstR</i> ^{RS-H}	9641.2	
	9662.3	22.3	<i>CstR</i> ^{RS-H} + Na	9663.2	
	19280.1	-	<i>CstR</i> ₂ ^{RS-SR'}	19280.4	
CstR + 5x GSSH	9639	-	<i>CstR</i> ^{RS-H}	9641.2	
	9671.1	32.1	<i>CstR</i> ^{RS-SH}	9673.3	
	9702.2	63.2	<i>CstR</i> ^{RS-SSH}	9705.3	
	19277.1	-	<i>CstR</i> ₂ ^{RS-SR'}	19280.4	
	19308.4	31.3	<i>CstR</i> ₂ ^{RS-S-SR', R''S-SR'''}	19312.5	
	19339.9	62.8	<i>CstR</i> ₂ ^{RS-S-SR', R''S-S-SR''''}	19344.5	
19373.6	96.5	<i>CstR</i> ₂ ^{RS-S-S-SR', R'S-S-SR''''}	19376.6		

crosslinked product observed following reaction with GSSG. Reaction with GSSG is consistent with *S*-glutathionylation of one cysteine followed by resolution by the other with release of GSH (Fig. 25G). Finally, the CstR reaction was repeated in the absence of the metal chelator EDTA and a series of cross-linked species analogous to the Na₂S₄ reaction were observed (Fig. 25H). This suggests that either metal contamination or oxygen leads to the formation of per- or polysulfide contamination, resulting in a reaction with CstR. In addition, lab stocks of NaHS contain a small but measurable polysulfide contamination (Appendix Fig. 2). We conclude that CstR preferentially reacts with the more oxidized, electrophilic, internal sulfur atoms within inorganic polysulfide rather than HS⁻ directly.¹²⁷ The chemical speciation of these more oxidized forms of sulfur, including sulfane S⁰, are not known *in vivo*.

Confirmation of di-, tri-, and tetrasulfide assignments by high-resolution tandem mass spectrometry. The LC-ESI-MS experiments provided reaction profiles for a number of sulfur compounds but did not allow for unambiguous assignment of the reaction products. To this end, a CstR sample containing these cross-links was then digested with trypsin and analyzed by high-resolution tandem mass spectrometry on an LTQ-orbitrap mass spectrometer. The highest intensity peaks containing CstR cross-links were in the +4 charge state as ²⁴MMEEGK|DCK|DVITQISASK⁴² (Peptide “A”, where “|” indicates a missed tryptic cleavage site) and ⁴⁸LMGIIISENLIIECVK⁶² (Peptide “B”) for the Cys31 and Cys60’-containing peptides, respectively (Table 7). Upon inspection of the high mass accuracy LTQ data, we identified a mass corresponding to the Cys31-Cys60’ disulfide cross-linked peptides at 946.977 Da (946.978 Da expected; Table 7). This

Table 7. Monoisotopic masses of di-, tri-, and tetrasulfide cross-linked parent ions in the +4 charge state. Masses of tryptic peptides were observed by high-resolution tandem mass spectrometry. Asterisks (*) indicate masses that were assigned as sulfur as opposed to two oxygen atoms based on the fragmentation pattern of the corresponding peptide (see Fig. 26 and Fig. 27).

CstR Modification	Monoisotopic Mass (Da)	
	Calculated	Observed
RS-SR'	946.978	946.977
+ O	950.977	950.976
+ 2 O	954.976	954.969*
RS-S-SR'	954.972	954.969
+ 2 O	962.969	962.963*
RS-S-S-SR'	962.965	962.963

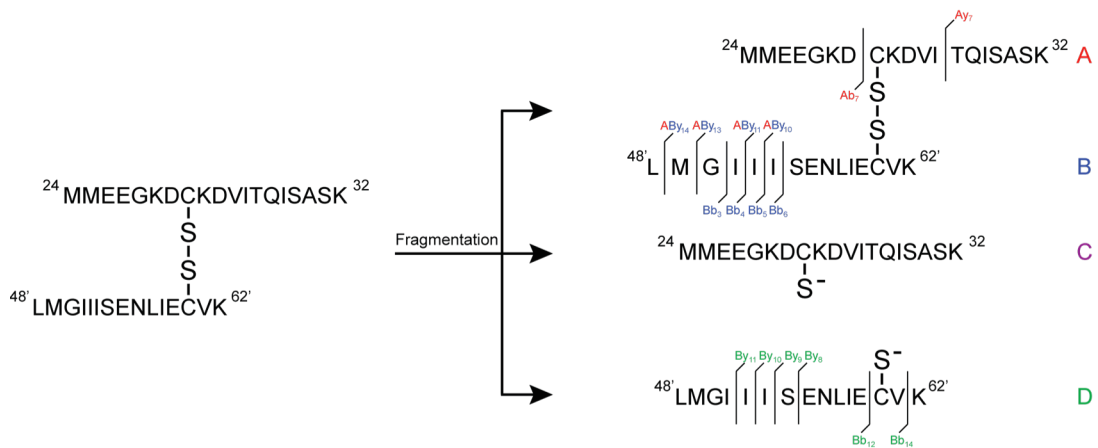
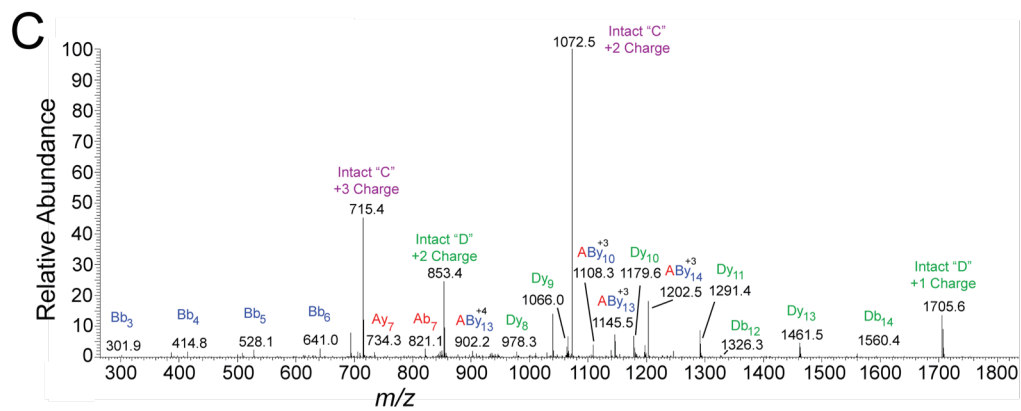
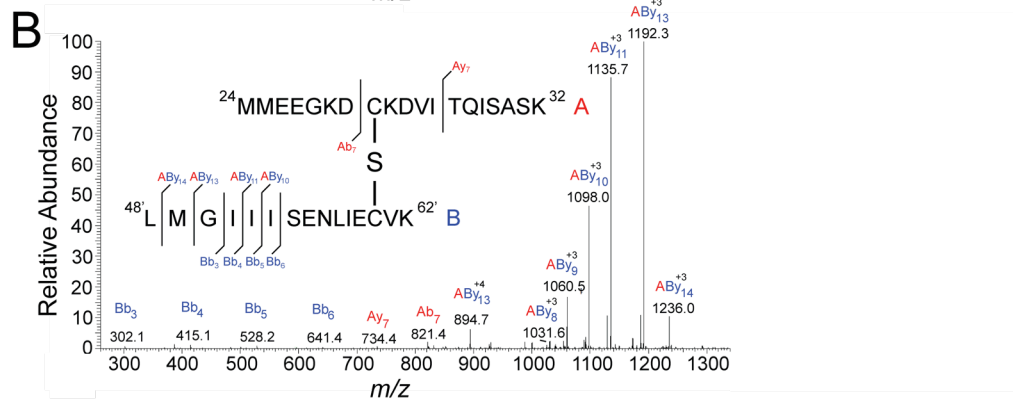
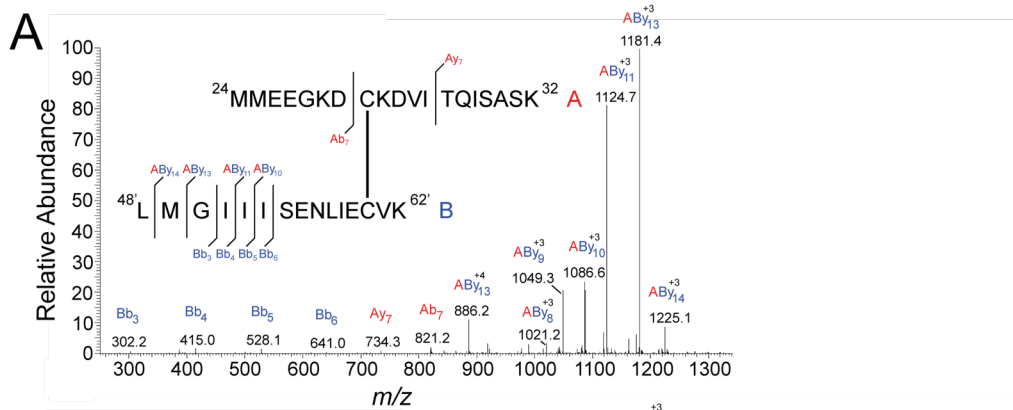


Figure 26. High-resolution tandem mass spectrometry confirms di-, tri-, and tetrasulfide mass shift assignments. Fragmentation patterns of peptides identified containing di-, tri-, and tetrasulfide masses. Peptide A (red), $^{24}\text{MMEEGKDCKVITQISASK}^{42}$, includes Cys31 and Peptide B (blue), $^{48}\text{LMGIIISENLIECVK}^{62}$, includes Cys60'. Peptide fragments were assigned relative to either peptide "A" or "B" where Bb_3 corresponds to the peptide fragment b ion $^{48}\text{LMG}^{50}$ with a mass of 302 Da. Cross-linked peptides are denoted as " AB_{yn} " where peptide "A" remained intact and fragmentation occurred on peptide "B". Inset: map of fragmentation pattern. (A) Disulfide. (B) Trisulfide. (C) Tetrasulfide

assignment was confirmed by inspection of the fragmentation pattern (Fig. 26A) and previous data (Fig. 14 and 15, Chapter 2).¹⁶² We next searched for masses corresponding to the addition of one or two sulfur atoms and identified peaks at 954.969 Da (954.972 Da expected) and 962.963 Da (962.965 Da expected), respectively. The mass shifts between the di- and trisulfide cross-linked peptides corresponds to the monoisotopic mass of ³²S adducts at +31.968 Da (31.970 Da expected) and +63.944 Da (63.941 Da expected) for the di- and tetrasulfide, respectively (Fig. 26A-C). The tri- and tetrasulfide assignment is further confirmed by inspection of the fragmentation pattern of the 954.969 and 962.965 Da peptides. This reveals a series of cross-linked A and B peptides that contain either a +32 or +64 Da mass shift relative to the disulfide, indicating that the observed mass shifts are due to sulfur atoms (Fig. 26) and not oxidation of methionine residues (Fig. 27).

Reaction of CstR with RSS Negatively regulates DNA binding in vitro. After establishing that CstR reacts with per- and polysulfides to form interprotomer di-, tri-, and tetrasulfide bonds, we sought to determine if these post translational modifications were sufficient to negatively regulate DNA *in vitro*. To test this, Na₂S₄-reacted CstR-*cst* OP1 operator DNA binding affinity was measured by fluorescence anisotropy (Fig. 28). For reference, fully reduced CstR binds to either *cst* operator site, OP1 or OP2, with similar affinities, of $\approx 10^7$ M⁻¹.⁶ When the titration is performed with Na₂S₄-reacted CstR, the binding affinity decreased by ≈ 200 fold (Fig. 28, Table 8). This result is consistent with strong derepression of the *cst* operon *in vivo*.

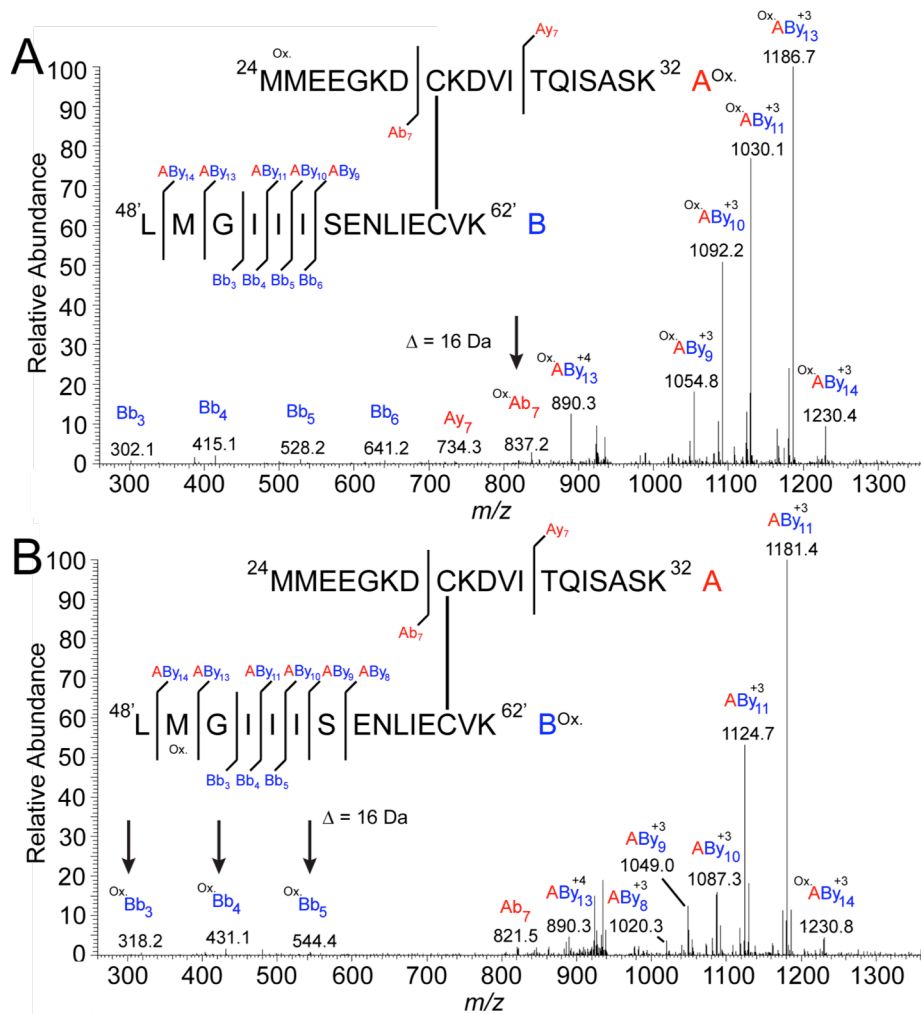


Figure 27. Fragmentation data of sulfide-treated CstR samples in not attributed to methionine oxidation of crosslinked CstR. Cross-linked peptides containing a single Met oxidation event on either the A peptide (A) or on the B-peptide (B) were identified from an aerobically-digested sample. The parent ions each have a mass of 950.977 Da (950.996 Da expected) in the +4 charge state but are differentiated from sulfur (S) adducted crosslinked peptides by their unique fragmentation pattern. For example, the Ab₇ fragment contains the “A” peptide Met residue with a mass of 821.3 Da and 837.3 Da for the reduced and oxidized forms, respectively. If two oxidations occur on the “A” peptide, the expected mass is 853.3 Da (panel A). An analogous Met oxidation analysis can potentially be found for the “B” peptide with the Bb₃₋₆. (panel B). If the parent ion contained a +32 Da shift and the Met residues in the fragmentation spectra display a combined +32 Da or +64 Da mass shift, the shifts would be attributed to Met oxidation and not a trisulfide or tetrasulfide crosslinked Cys31-Cys60’ peptide, respectively. These data ensure that the +32 Da and +64 Da shifts observed in so-designated trisulfide and tetrasulfide cross-linked peptides (Fig. 26) are due to sulfur and not multiple Met oxidation events.

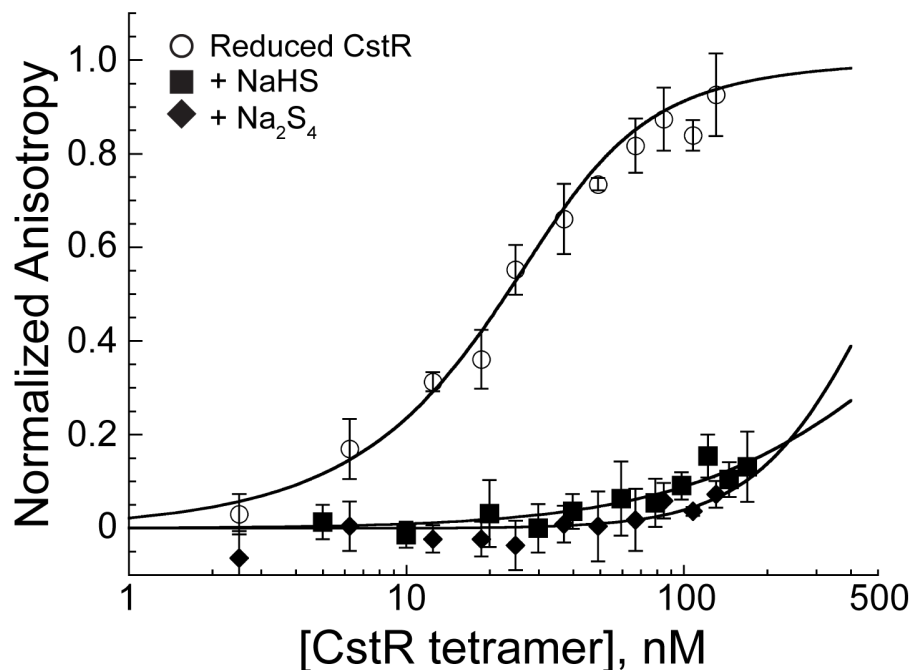


Figure 28. Reaction of CstR with sulfide negatively regulates DNA operator binding. Fluorescence anisotropy titrations of fully reduced CstR (open circles) and NaHS- (closed squares) or Na₂S₄-reacted CstR (closed diamonds) with fluorescently-labeled *cst* OP1-containing DNA. Data were fit to a sequential tetramer binding model where two non-dissociable tetramers bind stepwise to one operator DNA binding site. Stepwise binding constants, K_1 and K_2 , were used to determine the average macroscopic binding constant, K_{tet} ($K_{tet} = (K_1 \cdot K_2)^{1/2}$). WT CstR-OP1 affinity is $7.4 (\pm 1.8) \times 10^7 \text{ M}^{-1}$ (see Table S1 for all previously determined K_{tet} values)^{6,162}. while K_{tet} for NaHS- and Na₂S₄-reacted CstRs have upper limits of $0.06 \pm 0.05 \times 10^7 \text{ M}^{-1}$ and $0.03 \pm 0.03 \times 10^7 \text{ M}^{-1}$, respectively. Binding curves represent a single representative titration. Conditions: 10 nM *cst* OP1 DNA, 10 mM HEPES, 0.2 M NaCl, pH 7.5, 25 °C.

Table 8: Summary of CstR DNA binding constants following reaction with NaHS or Na₂S₄. CstR association equilibrium constants (K_{tet}) were obtained for *cst* OP1 by fluorescence anisotropy titrations. All experiments were performed with fluorescently labeled *cst* OP1 unless otherwise noted. Conditions: 10 mM HEPES, 200 mM NaCl, 25.0 °C, anaerobic.

Protein	$K_{\text{tet}} (\times 10^7) \text{ M}^{-1}$
	6.3 (± 0.5) ^a
	25 (± 5) ^b
CstR ^{RSH}	6 (± 5) ^{b*}
	10 (± 9) ^{b†}
	7.4 (± 1.8) ^c
CstR + NaHS	0.06 (± 0.05) ^c
CstR + Na ₂ S ₄	0.03 (± 0.03) ^c

^aFrom Luebke, J. et al. (2013),¹⁶² Chapter 2

^bFrom Grosseohme, N. et al (2011)⁶

^cFrom Luebke, J. et al. (2014),^{13,118} this Chapter

*Determined from competitive association with unlabeled competitors

†CstR-*cst* OP2 binding affinity

The cst operon is required for Na₂S and Na₂S₄ Stress Resistance. CstR reacts with per- and polysulfides but not sulfide *in vitro* (Fig. 25), however, NaHS induces the *cst* operon *in vivo* (Fig. 24). We sought to test if Na₂S and Na₂S₄ elicit the same response *in vivo*. Indeed, the *cst* operon is required for stress resistance of both Na₂S and Na₂S₄ and both induce the *cst* operon (Fig. 29). Despite differences in reactivity with the regulator CstR (Fig. 25), both species elicit the same response in *S. aureus*. This finding is in further support of a model in which sulfide, S²⁻, is converted to per- and/or polysulfides, which are sensed by CstR in the cell.

CsoR is not functionally analogous to CstR. To fully differentiate CstR and CsoR *in vivo*, we complemented the $\Delta cstR$ strain with *S. aureus* CsoR⁶ ($\Delta cstR$:CsoR) and stressed the cells with NaHS. In this experiment, constitutively expressed CsoR fails to restore growth in HHWm+TS under NaHS stress (Fig. 30A). This suggests that CsoR does not sense sulfide stress or that CsoR lacks the ability to bind the *cst* operator sites *in vivo* or a combination of both effects. In addition, NaHS stress does not induce *copA*, which is under control of CsoR, in WT *S. aureus* (Fig. 30B). Lastly, CsoR was reacted with Na₂S₄ polysulfide *in vitro* under the same conditions used for CstR. We show that CsoR reacts poorly with Na₂S₄ but does form a series of low-abundance cross-linked species (Fig. 30C-D, Table 9). These results are consistent with the inducer specificity model of CstR and CsoR.

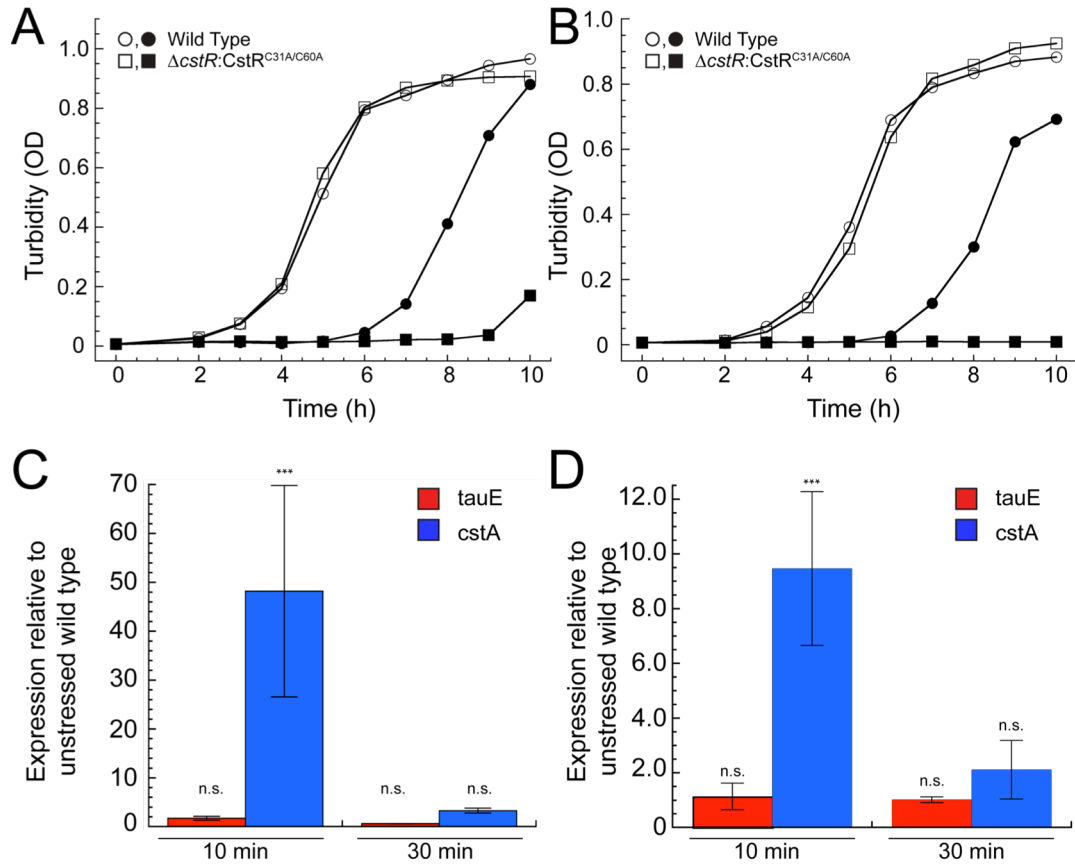


Figure 29. The *cst* operon is required for polysulfide and sodium disulfide stress resistance. (A-B) Growth curves of WT (circles) and $\Delta cstR:CstR^{C31A/C60A}$ (squares) *S. aureus* grown in the absence (open symbols) or presence (closed symbols) of either (A) 25 μM sodium tetrathiolane (Na_2S_4) or (B) 0.2 mM sodium sulfide (Na_2S). Cells were grown aerobically in HHWm+TS at 37 °C with shaking and data points correspond to a single representative growth curve. (C-D) Quantitative RT-PCR experiments for WT and mutant *S. aureus* cultures grown to an OD₆₀₀ of 0.2 and challenged with either (C) 25 μM Na_2S_4 or (D) 0.2 mM Na_2S added to the growth medium at $t=0$. Aliquots for analysis were collected at 10 and 30 min post addition.

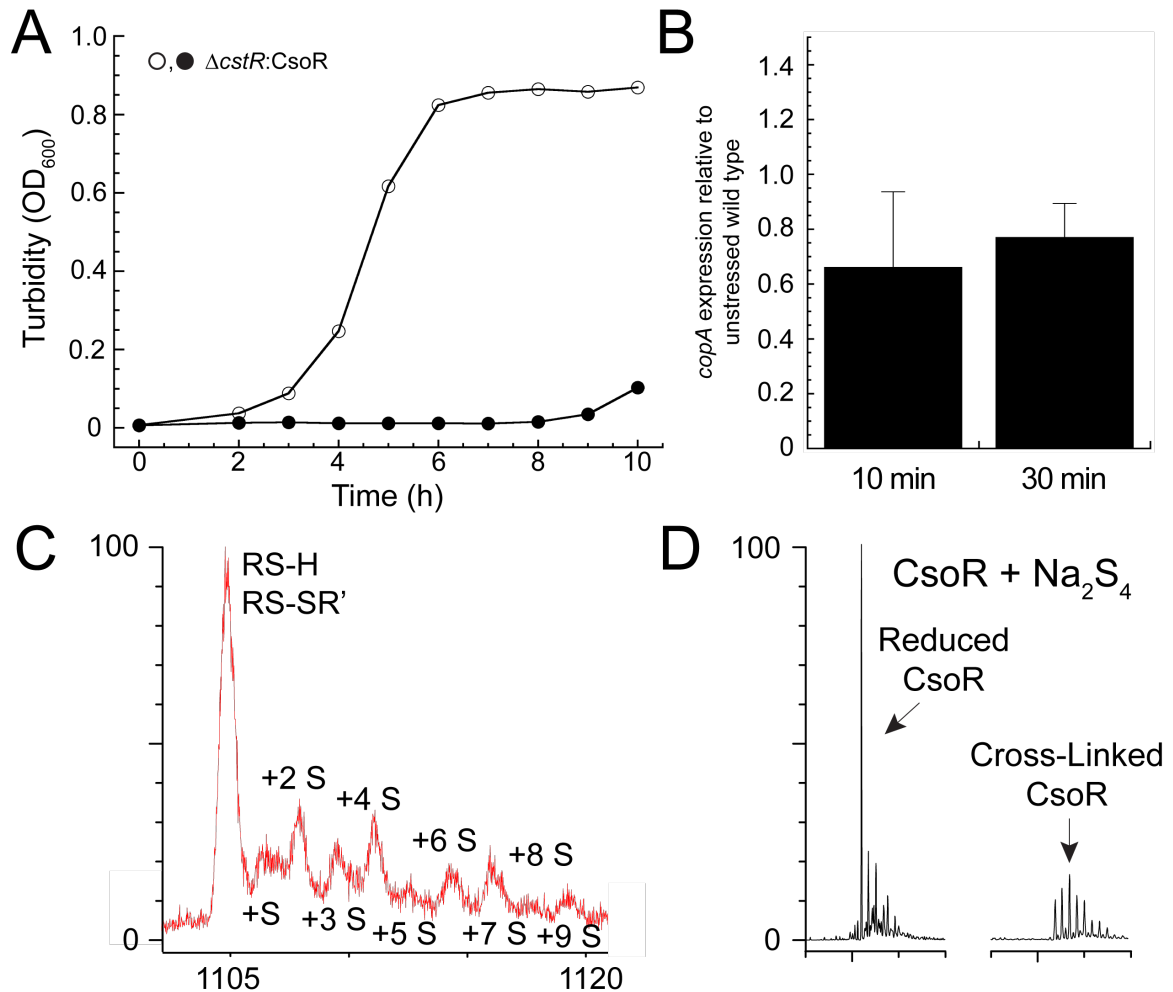


Figure 30. CsoR is not functionally analogous to CstR. (A) Growth curves of $\Delta cstR$ complemented with CsoR ($\Delta cstR:CsoR$) in the absence (open symbol) or presence (closed symbol) of 0.2 mM NaHS stress. Cells were grown aerobically in HHWm+TS at 37 °C with shaking. (B) RT-PCR of *copA* in WT *S. aureus* following addition of 0.2 mM NaHS stress is not induced, further establishing no *in vivo* crosstalk between CsoR and CstR regulatory pathways. *copA* is under the control of CsoR.⁶ Aliquots were collected before, and 10 and 30 min post addition of 0.2 mM NaHS at OD₆₀₀~0.2. (C-D) LC-ESI-MS of CsoR following reaction with Na₂S₄. The *S. aureus* Cu(I) sensor CsoR was reacted with a 5-fold excess of Na₂S₄ for 17 h and analyzed by LC-ESI-MS. (C) Mass to charge ratios of the +10/20 charges state indicate the formation of a series of sulfur cross-linked CsoR protomers with up to nine total sulfur atoms. (D) Deconvoluted spectra indicating the relative abundance of reduced to cross-linked species.

Table 9. Summary of LC-ESI-MS deconvoluted masses obtained from CstR reaction with LMW sulfur compounds. All mass shifts are relative to either the reduced or disulfide form of CsoR as indicated by (-). Italics represent species present in control samples. No reaction was observed with 5x NaHS.

Protein	M _r Observed (Da)	Mass Shift	Assignment	M _r Expected (Da)
CsoR + 25x NaHS	11035.5	-	<i>CsoR^{RS-H}</i>	11036.6
	11057.6	22.1	<i>CsoR^{RS-H} + Na</i>	11056.6
CsoR + 5x Na ₂ S ₄	11037.7	-	<i>CsoR^{RS-H}</i>	11036.6
	11069.2	31.5	CsoR ^{RS-SH}	11068.7
	11101.0	63.3	CsoR ^{RS-SH} , CsoR ^{R'S-SH}	11100.7
	11149.6	111.9	CsoR ^{RS-SSH} , CsoR ^{R'S-SH}	11132.8
	22075.5	-	CsoR ₂ ^{RS-SR'}	22071.2
	22106.0	30.5	CsoR ₂ ^{RS-S-SR'}	22103.2
	22138.4	62.9	CsoR ₂ ^{RS-S-SR', R''S-S-SR'''*}	22135.2
	22170.0	94.5	CsoR ₂ ^{RS-S-S-SR', R'S-S-SR'''}	22167.3
	22202.9	127.4	CsoR ₂ ^{RS-S-S-SR', R''S-S-S-SR'''}	22199.3
	22234.3	158.8	CsoR ₂ ^{RS-S-S-S-SR', R''S-S-S-SR'''}	22231.3
	22267.1	191.6	CsoR ₂ ^{RS-S-S-S-SR', R''S-S-S-S-SR'''}	22263.3
	22299.2	223.7	CsoR ₂ ^{RS-S-S-S-S-SR', R''S-S-S-S-S-SR'''}	22295.4
	22331.4	255.9	CsoR ₂ ^{RS-S-S-S-S-SR', R''S-S-S-S-S-SR'''}	22327.4
	22363.2	287.7	CsoR ₂ ^{RS-S-S-S-S-SR', R''S-S-S-S-S-SR''' + S}	22359.4

DISCUSSION

In the work presented in this chapter, we establish that CstR is a per- and polysulfide-sensing regulator in *S. aureus*. Persulfide sensing by CstR leads to transcriptional derepression of an operon that is hypothesized to be a sulfide oxidation system where all of the downstream components, *cstA*, *cstB*, and *sqr*, are required to mitigate the effects of sulfide toxicity, particularly when the cells are grown in chemically-defined growth medium, HHWm+TS (Fig. 22-24). The negative growth defects are detectable but relatively more modest when *S. aureus* is grown in HHWm+Cys or rich TSB medium (Fig. 22B-C). This observation is consistent with the proposal that sulfide toxicity interferes directly with cellular sulfur assimilation and these effects are more pronounced when *S. aureus* is forced to produce cysteine from an inorganic source such as TS. The mobilizable sulfane sulfur in TS is likely first “fixed” as a cysteine persulfide by one of five cellular thiosulfate sulfur transferases (rhodanases) (Fig. 31), which is ultimately trafficked to the cysteine biosynthesis complex via the activity of O-acetyl-L-serine sulfhydrylase (OASS; CysK), perhaps via thioredoxin/thioredoxin reductase system or to other cellular needs, e.g., Fe-S cluster biogenesis (Fig. 31). The identity of those rhodanases that function in this process are not known, although it is interesting to note that two are found in the *cst* operon itself (*cstA* and *cstB*). One possible scenario is that high intracellular persulfide or polysulfides¹³⁰ poison key sulfur shuttling steps and/or maintenance of cellular reduction potential, or leads to an increase in deleterious proteome S-sulfhydration¹⁹³ that induction of the *cst* operon serves to mitigate. Additional experimentation will be necessary to elucidate the speciation of LMW and protein-bound per- and polysulfides in the cell.

The genes in the *cst* operon predicted to be responsible for mitigation of sulfide stress are strongly transcriptionally induced by RSS as NaHS, Na₂S, or Na₂S₄. Transcriptional derepression is observed in mid-log cells in response to sulfide toxicity at 10 min post-addition of sulfide stress to the growth media. By 30 min, expression of the operon has returned to baseline. These kinetics of mRNA induction (Fig. 24) mirror the temporal aspects of an acute phase response, similar to those observed in proteomics profiles in *S. aureus* COL strain by a number of inducers.¹⁹² The kinetics of the CstR-dependent induction response may be indicative that the *cst* operon functions in (poly)sulfide homeostasis under normal housekeeping conditions. Additional evidence in support of a homeostatic control is the initially puzzling finding that either too much or too little expression of the CstR-regulated enzymes gives rise to the same strong growth defect on HHWm+TS under aerobic growth conditions (Fig. 22A). This suggests that overexpression of *cstA*, *cstB* and *sqr* may well divert TS-derived sulfur from cellular rhodanases dedicated to pushing sulfur into cysteine biosynthesis and other metabolite needs, *e.g.*, to sulfur-containing metabolites of Fe-S biogenesis, to sulfide oxidation along with NaHS and thus depriving the cell of useable sulfur (Fig. 31). On the other hand, too little of the sulfide oxidation system may essentially overrun the ability of the organism to detoxify sulfide stress, resulting in disruption of metal centers in proteins and other deleterious effects.

To better understand the sulfur species CstR may sense in the cell, recombinant CstR was reacted with three possible sources, Na₂S, Na₂S₄, and GSSH which represent sulfide, inorganic polysulfide, and an organic persulfide or hydrosulfide, respectively. Our results indicate that CstR preferentially reacts with the sulfane sulfur (S⁰) within

tetrasulfide and the related organic persulfide but not sulfide (S^{2-}) to form cross-linked adducts with mass shifts of approximately +32, +64, +96, and +128 Da as determined by LC-ESI-MS (Fig. 25, Table 6). The mass shifts were confirmed as di-, tri-, and tetrasulfides by high-resolution tandem mass spectrometry (Table 7, Fig. 26). These results are consistent with previous observations indicating that cysteine thiols do not react directly with sulfide but are capable of reacting with the sulfane sulfur of a per- or polysulfide.^{127,130}

The precise chemical inducer(s) of the *cst* operon in cells is unknown but LMW inorganic polysulfides or organic persulfides and polysulfides are possible candidates. Each gives rise to the same product profile as polysulfide (Fig. 25) and contains an internal, more electrophilic S^0 atom as part of a sulfur chain. Bacillithiol persulfide, BSSH, or cysteine persulfide, CysSSH, are possible candidates in *S. aureus* since this organism does not produce the model LMW thiol GSH and therefore would not encounter GSSH. Such hydrodisulfides (persulfides) are predicted to be formed from the reaction of oxidized bacillithiol (BSSB) and cystine with excess HS^- ,¹ while the former is formed noncatalytically in solutions of sulfide itself¹³⁰ or enzymatically via the action of SQR (Fig. 21).¹⁹⁴ In addition, the spontaneous formation of per- and polysulfides can occur following sulfide oxidation to a sulfenic acid^{44,195} or metal-catalyzed sulfide radical (HS^\bullet) formation,¹²⁷ both of which are readily capable of reacting with other sulfur species in the cell. The enzymes CBS and CSE also readily produce per- and polysulfides from the catabolism of cystine (Fig. 20)¹ but this is unlikely in the context the sulfide stress conditions used here. In any case, the DNA binding activity of CstR is negatively regulated following formation of di-, tri-, and tetrasulfides *in vitro*. Although

derivatization of the more N-terminal cysteine (Cys31) is sufficient for negative regulation of DNA binding *in vitro*,¹⁶² *in vivo* studies reveal that both reactive (Cys31) and resolving (Cys60) cysteines are essential to induce the operon under sulfide stress.¹³ The regulatory post-translational modification in cells is unknown for CstR, but likely involves a Cys31-Cys60' interprotomer mixed disulfide bond.

We favor the hypothesis that under conditions of acute sulfide stress in *S. aureus*, sulfide reacts cystine, BSSB, metal ions, and/or ROS to form per and polysulfides (Fig. 31). The sulfane sulfur as cysteine persulfides, bacillithiol persulfides and/or polysulfides may then go on to react with CstR, thereby inducing the *cst* operon. Further studies are required to identify the chemical nature of the cellular adducts of CstR in sulfide-stressed cells, as well as to more fully characterize the entire LMW and proteomic pools of *S*-sulfhydrated species in cells, and how these pools change upon sulfide stress. In this context, it is interesting to note that in ETHE1 (CstB)-deficient mice, significant protein *S*-sulfhydration is proposed to accumulate as a result of sulfide toxicity.¹⁹³ It is also of interest to connect previous findings, which establish that nitrite stress in *S. aureus* biofilms induces the *cst* operon (see Fig. X, Chapter 5),¹⁹⁰ with the persulfide induction of the *cst* operon reported here. One possibility is that elevated nitric oxide and increased endogenous H₂S production required for molybdopterin and Fe-S cluster biogenesis needed for nitrate/nitrite reductases, for example,¹⁹⁰ converge to form thionitrous acid (HSNO), nitroxyl (HNO), and possibly polysulfides.^{86,89} Indeed, recent work suggests a significant NO•/H₂S interplay in cardiovascular vasodilation which has been traced to HNO-mediated disulfide bond formation in a sensory chemoreceptor channel.⁸⁷ These studies make the prediction that CstR may sense nitroxyl directly.

Preliminary experiments designed to test this hypothesis are presented and discussed in Chapter 5.

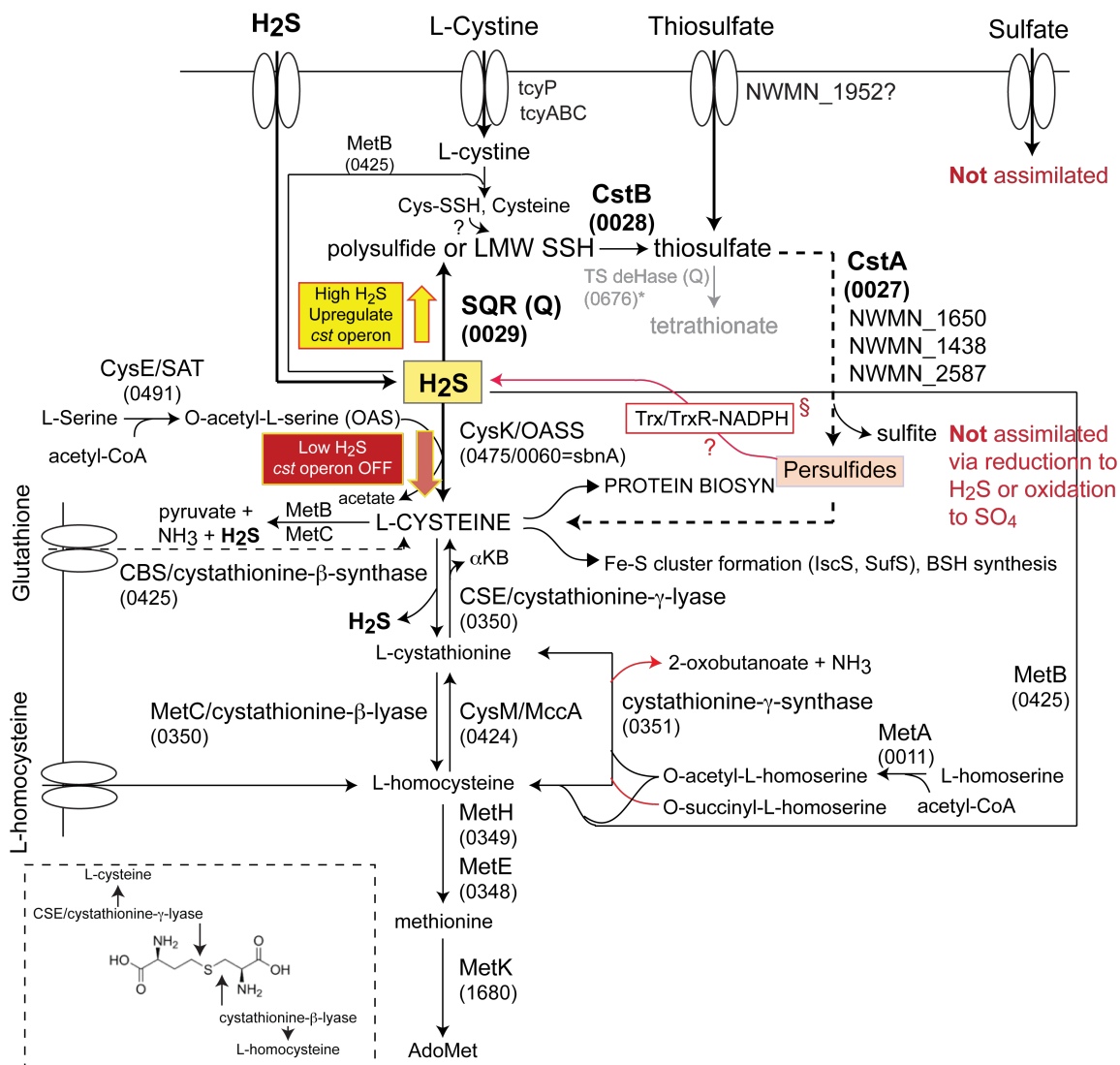


Figure 31. Abbreviated rendering of sulfur assimilation and hydrogen sulfide metabolism in *S. aureus* strain Newman. The 4-number (wxyz) *S. aureus* strain Newman gene locus tags (NWMN_wxyz) are given for each enzyme that is annotated with a standard abbreviation based on recent work.¹³⁷ OASS: O-acetyl-L-serine sulfhydrylase; SAT + OASS: cysteine synthase complex. The TS quinone-dependent dehydrogenase marked with an asterisk and shaded grey (NWMN_0676) is likely not functional given the absence of a gene encoding the small subunit. §, highlighted to implicate a reductive path to the generation of H₂S as a substrate for OASS from cellular protein-bound persulfides.¹ The large yellow and red arrows illustrate the concept of sulfide homeostasis, which is dictated by the coordinate action of H₂S detoxification (by proteins encoded by the *cst* operon) and assimilatory pathways.

CHAPTER IV

CYSTEINE REACTIVITY AND FUNCTIONAL CHARACTERIZATION OF WILD-TYPE AND MUTANT CstRs and CsoRs

INTRODUCTION

All microorganisms, irrespective of their specific niche(s), continuously monitor their immediate microenvironment and must be capable of responding to changes in cellular redox status. To achieve this, bacteria often employ transcriptional regulatory proteins that sense a specific stressor or class of stressors. These proteins control the expression of genes products that detoxify or repair damage caused by a particular stressor (Fig. 2, Chapter 1). Regulators often retain similar structural scaffolds but sense markedly different stressors. The paralogous transcriptional regulators, CstR and CsoR from *S. aureus*, represents an excellent illustration of this. CstR and CsoR share 35% sequence identity and 65% similarity.⁶ *S. aureus* CsoR coordinates Cu(I) with high affinity through the two cysteine residues, Cys40 and Cys71, and the N δ 1 atom of a histidine in a trigonal S₂N coordination geometry. Cu(I)-binding leads to a decrease in DNA binding affinity and derepression of the copper efflux genes *copA*, a proposed P-type ATPase Cu(I) efflux pump, and *copZ*, a candidate Cu(I) chaperone.^{6,144} In contrast, CstR regulates expression of the *cst* operon that encodes enzymes responsible for mediating resistance to sulfide toxicity and reacts with the sulfane sulfur of both an inorganic polysulfide, e.g., Na₂S₄, or an organic persulfide, e.g., glutathione persulfide (GSSH) (see Chapter 3).¹³ Previous work has shown that there is no crosstalk between

CsoR and CstR *in vivo*^{6,13} but little is known about the factors that dictate copper vs. per- and polysulfide selectivity in these paralogous regulators.

There are several primary differences between the CstR and CsoR transcriptional regulators. CstR lacks a key Cu(I)-binding histidine residue as well as residues in the second coordination shell previously shown to be energetically linked to Cu(I)-mediated allosteric inhibition of DNA binding.^{144,150} These include a tyrosine and glutamate that form a hydrogen bonding network between the N ϵ 2 of the Cu(I)-binding histidine in *M. tuberculosis* CsoR (Fig. 32A).^{144,150} A second notable difference between CsoR and CstR is in the sequence near Cys31 of CstR where the local microenvironment harbors more positively charged residues while in CsoRs, the analogous residues are more negatively charged. The consensus sequence for CstR and CsoR are (G/E/D)-(K/R)-D-C-K-D and D- Φ -Y-C-D-D (Φ , hydrophobic), respectively (Fig. 32B). One simple hypothesis is that the intrinsic reactivity of the cysteine residues within these proteins may preclude CsoR from reacting with sulfur compounds. As the pK_a of a thiol increases, the reactivity decreases due to protonation. Likewise, cysteines with a lower pK_a are more likely to be a deprotonated thiolate and thus is far more nucleophilic (See Chapter 1).³⁹ The major alternative hypothesis is that CsoR and CstR are electrostatically tuned to attract positively charged Cu(I) cations or negatively charged sulfane sulfur anions, respectively.

In this chapter, show that CstR binds Cu(I) but that Cu(I) binding is insufficient to drive negative regulation of operator DNA binding. In addition, we probe the reactivity of the cysteine residues in CstR and CsoR by ratiometric pulsed-alkylation MALDI-TOF mass spectrometry.¹⁹⁶ We find that Cys31 in CstR is approximately 50-fold more reactive than the analogous cysteine, Cys41, in CsoR. In an effort to determine factors

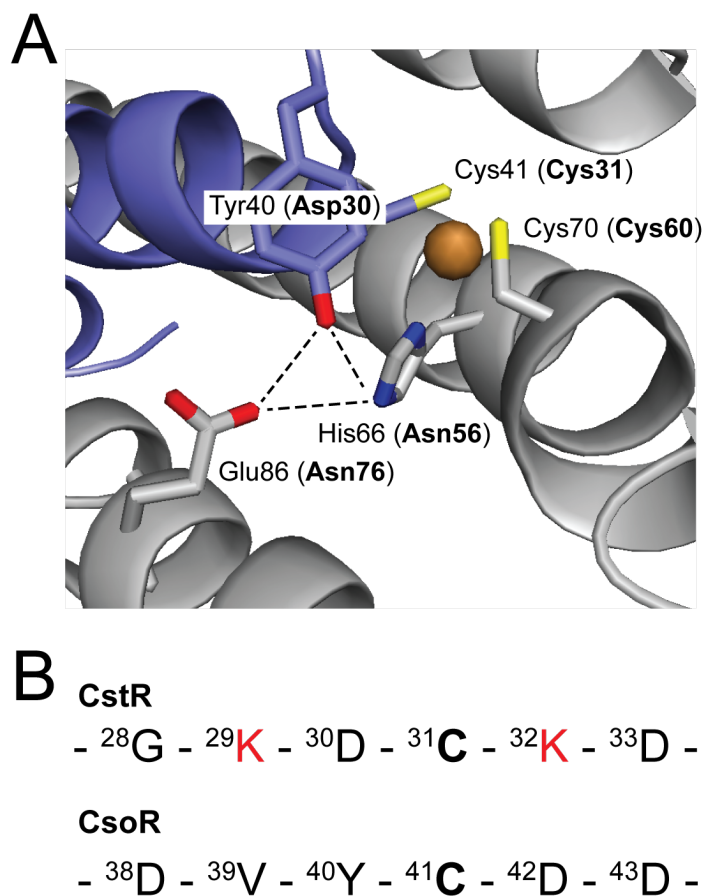


Figure 32. *M. tuberculosis* CsoR Cu(I) binding pocket and second coordination shell residues. (A) Residues involved in CsoR Cu(I) binding and residues involved in the second coordination shell. Modeled from *M. tuberculosis* CsoR¹⁴⁴ and annotated with *S. aureus* CsoR residues. In bold are the corresponding residues in *S. aureus* CstR. (B) *S. aureus* CstR lacks key residues in the second coordination shell but contains more positively charged (red) lysine residues near Cys31.

contributing to the difference in cysteine reactivity, we introduced mutations to lysine residues near Cys31 of CstR. These include either charge neutral (lysine to alanine) or charge reversal (lysine to aspartate) substitutions of Lys29 or Lys32 in CstR (see Fig. 32B). Surprisingly, our pulsed-alkylation experiments reveal that mutation of the lysine residues does not result in attenuation of Cys31 reactivity in CstR toward a neutral alkylating reagent. In light of this, we hypothesized that Lys29 and Lys32 in CstR may play an important role in sensing sulfide stress *in vivo*. Mutation of the lysine residues results in a negative growth phenotype for all *S. aureus* strains under sulfide stress with the exception of a K32A substitution which exhibits wild-type-like growth characteristics

MATERIALS AND METHODS

Plasmid Construction and Protein Purification. CstR cysteine and lysine mutant plasmids were prepared, expressed, and purified as described for WT and cysteine mutants in Chapter 2 with the exception of K32D CstR. During the ammonium sulfate precipitation, K32D CstR remained in the supernatant at 57% (0.35 g/mL) ammonium sulfate and precipitated at 93% (0.65 g/mL). The 93% ammonium sulfate pellet was resuspended in and dialyzed against buffer A (25 mM Tris, 5 mM DTT, 1 mM EDTA, pH 8.0) with 100 mM NaCl at 4°C. The protein was then loaded onto a Q sepharose anion exchange column (Pharmacia) equilibrated with buffer A and 100 mM NaCl and eluted with a linear gradient to buffer A and 500 mM NaCl over 15 column volumes. Fractions containing K32D CstR were collected, concentrated and loaded onto a pre-graded G200 10/60 gel filtration column (GE Healthcare) equilibrated with buffer A and

500 mM NaCl. Fractions containing K32D CstR were again collected, concentrated, and prepared for anaerobic work as described in Chapter 2.

CstR Cu(I) Binding and Affinity Measurements. A fresh Cu(I) stock was prepared anaerobically for each experiment in 10 mM HEPES, 200 mM NaCl, pH 7.0 by dissolution of solid Cu(I) chloride followed by centrifugation to remove insoluble particulates. The supernatant was serially diluted and [Cu(I)] measured by atomic absorption spectroscopy (PerkinElmer AAS-400). Initial Cu(I) binding experiments were performed by direct titration of Cu(I) at a 1:1 molar ratio with apo-CstR and measuring absorbance by UV-VIS spectroscopy. Apo-CstR (20 μ M) was measured by UV-Vis and subtracted from the Cu-CstR sample essentially as previously described.^{144,197}

To determine CstR Cu(I) binding affinity, a bicinchoninic acid (BCA) assay was performed as previously described:^{198,199} 120 μ L aliquots containing 10.0, 18.9, or 29.6 μ M Cu(I) and 30, 50, or 70 μ M BCA, respectively, were titrated with increasing fully reduced CstR titrant. Prior to CstR addition, all Cu(I) is bound as Cu-BCA₂ complex with an absorption band at 562 nm (A_{562}). An extinction coefficient of 7700 M⁻¹ cm⁻¹ was used to determine Cu(I):BCA₂ concentration. All titrations were globally fit to a direct competition binding model using Dynafit¹⁷⁴ as previously described (Appendix Fig. 5).¹⁹⁹

Cysteine Pulsed-Alkylation Reactivity Assay. Sample preparation for pulsed-alkylation mass spectrometry was adapted from the original report of the technique¹⁹⁶ and optimized for CstR and CsoR. All experiments were carried out anaerobically in a glovebox in a buffer containing 10 mM HEPES and 200 mM NaCl at pH 7.0. CstR, CstR mutants, and

CsoR proteins were reacted with a 3-fold thiol excess of d_5 -N-ethylmaleimide (NEM, pulse). At discrete time points, 50 μ L aliquots were removed and quenched with an equal volume of a solution containing a 900-fold thiol excess of H₅-NEM (chase) with 100 mM Tris pH 8.0, and 8 M urea. After a 1 h chase, quenched reactions were removed from the glovebox and precipitated on ice with a final concentration of 12.5% trichloroacetic acid (TCA) for 1.5 h. Precipitated protein was pelleted by centrifugation at 4° C. The supernatant was removed, and the pellet washed twice with ice-cold acetone. The washed pellet was vacuum centrifuged to dryness at 45° C and re-suspended in 10 μ L digest buffer (20 mM ammonium bicarbonate, 10% acetonitrile, 50:1 protein:trypsin ratio, pH 8.2). CstR and CstR lysine substitution mutants were digested for 1 h and CsoR for 0.5 h at 37° C. Tryptic digests were quenched with a final concentration of 1% trifluoroacetic acid (TFA) and spotted on a MALDI plate with α -cyano-4-hydroxycinnamic acid (CCA) matrix with a 5:1 matrix:sample ratio for analysis. For examination of the pH-dependence of the reaction, the same experiment was carried out in the following buffers; Mes for pH 6.0-6.5, HEPES for pH 7.0-7.5, and Tris for pH 8.0-9.0.

Acquiring and Analyzing MALDI-TOF Spectra. MALDI-TOF mass spectra were collected and analyzed in triplicate using a Bruker Autoflex III MALDI-TOF mass spectrometer with a 200 Hz frequency-tripled Nd:YAG laser (355 nm) and Flex Analysis software (Bruker Daltonics, Billerica, MA). Cysteine-containing peaks were identified by monoisotopic mass and resolved as alkylated with heavy d_5 -NEM (+130.0791 Da) or light H₅-NEM (+125.0477 Da) with little to no detectable unmodified peptide (data not shown). The theoretical distribution and peak areas were determined using the averagine

algorithm²⁰⁰ and quantified by summing the total peak areas of the full isotopic distribution. Relative peak areas were used to determine the mol fraction of H₅-NEM labeled peptide, $\Theta(\text{H}_5)$, as defined by Equation 1. $A(\text{H}_5)$ and $A(d_5)$ correspond to the area (A) of the isotopic distribution of H₅-NEM or d₅-NEM alkylated peptide, respectively. To obtain the pseudo-first order rate constant of alkylation, k , $\Theta(\text{H}_5)$ was plotted as a function of pulse time, t , and fit to Equation 2. In some instances, a fit to a sum of two exponentials was used, Equation 3. The second-order rate constant was obtained by dividing k by the concentration of d₅-NEM in the pulse.

$$\text{Equation 1: } \Theta(\text{H}_5) = \frac{A(\text{H}_5)}{A(\text{H}_5) + A(d_5)}$$

$$\text{Equation 2: } \Theta(\text{H}_5) = \Theta(\text{H}_5)_{t_0} \cdot e^{-kt}$$

$$\text{Equation 3: } \Theta(\text{H}_5) = \Theta(\text{H}_5)_{t_0-t_{\text{slow}}} \cdot e^{-k_{\text{fast}}t} + \Theta(\text{H}_5)_{t_0-t_{\text{fast}}} \cdot e^{-k_{\text{slow}}t}$$

Fluorescence Anisotropy Titrations. These experiments were performed as described in Chapter 2.

*Construction of Cysteine and Lysine Mutant ΔcstR *S. aureus* Strains.* ΔcstR *S. aureus* was complemented with pOS1-P_{lgt} plasmid containing the indicated lysine mutant CstR as described in Chapter 3. Plasmid DNA was maintained by the addition of 10 $\mu\text{g mL}^{-1}$ chloramphenicol (Cm) to all plates and growth media.

S. aureus Growth Curves. Growth curves were performed as described in Chapter 3.

RESULTS

CstR binds Cu(I) but Cu(I) binding does not negatively regulate cst operator DNA binding. *CstR* and the *bona fide* copper sensor *CsoR* from *S. aureus* strain Newman are 31% identical but function independently in the same cytoplasm (Fig. 30, Chapter 3).^{6,13} *CstR* and *CsoR* partition into separate clades on the basis of a global sequence alignment and exhibit no crosstalk *in vivo*.^{6,13,145} For example, in qRT-PCR experiments, the addition of copper salts does not result in induction of *CstR*-regulated genes and *CsoR*-regulated genes are not induced under conditions of sulfide stress.^{6,13} To further probe this dichotomy of function, a series of anaerobic Cu(I) binding experiments were performed by directly titrating Cu(I) into *CstR* up to a 1:1 stoichiometry (Cu(I):protomer) and measuring the UV-Vis absorption band for S⁻ to Cu(I) charge transfer (Fig. 33A). This experiment yielded results similar to that of other *CsoR* proteins¹⁴⁴ and reveals that *CstR* binds Cu(I) stoichiometrically under these conditions. We next determined the *CstR*:Cu(I) binding affinity by titrating reduced *CstR* into a solution of Cu(I):BCA₂ (bicinchoninic acid; log K_{Cu} =17.2) and observing the change in absorption of the Cu(I):BCA₂ complex (A_{562}) as a result of Cu(I) binding by *CstR* (Fig. 33B). Global analysis of three independent experiments carried out at different Cu(I):BCA₂ concentrations reveals log K_{Cu} =14.0 (± 0.3). This value is four orders of magnitude weaker than *S. aureus* *CsoR* (18.0 ± 0.1) and is in fact, within a factor of ≈ 5 of K_{Cu} for to H64A *S. aureus* *CsoR* (14.5 ± 0.1)⁶ and the analogous H61A *M. tuberculosis* *CsoR* (14.7 ± 0.4).¹⁵⁰ The H61A *CsoR* mutation in *M. tuberculosis* *CsoR* is known to form a bis-thiolate coordination complex,¹⁴⁴ similar to what is likely to be formed by *CstR* on the basis of an absorption spectrum dominated by Cu(I)-S bonds (Fig. 33A).

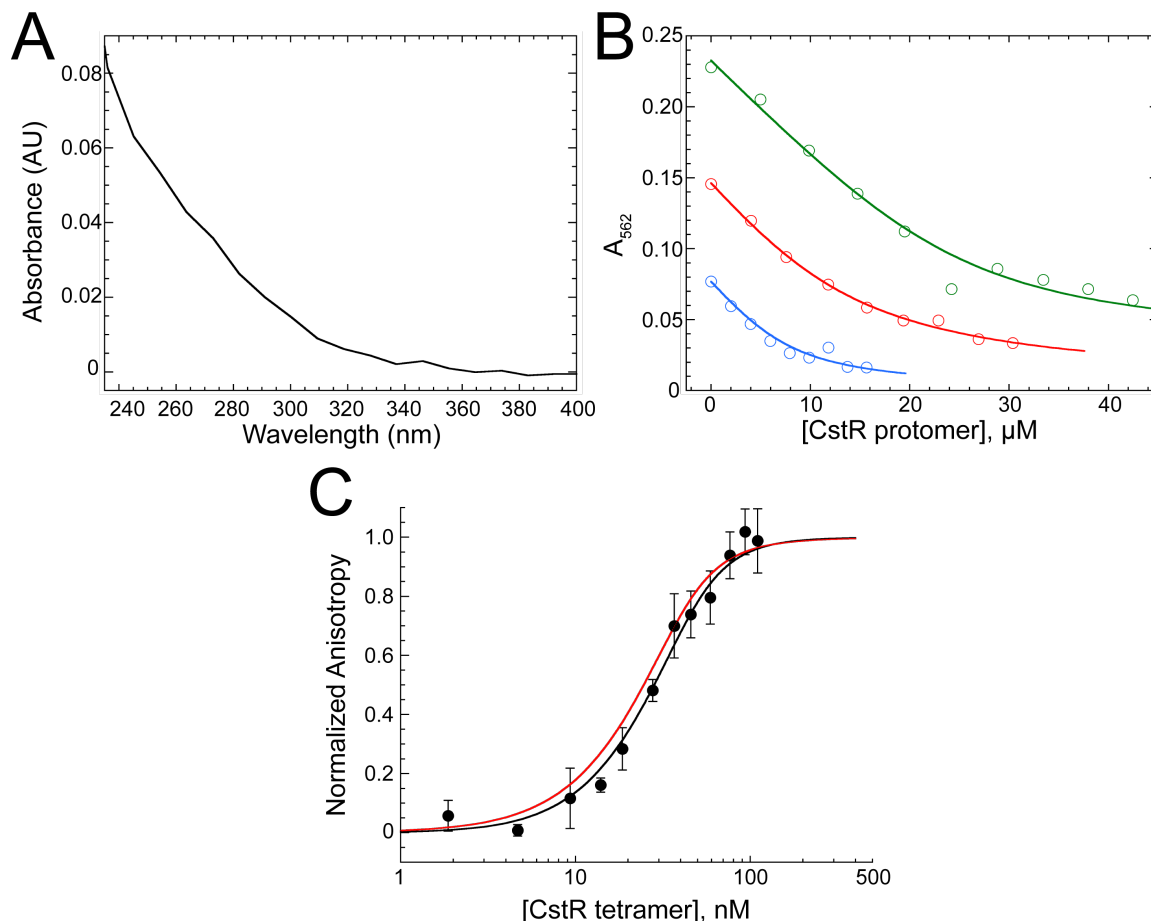


Figure 33. CstR forms a modest affinity complex with Cu(I) and metal binding does not negatively regulate *cst* DNA binding. (A) Apoprotein-subtracted UV-Vis spectrum of 1:1 Cu(I):CstR. This spectrum is characterized by intense absorption from S^- to Cu(I) ligand-to-metal or metal-to-ligand charge transfer transitions in the UV region.^{144,197} (B) Representative Cu(I)-bicinchonic acid competition assays with apo CstR. Binding curves were obtained under anaerobic conditions. Open symbols represent the A_{562} of the Cu(I):BCA₂ complex and the solid lines represent the global fitting of three individual experiments to a single-site binding, direct competition model. The global Cu(I):CstR binding constant was calculated to be $1.0 \pm 0.4 \times 10^{14} \text{ M}^{-1}$. *Green*: 29.6 μM Cu(I), 70 μM BCA. *Red*: 18.9 μM Cu(I), 50 μM BCA. *Blue*: 10.0 μM Cu(I), 30 μM BCA. (C) Representative fluorescence anisotropy titration of Cu(I)-bound CstR to a fluorescently labeled *cst* OP1 DNA fragment. The macroscopic binding constant, K_{tet} , was determined to be $4.3 \pm 1.7 \times 10^7 \text{ M}^{-1}$. The *red* line is a simulated curve defined by the binding parameters for apo-reduced CstR (see Fig. 28, Chapter 3) under the same solution conditions ($K_{\text{tet}} = 6.3 \pm 0.5 \times 10^7 \text{ M}^{-1}$).

We next determined the impact of Cu(I)-binding by CstR on *cst* OP1 DNA affinity. In this experiment, Cu(I)-bound CstR binds to the *cst* OP1 operator DNA with an affinity that is similar to that of apo-reduced CstR (Fig. 33C). Thus, despite the fact that CstR binds Cu(I), Cu(I) binding does not allosterically drive dissociation of CstR from *cst* operator DNA *in vitro* or *in vivo*.⁶ Furthermore, the Cu(I) affinity is such that the intracellular Cu(I) concentration is unlikely to rise to a level required to be bound by CstR, due to regulation by CsoR.²⁰¹

Cys31 of CstR is approximately 50-fold more reactive than the analogous residue, Cys41, in CsoR at pH 7.0. CstR reacts with a sulfane sulfur from a per- or polysulfide donor to negatively regulate DNA binding while CsoR poorly reacts with these species under the same conditions (See Chapter 3).¹³ To better understand the difference of intrinsic cysteine reactivity between CstR and CsoR, we performed pulsed alkylation mass spectrometry experiments¹⁹⁶ with the neutral alkylating reagent, N-ethylmaleimide (NEM) at pH 7.0 under anaerobic conditions. In these experiments, CsoR or CstR were reacted with a 3-fold thiol excess of deuterium-labeled “heavy” NEM (*d*₅-NEM, pulse). After a discrete time, an aliquot was removed and added to a denaturing buffer with a vast excess of “light” NEM (H₅-NEM, chase) (Fig. 34) to alkylate any unreacted cysteine residues. Following this pulse-chase alkylation protocol, proteins were precipitated with TCA and washed with acetone and digested with trypsin in ammonium bicarbonate at pH 8.0. The resulting tryptic peptides were analyzed by MALDI-TOF mass spectrometry. The cysteine-containing peptides were observed as either H₅-NEM or *d*₅-NEM alkylation adducts (Table 10). Following a reaction time course for each protein (Fig. 35), the mol

fraction of H₅-NEM alkylation was determined by summing the peak area of the full isotopic distribution of H₅- or d₅-NEM alkylated peptides and fit to a second order rate constant (Fig. 36). Remarkably, the reaction of Cys31 in CstR is complete within 5 min while the analogous residue, Cys41 in CsoR, is only ≈20% complete after 90 min under these conditions (pH 7.0). Fitting of these kinetic data reveals a 50-fold difference in the magnitude of the second order rate constant (Fig. 36, Table 11). In contrast, Cys70 of CsoR is 2.5 times more reactive than the analogous Cys60 of CstR.

The results presented above reveal that the more C-terminal cysteines of CstR (Cys60) and CsoR (Cys70) have similar reactivities while the more N-terminal cysteines, Cys31 and Cys41, respectively, differ dramatically in reactivity at pH 7.0. These results suggest that the difference in relative reactivity of the N-terminal cysteine in CstR specifically endows CstR with the ability to react with a per- or polysulfide donor. This is consistent with the observation that perturbation of Cys31 is both necessary and sufficient to drive negative regulation of DNA binding of CstR *in vitro*. Indeed, experiments aimed to determine the pK_a of Cys31 of CstR and Cys41 of CsoR reveal that Cys31 has a pK_a of ≈8.6 while Cys41 is ≈9.3 (Fig. 37). The pK_a of Cys31 is similar to that of a free thiol, 8.5-9.0,⁴⁴ while Cys41 elevated consistent with decreased reactivity over the entire pH range of 6.0-8.5 (Fig. 37) The sum of these results suggests that the environment near Cys41 in CsoR makes deprotonation less favorable than in CstR and might be traced to acidic residues in the vicinity of the sulfhydryl group (Fig. 32B).

Mutation of CstR Lysine Residues does not Attenuate Cysteine Reactivity. By sequence alignment, CstRs appear to contain more positively-charged residues near the N-terminal

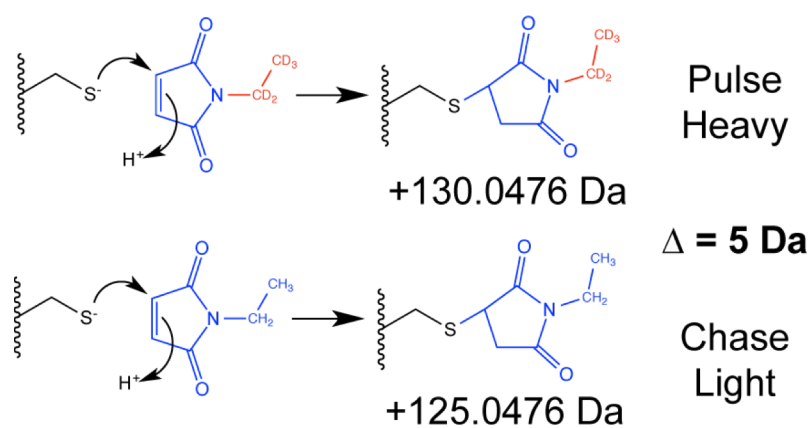


Figure 34: Reaction schematic of the pulse-chase alkylation reaction. Each protein was reacted with a 3-fold thiol excess of heavy NEM (d_5) for a defined time and chased with an excess of light (H_5) NEM. A summary of H_5 -NEM and d_5 -NEM alkylated peptides is available in Table 10.

Table 10. Summary of observed and calculated monoisotopic masses for cysteine-containing peptides. Cysteines were alkylated with either H₅-NEM or d₅-NEM followed by tryptic digest. Peptides were detected by MALDI-TOF mass spectrometry.

Cys31	Peptide	Sequence	Mass of Cys-Containing Peptides (Da)				
			Cys-SH Calc.	Cys-S-d ₅ -NEM Calc. Obs.		Cys-S-H ₅ -NEM Calc. Obs.	
CstR	24-42	(K)MMEEGKDCKDVITQI SASK(S)	2113.0	2243.1	2243.1	2238.0	2238.0
K29A	24-42	(K)MMEEGADCKDVITQI SASK(S)	2055.9	2186.0	2185.7	2181.0	2180.8
K29D	24-42	(K)MMEEGDDCKDVITQI SASK(S)	2099.9	2230.0	2230.0	2225.0	2225.0
K32A	30-42	(K)DCADVITQISASK(S)	1350.7	1480.7	1480.8	1475.7	1475.8
K32D	24-42	(K)MMEEGKDCDDVITQI SASK(S)	2099.9	2230.0	2230.1	2225.0	2225.1
CsoR	34-49	(R)MIEEDVYCDDVLTQIR (A)	1941.9	2072.0	2072.0	2066.9	2066.9
Cys60	Peptide	Sequence	Cys-SH	Cys-S-d ₅ -NEM		Cys-S-H ₅ -NEM	
CstR					1804.9		1799.9
K29A					1805.0		1800.1
K29D	48-62	(R)LMGHIISENLIIECVK(A)	1674.9	1805.0	1804.9	1800.0	1799.9
K32A					1804.9		1799.9
K32D					1805.0		1799.9
CsoR	69-93	(K)SCIMNKVNQGAQEEA MEELLVTFQK(L)	2840.4	2970.4	2970.4	2965.4	2965.5

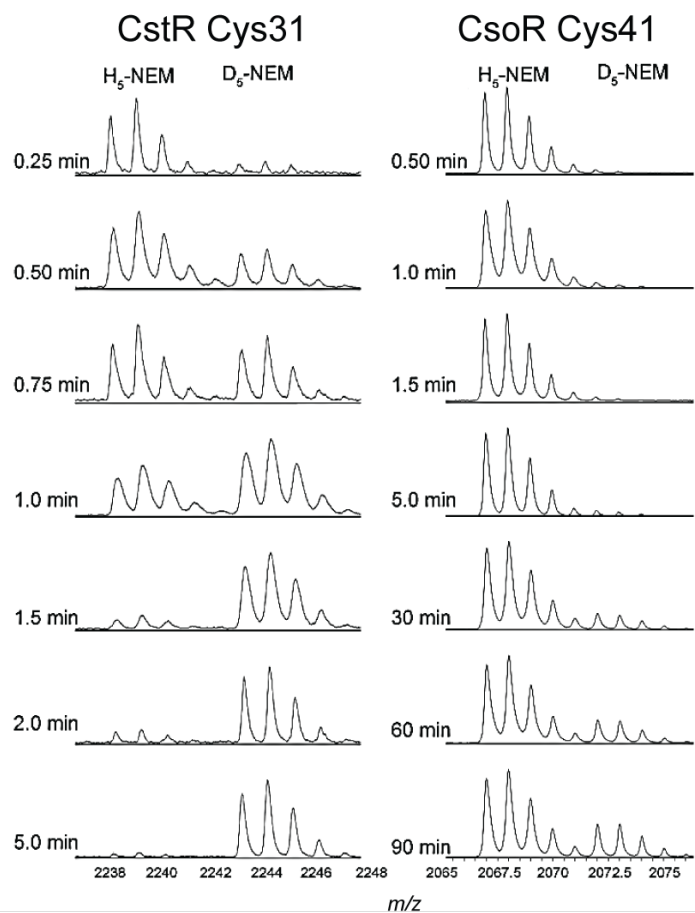


Figure 35. Series of MALDI-TOF mass spectra obtained for CstR Cys31 and CsoR Cys41. Representative MALDI-TOF spectra obtained for Cys31 of CstR (left) and Cys41 of CsoR (right) through the pulsed alkylation time course. Peaks were identified by monoisotopic mass and theoretical isotope distribution calculated using the averagine algorithm.²⁰⁰

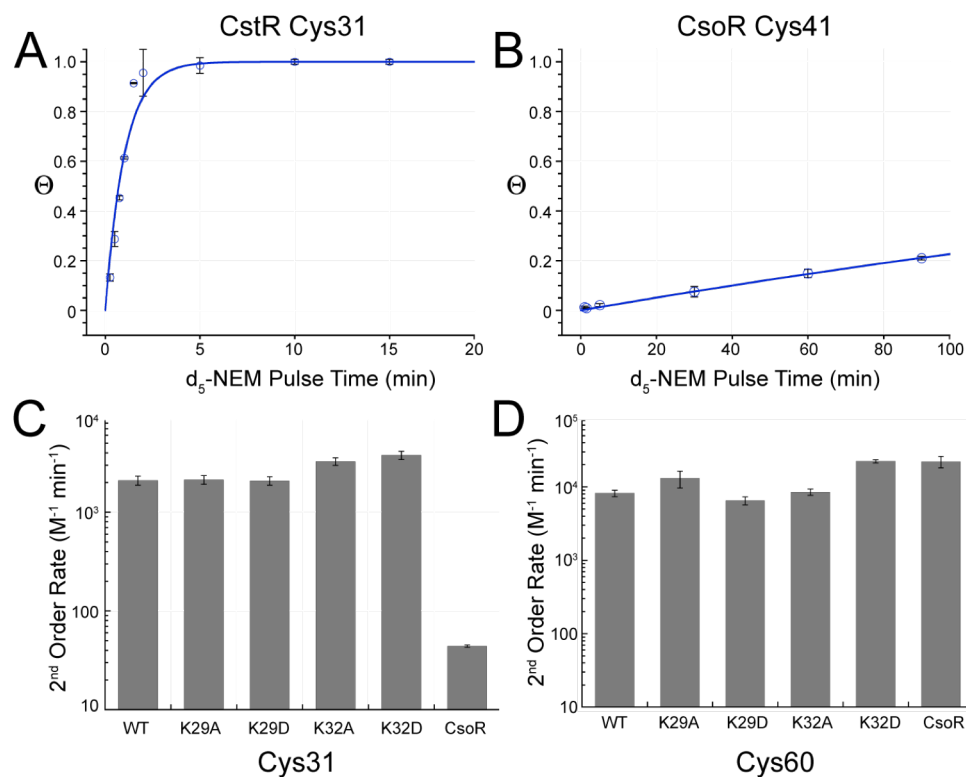


Figure 36. Data analysis of pulsed-alkylation cysteine reactivity experiments. (A-B) Mol fraction (Θ) of d_5 -NEM labeled peptide as determined by integration of the H_5 and d_5 -NEM peak areas from Fig. 35. (C-D) Summary of 2nd order reaction rates for each protein and cysteine tested. Note: In *S. aureus* CsoR, Cys41 and Cys70 and analogous to CstR Cys31 and Cys60, respectively. Conditions: 10 mM HEPES, 200 mM NaCl, pH 7.0, anaerobic.

Table 11: Summary of pulsed alkylation rate constants

CstR	Cys31	Cys60	
	Second Order Rate Constant ($M^{-1} \text{min}^{-1}$)	K_{fast} Second Order Rate Constant ($M^{-1} \text{min}^{-1}$)	K_{slow} Second Order Rate Constant ($M^{-1} \text{min}^{-1}$)
WT	2100 (± 200)	8200 (± 800)	610 (± 170)
K29A	2100 (± 200)	13100 (± 3400)	1800 (± 200)
K29D	2100 (± 200)	6500 (± 800)	500 (± 160)
K32A	3300 (± 300)	8500 (± 800) ^b	-
K32D	3800 (± 400)	22000 (± 1200) ^b	-
CsoR ^a	44 (± 1.2)	22000 (± 4000)	200 (± 50)

^aCorresponding cysteine residues in CsoR are Cy41 and Cys70

^bK32A and K32D Cys60 pulsed alkylation displayed single exponential kinetics

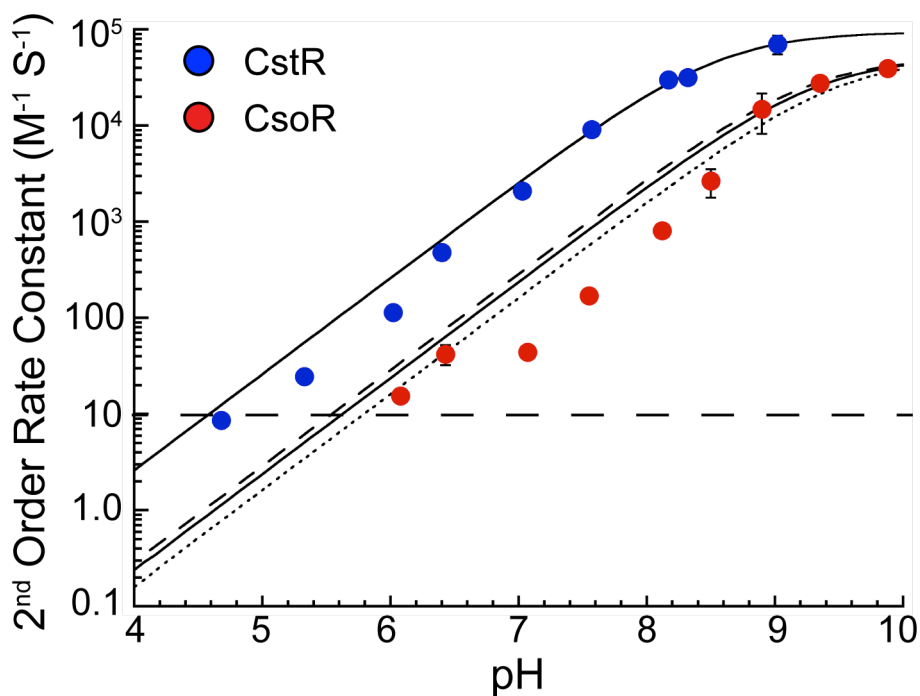


Figure 37. Observed pK_a of Cys41 of CsoR is approximately 1 pH unit higher than Cys31 of CstR. Summary of second order rate constants obtained for Cys31 of CstR for the pH range of 4.5-9.0 and Cy41 of CsoR between 6.0 and 10.0. The pK_a was calculated to approximately 8.6 ± 0.1 for Cys31 of CstR and 9.3 ± 0.1 for Cys41 of CsoR (solid line). Simulations of a Cys41 pK_a of 9.25 (dashed) and 9.5 (dotted) are also included. Error bars represent the standard deviation from at least three independent experiments. The horizontal dashed line represents the lower limit of reactivity that can be determined from the experimental protocol used here.

cysteine, Cys31, (G/E/D)-(K/R)²⁹-D-C-K³²-D, than the analogous residue in CsoRs, D- Φ -Y-C-D-D (Φ , hydrophobic). Overall, CsoRs tend to cluster more negatively-charged residues near the N-terminal cysteine residue. We next introduced charge neutral or charge reversal substitutions as alanine or aspartate, respectively, to either Lys29 or Lys32 to create K29A, K29D, K32A, and K32D CstRs. Each mutant protein was subjected to the same pulsed alkylation protocol performed for WT CstR and CsoR and second order rate constants were extracted from these data (Fig. 36). We find that mutation of Lys29 or Lys32 to alanine or aspartate does not substantially attenuate the reactivity of Cys31 toward the neutral alkylating reagent NEM at pH 7.0 (Fig. 36C-D, Table 11). In fact, mutation of Lys32 slightly increases the reactivity of Cys31 by a factor of ~ 1.5 (K32A) or ~ 2 (K32D) (Table 11). These results collectively suggest that Lys29 and Lys32 are *not* involved in the stabilization of a thiolate anion on Cys31 and therefore do not influence the intrinsic cysteine reactivity. This is fully consistent with the pK_a estimated from experiments of the pH-dependence of reactivity (Fig. 37) which is ≈ 8.5 for a typical solvent-exposed cysteine. There may be other residues responsible for controlling Cys31 reactivity or greater solvent exposure of Cys31 in CstR than Cys41 in CsoR, consistent with a higher pK_a for Cys41 in CsoR at ≈ 9.3 . Structural studies of *S. aureus* CsoR and CstR will be necessary to fully address the contributions from solvent exposure to cysteine reactivity.

CstR lysine mutants inhibit S. aureus growth under sulfide stress. NEM is a neutral alkylating reagent that largely reports on intrinsic cysteine reactivity. The lack of attenuation in cysteine reactivity of the CstR lysine mutants does not report on the

functional viability of CstR in the cell. To this end, a $\Delta cstR$ *S. aureus* strain was complemented with K29A, K29D, K32A, or K32D *cstR* alleles carried on the pOS1-P_{lgt} plasmid. These strains, $\Delta cstR:CstR^{K29A}$, $\Delta cstR:CstR^{K29D}$, $\Delta cstR:CstR^{K32A}$, and $\Delta cstR:CstR^{K32D}$ *S. aureus* were then stressed with 0.2 mM NaHS to determine growth phenotypes. Under sulfide stress conditions, the $\Delta cstR:CstR^{K29A}$, $\Delta cstR:CstR^{K29D}$, and $\Delta cstR:CstR^{K32D}$ strains fail to complement the $\Delta cstR$ strain while the $\Delta cstR:CstR^{K32A}$ strain successfully complemented (Fig. 38, compare Fig. 37C with Fig. 22A, Chapter 3). These findings indicate that the lysine residues near Cys31 of CstR are functionally important for mitigating sulfide stress despite having little influence on cysteine reactivity toward the neutral alkylating reagent NEM *in vitro*.

Fluorescence anisotropy titrations of CstR lysine mutants and cst OPI. To further explore the underlying origin of the observed lysine mutant growth phenotypes, fluorescent anisotropy titrations of fully reduced CstR lysine substitution mutants was performed to determine the DNA binding characteristics. K29A, K32A, and K32D CstR each bound to *cst* OPI with an affinity similar to reduced WT CstR. In contrast, K29D CstR binds weakly to *cst* OPI (Fig. 39, Table 12). The physiological effect of K29D CstR may therefore derive from an inability to repress the *cst* operon *in vivo*, much like the $\Delta cstR$ strain, which also fails to grow in the presence of 0.2 mM NaHS stress. In contrast, the K29A and K32D mutants are excellent candidates as either “reactivity” mutants, in which the reactivity toward the physiological RSS is attenuated, or as “allosteric” mutants, in which chemical reactivity is retained but no longer results in dissociation from operator DNA following reaction. An assignment of K29A or K32D CstRs as

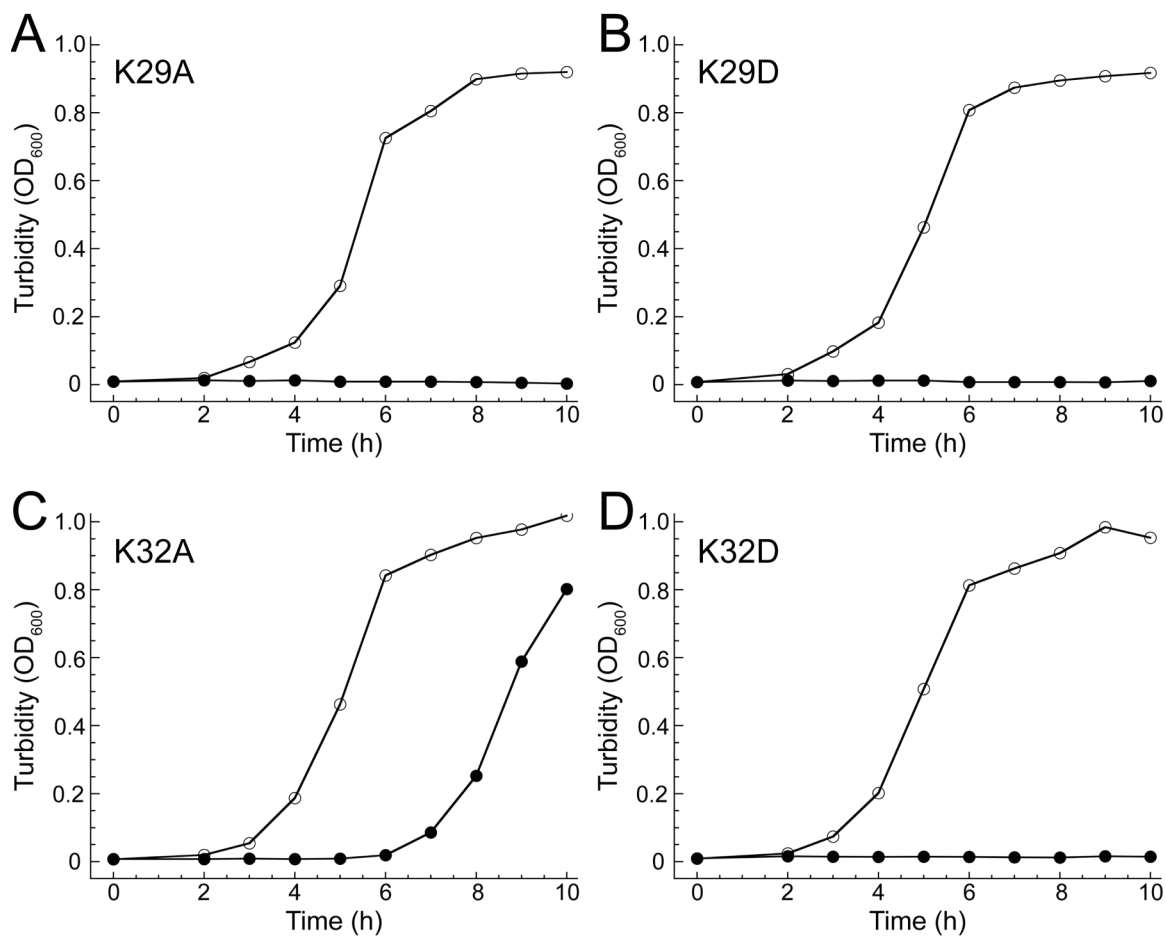


Figure 38. CstR lysine mutants impact *S. aureus* growth under sulfide stress. Representative growth curves of $\Delta cstR$ *S. aureus* complemented with lysine mutations at position 29 (A-B) or 32 (C-D) in the absence (*open* symbols) or presence of 0.2 mM NaHS (*closed* symbols) in HHWm+TS at 37 °C with shaking. (A) $\Delta cstR$:CstR^{K29A}, (B) $\Delta cstR$:CstR^{K29D}, (C) $\Delta cstR$:CstR^{K32A}, and (D) $\Delta cstR$:CstR^{K32D}.

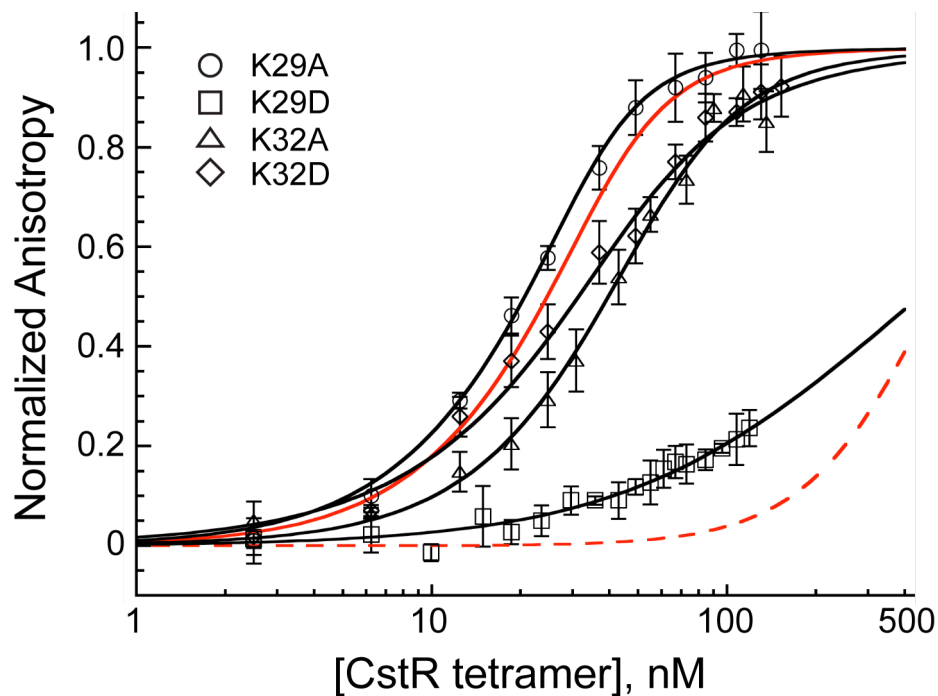


Figure 39. K29D CstR does not bind to *cst* OP1. Fluorescence anisotropy titrations of fully reduced CstR lysine mutants with fluorescently-labeled *cst* OP1. Data were fit to a sequential tetramer binding model where two non-dissociable tetramers bind stepwise to one operator DNA binding site. Stepwise binding constants, K_1 and K_2 , were used to determine the average macroscopic binding constant, K_{tet} ($K_{tet} = (K_1 \cdot K_2)^{1/2}$). For comparison, WT CstR-OP1 affinity is $7.4 (\pm 1.8) \times 10^7 \text{ M}^{-1}$ and the fit is represented as a solid red line while Na_2S_4 -reacted CstR has an affinity of $0.03 \pm 0.03 \times 10^7 \text{ M}^{-1}$ and shown as the dashed red line (See Fig. 28, Chapter 3). Binding curves represent a single representative titration. Conditions: 10 nM *cst* OP1 DNA, 10 mM HEPES, 0.2 M NaCl, pH 7.5, 25 °C.

Table 12. Summary of macroscopic binding constants of CstR lysine mutants. CstR lysine mutant association equilibrium constants (K_{tet}) for *cst* OP1 obtained from fluorescence anisotropy titrations. All experiments were performed with fluorescently labeled *cst* OP1. Conditions: 10 mM HEPES, 200 mM NaCl, 25.0 °C, anaerobic.

Protein	K_{tet} ($\times 10^7$) M^{-1}
WT CstR	7.4 (± 1.8) ^a
WT CstR + Cu(I)	4.3 (± 1.7) ^a
K29A CstR	11 (± 3)
K29D CstR	0.56 (± 0.2)
K32A CstR	2.6 (± 0.9)
K32D CstR	5.3 (± 1.1)
CstR ₂ ^(RS-SR)	0.11 (± 0.11) ^b
CstR+Na ₂ S ₄	0.03 (± 0.03) ^a

^aFrom Luebke, J. et al. (2014),¹³ Chapter 3

^bFrom Luebke, J. et al (2013),¹⁶² Chapter 2

“reactivity” or “allosteric” mutants can be readily evaluated using a combination of qRT-PCR induction experiments (see Fig. 24, Chapter 3), determination of DNA binding properties of oxidized vs. reduced CstR lysine substitution mutants (see Fig. 28, Chapter 3), and determination of the relative reaction rates of these mutants toward per- and polysulfides. These experiments are in progress.

DISCUSSION

In this chapter, we attempt to pinpoint molecular features that distinguishes *S. aureus* CstR from CsoR. It was previously established that CstR does not respond to copper stress *in vivo*.⁶ Here we show that CstR binds Cu(I) with high affinity with a log K_{Cu} of 14.0 ± 0.3 but Cu(I)-binding does not drive negative regulation of DNA binding (Fig. 31).¹³ CstR Cu(I) binding is four orders of magnitude lower than that of CsoR, log K_{Cu} of 18.1 ± 0.5 .⁶ The observed CstR Cu(I)-binding affinity is similar to CsoR mutants where the Cu(I)-binding histidine residue is removed.¹⁵⁰ In both proteins, Cu(I)-binding fails to disassemble protein-operator DNA complexes.^{6,150} Likewise, CsoR does not function as an RSS sensor *in vivo* and displays little reactivity toward RSS *in vitro* (Fig. 30, Chapter 3). The underlying factors contributing to the copper vs per- and polysulfide sensing are of a fundamental importance to understanding ligand discrimination in these paralogous transcriptional regulators.

We hypothesized that the cysteine residues in CstR are intrinsically more reactive than those in CsoR. To test this, we performed pulsed-alkylation mass spectrometry²⁰² to determine relative cysteine reactivities over a wide range of pH values (Fig. 36-37, Table 11). Here, we observe a striking differences between the N-terminal cysteine residues,

Cys31 of CstR and Cys41 of CsoR. This result is consistent with a lower pK_a for Cys31 of CstR vs. Cys41 of CsoR (Fig. 36) and is maintained over a pH range of 6-8.5 (Fig. 37). However, the apparent pK_a of Cys31 is not readily distinguished from a solvent exposed sulfhydryl group.

Although the structure of CstR is unknown, it could be hypothesized that *S. aureus* CsoR and CstR have comparable solvent exposures and that charged residues near Cys31 of CstR may influence the pK_a and therefore reactivity. However, mutations of Lys29 or Lys32 to alanine or aspartate, similar to those found in CsoRs, do not lead to an attenuation of Cys31 reactivity toward the neutral alkylating reagent NEM at pH 7.0 (Fig. 36, Table 11). This leads us to propose that the lysine residues in CstR electrostatically tune CstR to provide selectivity to negatively-charged sulfane sulfur donors, e.g., per- and polysulfides vs. the positively charged Cu(I) anion in CsoR. Inspection of the Cu(I) binding pocket in *M. tuberculosis* CsoR reveals a negatively charged aspartate next to the N-terminal cysteine residue as Asp39. The negative charge from the aspartate lies directly over the Cu(I) binding pocket in *M. tuberculosis* CsoR (Fig. 40). The analogous residue in CstR is Lys29 which is conserved in many predicted CstRs (Fig. 32B and Fig. 9, Chapter 1). Lys32 is specific to CstRs (Fig. 9, Chapter 1) and it should be noted that this position in most CsoRs is either a negatively charged or hydrophobic residue (Fig. 32B).^{144,203} Therefore, this particular lysine may not actually be involved in ligand discrimination but in some way allosterically in DNA binding. The corresponding residue in *M. tuberculosis*, Val37, is buried in the dimer-dimer interface (Fig. 40C-D). These observations lead to a hypothesis in which the reversal of CsoR vs CstR at position 29 may provide an electrostatic basis for ligand discrimination. The negatively charged

binding pocket of CsoR would attract positively charged Cu(I) cations while a negatively charged CstR ‘binding pocket’ would attract negatively charged per- and polysulfide anions.

Initial *in vivo* experiments were performed to test this hypothesis using a $\Delta cstR$ *S. aureus* strain complemented with K29A, K29D, K32A, or K32D CstRs. We observed that mutation of a charged residue at position 29 results in loss of viability under sulfide stress. The K29A substitution binds to *cst* operator DNA *in vitro* (Fig. 39, Table 12) but this mutation is not viable *in vivo*. The loss of viability of the K29D substitution is likely due to an order of magnitude decrease in *cst* operator DNA binding affinity *in vitro* (Fig. 39, Table 12). The $\Delta cstR:CstR^{K29D}$ strain would therefore function essentially as a $\Delta cstR$ strain, which does not grow under sulfide stress (Fig. 22, Chapter 3). At residue position 32, a charge-neutralizing mutation, K32A, results in wild-type-like DNA binding and no growth phenotype under sulfide stress. However, the charge reversal mutant, K32D, binds *cst* operator DNA with wild-type-like affinity but loses viability under sulfide stress. Lys32 may stabilize an $\alpha 2$ - $\alpha 3$ helix interaction in the dimer interface architecture of CstR and provide a function similar to the N $\epsilon 2$ face of the Cu(I) ligand in *M. tuberculosis* CsoR and Glu86 (Fig. 32A, Fig 40C-D). In this model, Lys32 would not be involved in ligand discrimination, rather, this residue may function allosterically in CstR. In this scenario, the K32D mutant could react with a per- or polysulfide donor but the reaction no longer results in negative regulation of DNA binding. This is supported by the wild-type-like growth of the K32A substitution that successfully complements the $\Delta cstR$ *S. aureus* strain. Experiments to test this hypothesis are currently underway.

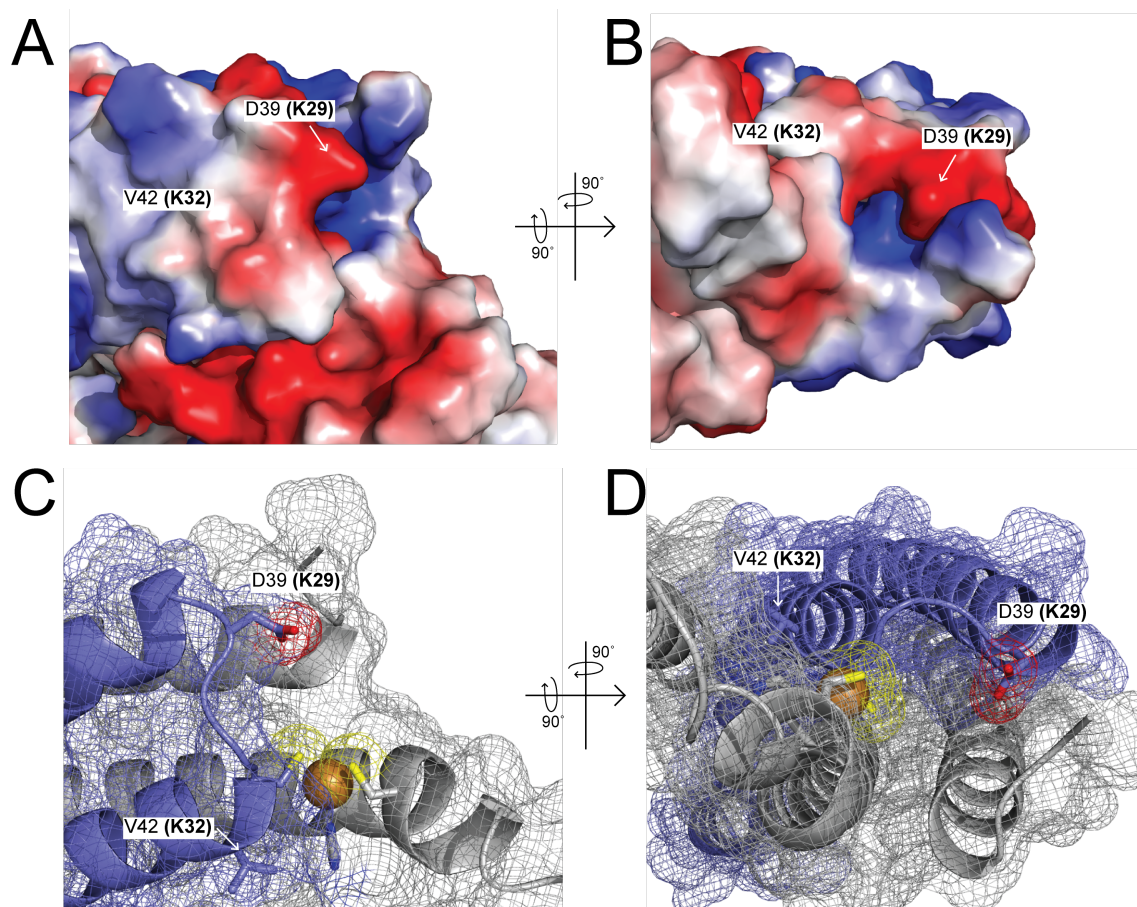


Figure 40. Analysis of the electrostatics near CsoR Cu(I) binding pocket. (A-B) Electrostatic representation near the Cu(I) binding pocket of *M. tuberculosis* CsoR.¹⁴⁴ (C-D) Mesh cartoon of the residues near the Cu(I) binding pocket. An aspartate is located directly above the N-terminal cysteine in CsoR. In CstR, the aspartate is a lysine residue (Lys29). The difference of an aspartate vs lysine may provide an electrostatic basis for ligand discrimination between these paralogous regulators. Val39 in CsoR is buried in the dimer-dimer interface. Residues given are for *S. aureus* CsoR and in bold are the corresponding residues for CstR.

CHAPTER V

SUMMARY AND PROSPECTIVE

SUMMARY

Sulfur is essential for many cellular components including cysteine, methionine, glutathione and related low molecular weight (LMW) thiols, biotin, molybdopterin, lipoic acid, and others.¹⁶³ These provide the basis for catalysis, protein structure, metal binding, and signaling. Cells have evolved mechanisms to acquire and then incorporate sulfur into these components. The major form of sulfur trafficked in the cell is generally accepted to be in the form LMW per- and polysulfides.¹ These are comprised of hydrodisulfides or persulfides (RSSH), hydropolysulfides (RS(S_n)SH), and polysulfides, (RS(S_n)SR) that are derived from organic LMW thiols, RSH, *e.g.*, glutathione.¹²⁹ These species are collectively known as reactive sulfur species (RSS) and were recently shown to accumulate to levels greater than 100 μ M.¹ RSS also includes other sulfur species such as hydrogen sulfide (H₂S).

The enzymatic production of LMW per- and polysulfides has been linked to the catabolism of cysteine by the action of the enzymes cystathionine β -synthase (CBS) and cystathionine γ -lyase (CSE).¹ The LMW per- and polysulfides are thought to undergo a reversible *S*-sulfhydration exchange reaction with protein-based thiols.^{127,181} At increasing concentrations, these species become toxic and poison cytochrome c oxidase of the electron transport chain and likely perturb other metal centers.¹¹³ This necessitates a detoxification system to maintain cellular homeostasis of RSS. This system has been well characterized in mammalian mitochondria and ultimately leads to a formal oxidation

state change of the central sulfur atom from S^{2-} to S^{6+} in both sulfate or thiosulfate.^{113,118,123} The underlying mechanisms that control the homeostasis of these species are poorly understood in bacteria.

In this dissertation, we establish that CstR is a persulfide- and polysulfide-sensing transcriptional repressor in *S. aureus*. CstR controls the expression of the *cst* operon⁶ that encodes what appears to be a complete sulfide oxidation system. Under conditions of acute sulfide toxicity, as Na_2S , $NaHS$ or Na_2S_4 , the downstream *cst* operon genes *cstA*, *cstB*, and *sqr* are strongly transcriptionally induced and are required for culture viability. Induction of the *cst* operon requires both cysteine residues in CstR to initiate a transcriptional response and mitigate sulfide stress. Mutation of cysteine residues in CstR results in failure to respond to sulfide stress and loss of culture viability.¹³

After establishing sulfide stress as an inducer of the *cst* operon, we pursued *in vitro* experiments with CstR to provide insight into potential *in vivo* species that are capable of reacting with CstR. Many very recent insights from the literature^{1,127,130} indicated that cysteine thiols do not react directly with sulfide (HS^-) and as expected, CstR does not react directly with sulfide. However, we establish that CstR reacts with an inorganic polysulfide (Na_2S_4) or an organic persulfide, GSSH, harboring more oxidized sulfur atoms to form a series of cross-linked adducts that contain 0-4 sulfur atoms that were assigned as di-, tri-, and tetrasulfides between Cys31 and Cys60' of CstR by high-resolution tandem mass spectrometry. These modifications were shown to negatively regulate DNA binding *in vitro*.¹³ Although the precise *in vivo* inducer is unknown, the sum of these experiments suggests that CstR likely senses per- and polysulfides in the

cell. These species can be formed non-enzymatically by reacting with metals, ROS, or oxidized LMW thiol species, e.g., BSSB.^{1,44,127}

In our model of *S. aureus* sulfide stress and homeostasis, per- and polysulfides are sensed through the cysteine residues in CstR, which leads to transcriptional derepression of the *cst* operon, the gene products of which provide *S. aureus* with a sulfide detoxification system (Fig. 41). Indeed, recent work published by our lab reveals that CstA is a sulfur transferase that reacts directly with both a protein-based persulfide and LMW per- and polysulfides to “consume” these highly reactive species. Further studies are required to identify the precise chemical nature of the cellular adducts of CstR in sulfide-stressed cells. In addition, characterization of the LMW pool of per- and polysulfides will provide insight on possible species sensed by CstR in the cell.

S. aureus encodes two CsoR family transcriptional regulators; a *bona fide* copper-sensing CsoR and the per- and polysulfide-sensing CstR.⁶ These proteins share a high degree of similarity and it was of interest to understand the basis for ligand discrimination of these paralogous repressors. Early work with CstR established that perturbation of Cys31 was both necessary and sufficient to negatively regulate DNA binding *in vitro*.¹⁶² This led us to hypothesize that the intrinsic reactivity of this cysteine may be greater than that of the analogous residue, Cys41, in CsoR, thus endowing CstR with the specific ability to react with per- and polysulfides. Indeed, Cys31 in CstR is approximately 50-fold more reactive than Cys41 in CsoR toward the neutral alkylating reagent NEM at pH 7.0. Experiments used to estimate the pK_a indicate that Cys31 of CstR is ≈ 8.6 , similar to a free cysteine thiol, and Cys41 of CsoR is ≈ 9.3 .

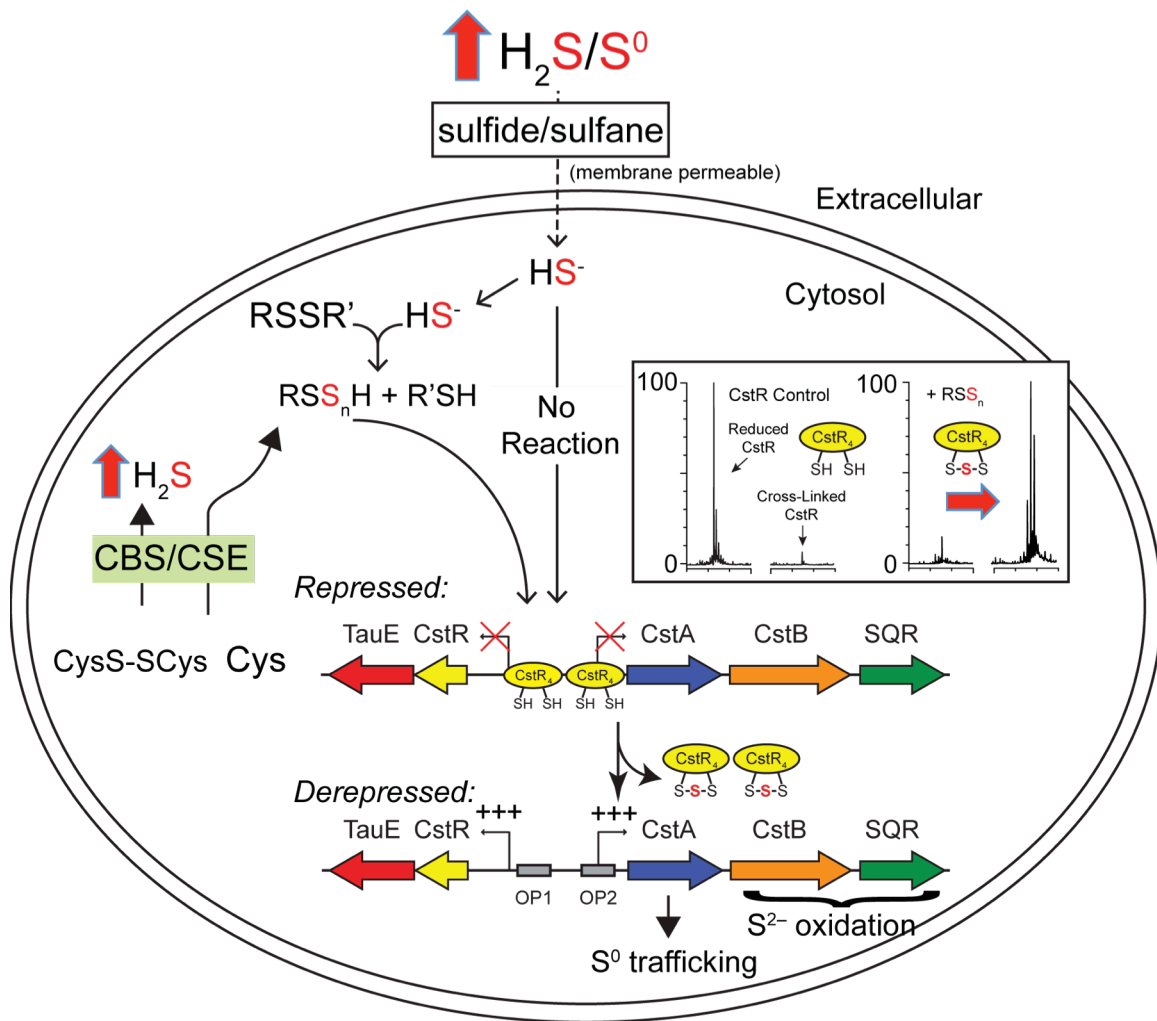


Figure 41. Model of sulfide homeostasis in *S. aureus*. In this model, sulfide stress leads to the formation of increased levels of intracellular RSS, specifically per- and polysulfides. These species can also be produced enzymatically by the action of CBS and CSE. Per- and/or polysulfides then react with CstR to form a series of di-, tri-, and tetrasulfide crosslinked species *in vitro*. The *in vivo* adducts of CstR are currently unknown but the reaction of CstR with these species leads to transcriptional derepression of the *cst* operon, which has been shown to be required to mitigate sulfide toxicity *in vivo*.

Residues near the N-terminal cysteine in CstRs are more positively charged, (G/E/D)-(K/R)-D-³¹C-K, while CsoRs cluster more negatively charged residues, D-Φ-Y-⁴¹C-D-D (Φ, hydrophobic). This difference lead us to hypothesize that the lysine residues may be involved in either tuning the pK_a and therefore the intrinsic reactivity of Cys31 in CstR allosterically or electrostatically tuning the binding pocket. Substitutions of lysine mutants near Cys31 of CstR to alanine or aspartate to create K29A, K29D, K32A, or K32D CstRs, did not strongly alter cysteine reactivity at pH 7.0. This suggests that neither lysine residue is involved in tuning the pK_a, a finding consistent with an experimentally determined pK_a that is near that of a typical sulfhydryl. However, *in vivo* experiments indicate that these lysine substitutions are functionally important. Of all of the substitution mutants, only a strain expressing K32A CstR is viable when stressed with sulfide. In contrast, a strain expressing a K29A substitution mutant is not viable *in vivo*. Neither charge reversal mutant, K29D or K32D CstRs, are viable either. Although K29D CstR does not bind to *cst* operator DNA with high affinity *in vitro*. Lys32 may be required for efficient allosteric switching upon di-, tri-, and tetrasulfide bond formation following reaction with a LMW per- or polysulfides, which may be unable to drive dissociation from the operator DNA. The sum of these experiments leads us to a hypothesis in which Lys29 provides the necessary electrostatics to allow for a Cys31 reaction with a per- or polysulfide donor while Lys32 may be in some way involved in allosteric negative regulation of DNA binding.

PROSPECTIVES

The cst operon and oxygen limiting conditions. Under conditions of low oxygen tension, sulfide has been identified as a growth-limiting determinant¹⁸ through poisoning cytochrome c oxidase and likely other metal-containing proteins in the cell. This necessitates a detoxification system to remove excess sulfide to prevent toxicity and maintain homeostasis. In the plant pathogen *A. tumefaciens*, loss of the sole sulfur dioxygenase (SDO), which corresponds to CstB in *S. aureus*, results in a loss of cellular viability when stressed with sulfide. Conversely, overexpression of the SDO resulted in increased viability. In *S. aureus*, the *cst* operon functions to mitigate the effects of sulfide toxicity (see Chapter 3) and we sought to determine the growth characteristics under low oxygen, or microaerophilic, conditions. To this end, *S. aureus* was grown in HHWm+TS and supplemented with nitrate (NO_3^-) to serve as the terminal electron acceptor. Under these conditions, sodium hydrosulfide is markedly more toxic and growth inhibition occurs at 5% of the concentration used in aerobic cultures, or 0.01 mM vs. 0.2 mM NaHS, respectively (Fig. 42A, compare to Fig. 22A, Chapter 3). To probe this further, we performed the same experiment with the ΔcstR *S. aureus* strain and observe a growth phenotype in which cells recover much more rapidly (Fig. 42B). This result is exactly opposite of our growth curve experiments performed under aerobic conditions (see Fig. 22A, Chapter 3). Conditions of low oxygen tension require *S. aureus* to adapt to a new environmental niche but does not necessarily result in induction of the *cst* operon.²⁰⁴ However, the molecular machinery under these conditions may be more sensitive to sulfide stress.

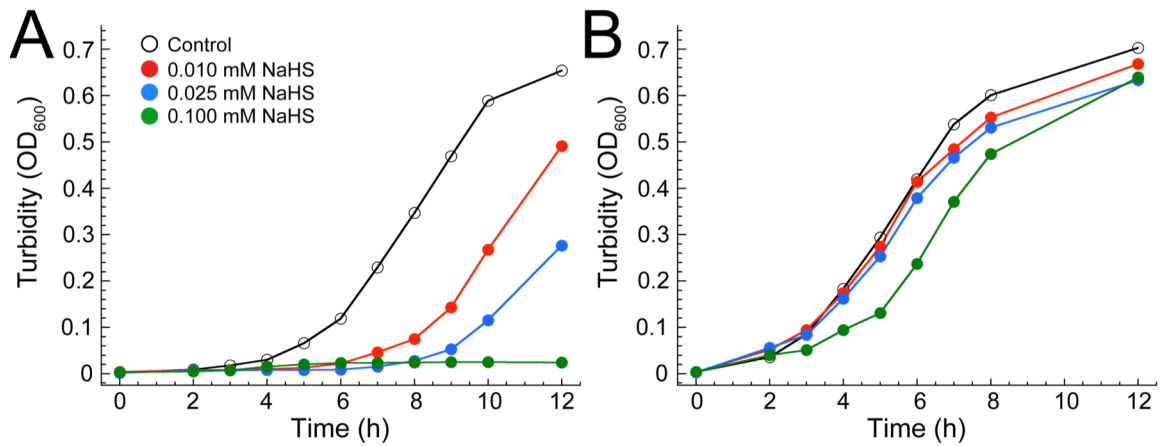


Figure 42. Growth of *S. aureus* under low oxygen conditions and sulfide stress. Under microaerophilic growth conditions, deletion of *cstR* results in an enhanced growth phenotype in the presence of NaHS stress. Growth curves of WT (A) and $\Delta cstR$ (B) *S. aureus* strains grown in the absence (open symbols) or presence (closed symbols) NaHS stress. Under oxygen limiting conditions, *S. aureus* is significantly more susceptible to sulfide stress. In the presence of increased expression of the *cst* operon (see Fig. 24, Chapter 3), $\Delta cstR$ *S. aureus* is less susceptible to sulfide stress. Conditions: HHWm+TS+NO₃⁻, microaerophilic, ±NaHS.

The cst operon and nitroxyl resistance. In a microarray study conducted prior to the discovery of CstR,⁶ the *cst* operon in *S. aureus* N315 strain was among the most highly induced operons, induced ≈ 30 -fold relative to cells in the absence of nitrite (Fig. 43A). In this study, *S. aureus* was grown anaerobically in a biofilm with nitrate (NO_3^-) as the terminal electron source and stressed with excess sodium nitrite (NO_2^-). Under these conditions, cells experience increased levels of NO stress from the reduction of nitrate and nitrite during anaerobic respiration,^{190,205} neither of which induce the *cst* operon under aerobic growth conditions (see Fig. 24, Chapter 3).^{13,189,206} This results in an induction of a general oxidative and nitrosative stress response, as well as high iron, which leads to the impairment of polysaccharide intercellular adhesion (PIA) synthesis and inhibition or dispersal of existing biofilms. Furthermore, these effects were promoted by slightly acidic pH and were found to be quenched by the addition of nitric oxide (NO) scavengers.¹⁹⁰ NO has since been shown to play a role in biofilm dispersal of *Pseudomonas aureginosa*²⁰⁷ and other bacteria²⁰⁸ through an unknown mechanism. The reason for the strong induction of *cst* operon is not readily apparent but may be related to controlling the interplay between hydrogen sulfide and nitric oxide. Emerging studies have demonstrated that HS^- and NO rapidly react, ultimately leading to the production of nitroxyl (HNO) (see Chapter 1).⁸⁷ One exciting possibility is that under conditions of elevated NO,¹⁹⁰ increased endogenous or exogenous sulfide converge to form thionitrous acid (HSNO), nitroxyl (HNO), and possibly polysulfides (Fig. 43B).^{86,89} Nitroxyl readily reacts with cysteine residues to form an *N*-hydroxysulfenamide which can be resolved by a second cysteine to form a disulfide bond and hydroxylamine (see Fig. 3, Chapter 1).^{84,87,88} The observation that sulfide and nitric oxide react to ultimately form

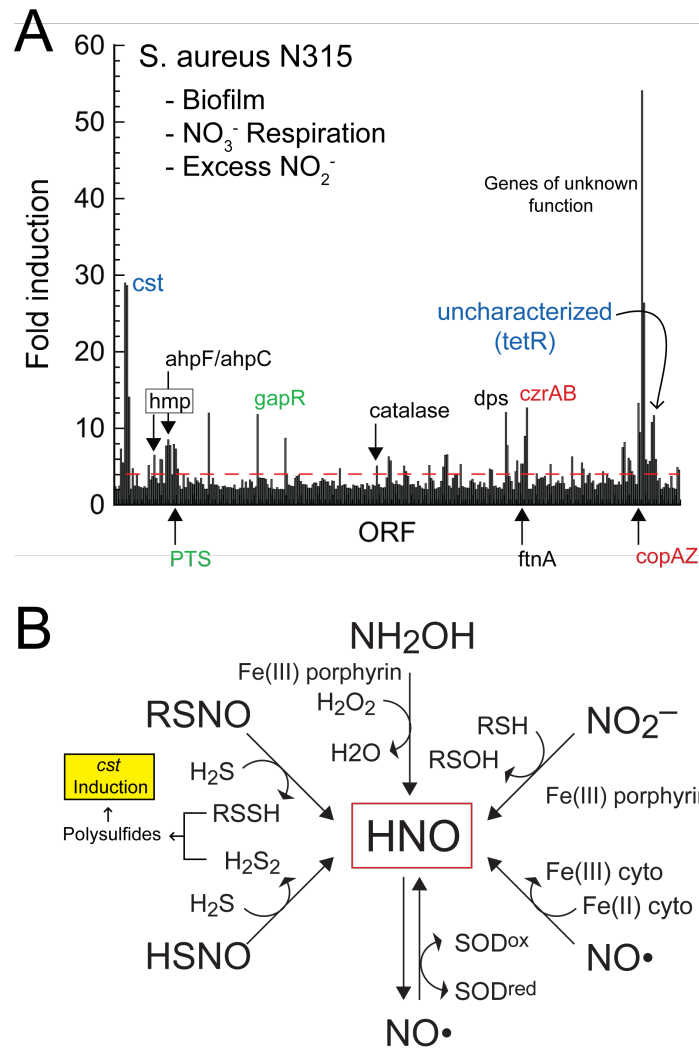


Figure 43. The *cst* operon is induced under biofilm growth conditions with nitrite stress. (A) Microarray data adapted from Schlag, et al. (2007).¹⁹⁰ The *cst* operon is one of the most highly induced operons under these conditions. (B) Intersection of nitrosative and RSS stressors ultimately lead to nitroxyl formation. Adapted from Wrobel, et al. (2014).²⁰⁹

nitroxyl introduces new complexity in the signaling roles of these compounds and the influence of nitroxyl on microorganisms is completely uncharacterized.

These studies make the prediction that CstR may sense nitroxyl directly. To this end, we performed growth curve and qRT-PCR experiments to assess if the *cst* operon is involved in HNO sensing and mitigation of HNO toxicity. WT and $\Delta cstR:CstR^{C31AC60A}$ *S. aureus* strains were grown in HHWm+TS in the presence or absence of 0.15 mM HNO stress introduced as Angelis Salt (Fig. 44A). These results indicate that failure to express the *cst* operon is deleterious to culture viability under conditions of HNO stress. To test if HNO stress induces the *cst* operon, qRT-PCR experiments were carried out. Indeed, HNO induces the *cst* operon in a manner similar to sulfide stress (Fig. 44b, compare with Fig. 24, Chapter 3). The functional implication of these results is not yet known but may be involved in biofilm dispersal. These observations speak to the strong interconnectedness of various reactive oxidative small molecule species and the difficulty in separating cellular signaling, cytoprotective roles, and toxicity. The intersection of microbiology and transcriptomics, mass spectrometry-based proteomics and metabolomics approaches, and structural biology promises new insights and understanding of redox biology at the host-pathogen interface.^{1,13,18,118,192}

There is much to be learned regarding our understanding sulfide stress and homeostasis and the chemistry involved in these processes. The ongoing development of mass spectrometry (MS)-based thiol proteomic approaches²¹⁰ that can be used to identify and quantify on a proteome-wide scale, a specific PTM^{ox} in response to a specific stressor, promises new insights into the cellular response to oxidative insult. These methods, in principal, will also allow the direct determination of the specific thiol

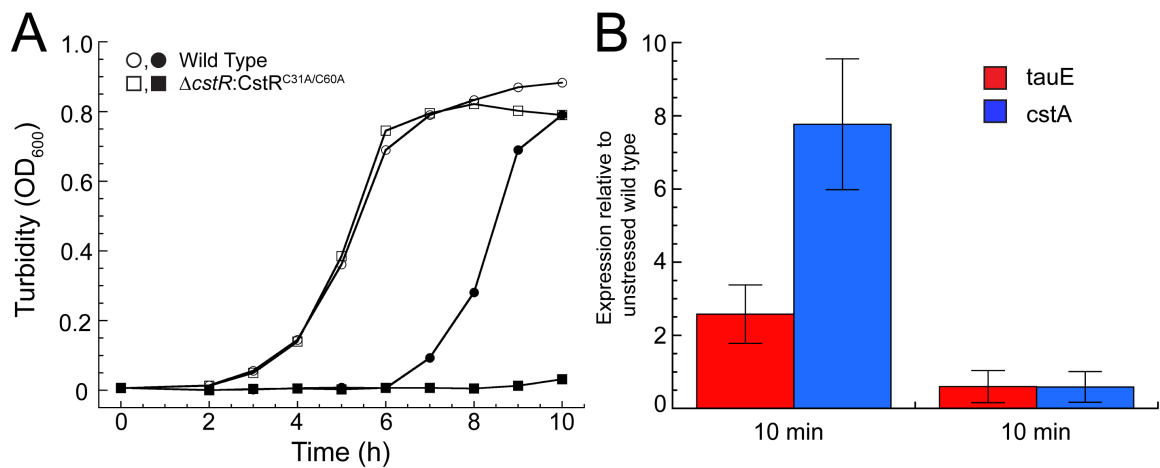


Figure 44. The *cst* operon is required for nitroxyl stress resistance. (A) Growth curves of WT (circles) and $\Delta cstR:CstR^{C31A/C60A}$ (squares) *S. aureus* grown in the absence (open symbols) or presence (closed symbols) of 0.15 mM nitroxyl (HNO). Cells were grown aerobically in HHWm+TS at 37 °C with shaking and data points correspond to a single representative growth curve. (B) Quantitative RT-PCR experiments for WT *S. aureus* cultures grown to an OD₆₀₀ of 0.2 and challenged with 0.15 mM HNO added to the growth medium $t=0$. Aliquots for analysis were collected at 10 and 30 min post addition. It is unknown if CstR react with HNO directly but HNO has been shown to rapidly react with protein cysteine thiols.⁸⁷

modifications of transcriptional regulatory proteins in bacterial cells. More importantly, they will allow the elucidation of the degree of global overlap among a number of distinct PTM^{ox} events, *e.g.*, sulfenylation²¹¹ vs. *S*-sulphydration^{1,127} vs. *S*-nitrosation.^{212,213} Indeed, the precise factors that control the specificity of a particular thiol for a given oxidant, beyond simple tuning of the global reactivity, remain incompletely understood. Although operon inducer specificity can be readily probed using conventional qRT-PCR¹³ and related proteomics approaches, structural methods and direct determination of PTM^{ox} in regulatory proteins isolated from cells^{10,214} will become critically important and are the subject of future work in our understanding of this area.

REFERENCES

- 1 Ida, T. *et al.* Reactive cysteine persulfides and S-polythiolation regulate oxidative stress and redox signaling. *Proc. Natl. Acad. Sci. U.S.A.* **111**, 7606-7611 (2014).
- 2 Lin, V. S., Chen, W., Xian, M. & Chang, C. J. Chemical probes for molecular imaging and detection of hydrogen sulfide and reactive sulfur species in biological systems. *Chem. Soc. Rev.*, doi:10.1039/C4CS00298A (2015).
- 3 Imlay, J. A. The molecular mechanisms and physiological consequences of oxidative stress: lessons from a model bacterium. *Nat. Rev. Micro.* **11**, 443-454 (2013).
- 4 Gray, M. J., Wholey, W.-Y. & Jakob, U. Bacterial responses to reactive chlorine species. *Annu. Rev. Microbiol.* **67**, 141-160 (2013).
- 5 Toledo, J. C. & Augusto, O. Connecting the chemical and biological properties of nitric oxide. *Chem. Res. Toxicol.* **25**, 975-989 (2012).
- 6 Grosseohme, N. E., Kehl-Fie, T. E., Ma, Z., Adams, K. W., Cowart, D. M., Scott, R. A., Skaar, E. P., Giedroc, D. P. Control of copper resistance and inorganic sulfur metabolism by paralogous regulators in *Staphylococcus aureus*. *J. Bio. Chem.* **286**, 13522-13531 (2011).
- 7 Robinson, J. Phagocytic leukocytes and reactive oxygen species. *Histochem. Cell Biol.* **131**, 465-469 (2009).
- 8 Bhat, S. A. *et al.* The mechanism of redox sensing in *Mycobacterium tuberculosis*. *Free Radic. Biol. Med.* **53**, 1625-1641 (2012).
- 9 Kumar, A. *et al.* Redox homeostasis in mycobacteria: the key to tuberculosis control? *Exper. Rev. Mol. Med.* **13**, e39 (2011).
- 10 Lee, J. W. & Helmann, J. D. The PerR transcription factor senses H₂O₂ by metal-catalysed histidine oxidation. *Nature* **440**, 363-367 (2006).
- 11 Kiley, P. J. & Beinert, H. The role of Fe-S proteins in sensing and regulation in bacteria. *Curr. Opin. Microbiol.* **6**, 181-185 (2003).
- 12 Watanabe, S., Kita, A., Kobayashi, K. & Miki, K. Crystal structure of the [2Fe-2S] oxidative-stress sensor SoxR bound to DNA. *Proc. Natl. Acad. Sci. U.S.A.* **105**, 4121-4126 (2008).
- 13 Luebke, J. L. *et al.* The CsoR-like sulfurtransferase repressor (CstR) is a persulfide sensor in *Staphylococcus aureus*. *Mol. Microbiol.* (2014).

- 14 Chim, N., Johnson, P. M. & Goulding, C. W. Insights into redox sensing metalloproteins in *Mycobacterium tuberculosis*. *J. Inorg. Biochem.* **133**, 118-126 (2014).
- 15 Brekasis, D. & Paget, M. S. A novel sensor of NADH/NAD⁺ redox poise in *Streptomyces coelicolor* A3(2). *EMBO J.* **22**, 4856-4865 (2003).
- 16 Vesić, D. & Kristich, C. J. A rex family transcriptional repressor influences H₂O₂ accumulation by *Enterococcus faecalis*. *J. Bacteriol.* **195**, 1815-1824 (2013).
- 17 Baker, J. L. *et al.* *Streptococcus mutans* NADH oxidase lies at the intersection of overlapping regulons controlled by oxygen and NAD⁺ levels. *J. Bacteriol.* **196**, 2166-2177 (2014).
- 18 Guimarães, B. G. *et al.* Plant pathogenic bacteria utilize biofilm growth-associated repressor (BigR), a novel winged-helix redox switch, to control hydrogen sulfide detoxification under hypoxia. *J. Biol. Chem.* **286**, 26148-26157 (2011).
- 19 Chen, H. *et al.* The *Pseudomonas aeruginosa* multidrug efflux regulator MexR uses an oxidation-sensing mechanism. *Proc. Natl. Acad. Sci. U.S.A.* **105**, 13586-13591 (2008).
- 20 Poor, C. B., Chen, P. R., Duguid, E., Rice, P. A. & He, C. Crystal structures of the reduced, sulfenic acid, and mixed disulfide forms of SarZ, a redox active global regulator in *Staphylococcus aureus*. *J. Biol. Chem.* **284**, 23517-23524 (2009).
- 21 Ji, Q. *et al.* Molecular mechanism of quinone signaling mediated through S-quinonization of a YodB family repressor QsrR. *Proc. Natl. Acad. Sci. U.S.A.* **110**, 5010-5015 (2013).
- 22 Drazic, A. & Winter, J. The physiological role of reversible methionine oxidation. *Biochim. Biophys. Acta* **1844**, 1367-1382 (2014).
- 23 Drazic, A. *et al.* Methionine oxidation activates a transcription factor in response to oxidative stress. *Proc. Natl. Acad. Sci. U.S.A.* **110**, 9493-9498 (2013).
- 24 Newton, G. L., Ta, P. & Fahey, R. C. A mycothiol synthase mutant of *Mycobacterium smegmatis* produces novel thiols and has an altered thiol redox status. *J. Bacteriol.* **187**, 7309-7316 (2005).
- 25 Newton, G. L. *et al.* Bacillithiol is an antioxidant thiol produced in *Bacilli*. *Nat. Chem. Biol.* **5**, 625-627 (2009).

- 26 Potter, A. J., Trappetti, C. & Paton, J. C. *Streptococcus pneumoniae* uses glutathione to defend against oxidative stress and metal ion toxicity. *J. Bacteriol.* **194**, 6248-6254 (2012).
- 27 Hwang, C., Sinskey, A. J. & Lodish, H. F. Oxidized redox state of glutathione in the endoplasmic-reticulum. *Science* **257**, 1496-1502 (1992).
- 28 Sharma, S. V. *et al.* Biophysical features of bacillithiol, the glutathione surrogate of *Bacillus subtilis* and other firmicutes. *ChemBioChem* **14**, 2160-2168 (2013).
- 29 Ordóñez, E. *et al.* Arsenate reductase, mycothiol, and mycoredoxin concert thiol/disulfide exchange. *J. Biol. Chem.* **284**, 15107-15116 (2009).
- 30 Van Laer, K. *et al.* Mycoredoxin-1 is one of the missing links in the oxidative stress defence mechanism of Mycobacteria. *Mol. Microbiol.* **86**, 787-804 (2012).
- 31 Gaballa, A. *et al.* Redox regulation in *Bacillus subtilis*: the bacilliredoxins BrxA(YphP) and BrxB(YqiW) function in de-bacillithiolation of S-bacillithiolated OhrR and MetE. *Antioxid. Redox Signal.* **21**, 357-367 (2014).
- 32 delCardayré, S. B., Stock, K. P., Newton, G. L., Fahey, R. C. & Davies, J. E. Coenzyme A disulfide reductase, the primary low molecular weight disulfide reductase from *Staphylococcus aureus* : purification and characterization of the native enzyme. *J. Biol. Chem.* **273**, 5744-5751 (1998).
- 33 Hirose, K., Ezaki, B., Liu, T. & Nakashima, S. Diamide stress induces a metallothionein BmtA through a repressor BxmR and is modulated by Zn-inducible BmtA in the cyanobacterium *Oscillatoria brevis*. *Toxicol. Lett.* **163**, 250-256 (2006).
- 34 Tottey, S. *et al.* Cyanobacterial metallochaperone inhibits deleterious side reactions of copper. *Proc. Natl. Acad. Sci. U.S.A.* **109**, 95-100 (2012).
- 35 Ma, Z. *et al.* Bacillithiol is a major buffer of the labile zinc pool in *Bacillus subtilis*. *Mol. Microbiol.*, n/a-n/a (2014).
- 36 Arunkumar, A. I., Campanello, G. C. & Giedroc, D. P. Solution structure of a paradigm ArsR family zinc sensor in the DNA-bound state. *Proc. Natl. Acad. Sci. U.S.A.* **106**, 18177-18182 (2009).
- 37 Foster, A. W., Osman, D. & Robinson, N. J. Metal preferences and metallation. *J. Biol. Chem.* **289**, 28095-28103 (2014).
- 38 Marino, S. M. & Gladyshev, V. N. Cysteine function governs its conservation and degeneration and restricts Its utilization on protein surfaces. *J. Molec. Biol.* **404**, 902-916 (2010).

- 39 Marino, S. M. & Gladyshev, V. N. Analysis and functional prediction of reactive cysteine residues. *J. Biol. Chem.* **287**, 4419-4425 (2012).
- 40 Salsbury, F. R., Knutson, S. T., Poole, L. B. & Fetrow, J. S. Functional site profiling and electrostatic analysis of cysteines modifiable to cysteine sulfenic acid. *Protein Sci.* **17**, 299-312 (2008).
- 41 Roos, G., Foloppe, N. & Messens, J. Understanding the pK_a of redox cysteines: the key role of hydrogen bonding. *Antioxid. Redox Signal.* **18**, 94-127 (2012).
- 42 Winterbourn, C. C. & Metodiewa, D. Reactivity of biologically important thiol compounds with superoxide and hydrogen peroxide. *Free Rad. Biol. Med.* **27**, 322-328 (1999).
- 43 Ferrer-Sueta, G. *et al.* Factors affecting protein thiol reactivity and specificity in peroxide reduction. *Chem. Res. Toxicol.* **24**, 434-450 (2011).
- 44 Reddie, K. G. & Carroll, K. S. Expanding the functional diversity of proteins through cysteine oxidation. *Curr. Opin. Chem. Biol.* **12**, 746-754 (2008).
- 45 Seo, Y. H. & Carroll, K. S. Quantification of protein sulfenic acid modifications using isotope-coded dimedone and iododimedone. *Angew Chem. Int. Ed.* **50**, 1342-1345 (2011).
- 46 Yin, Q. *et al.* In situ visualization and detection of protein sulfenylation responses in living cells through a dimedone-based fluorescent probe. *Org. Biomol. Chem.* **11**, 7566-7573 (2013).
- 47 Perkins, A., Poole, L. B. & Karplus, P. A. Tuning of peroxiredoxin catalysis for various physiological roles. *Biochemistry* **53**, 7693-7705 (2014).
- 48 Lee, J.-W., Soonsanga, S. & Helmann, J. D. A complex thiolate switch regulates the *Bacillus subtilis* organic peroxide sensor OhrR. *Proc. Natl. Acad. Sci. U.S.A.* **104**, 8743-8748 (2007).
- 49 Antelmann, H. & Helmann, J. D. Thiol-based redox switches and gene regulation. *Antioxid. Redox Signal.* **14**, 1049-1063 (2010).
- 50 Paget, M. S. & Buttner, M. J. Thiol-based regulatory switches. *Annu. Rev. Genet.* **37**, 91-121 (2003).
- 51 Ung, K. S. & Av-Gay, Y. Mycothiol-dependent mycobacterial response to oxidative stress. *FEBS Lett.* **580**, 2712-2716 (2006).
- 52 Pother, D.-C. *et al.* Diamide triggers mainly S-thiolations in the cytoplasmic proteomes of *Bacillus subtilis* and *Staphylococcus aureus*. *J. Bacteriol.* **191**, 7520-7530 (2009).

- 53 Dalle-Donne, I., Rossi, R., Colombo, G., Giustarini, D. & Milzani, A. Protein S-glutathionylation: a regulatory device from bacteria to humans. *Trends Biochem. Sci.* **34**, 85-96 (2009).
- 54 Chi, B. K. *et al.* S-Bacillithiolation Protects Against Hypochlorite Stress in *Bacillus subtilis* as Revealed by Transcriptomics and Redox Proteomics. *Mol. Cell. Proteomics* **10**, doi:10.1074/mcp.M111.009506 (2011).
- 55 Chi, B. K. *et al.* S-Bacillithiolation Protects Conserved and Essential Proteins Against Hypochlorite Stress in Firmicutes Bacteria. *Antioxid. Redox Signal.* **18**, 1273-1295 (2012).
- 56 Chi, B. K. *et al.* Protein S-Mycothioloation Functions as Redox-Switch and Thiol Protection Mechanism in *Corynebacterium glutamicum* Under Hypochlorite Stress. *Antioxid. Redox Signal.* **20**, 589-605 (2014).
- 57 Cole, J., Aberdein, J., Jubrail, J. & Dockrell, D. H. The role of macrophages in the innate immune response to *Streptococcus pneumoniae* and *Staphylococcus aureus*: mechanisms and contrasts. *Adv. Microb. Physiol.* **Volume 65**, 125-202 (2014).
- 58 Kolaczowska, E. & Kubes, P. Neutrophil recruitment and function in health and inflammation. *Nat. Rev. Immunol.* **13**, 159-175 (2013).
- 59 Joshua, M. & Thomas, A. C. Nitric oxide synthase: non-canonical expression patterns. *Front. Immunol.* **5** (2014).
- 60 Klebanoff, S. J., Kettle, A. J., Rosen, H., Winterbourn, C. C. & Nauseef, W. M. Myeloperoxidase: a front-line defender against phagocytosed microorganisms. *J. Leukoc. Biol.* **93**, 185-198 (2013).
- 61 Klebanoff, S. J. Myeloperoxidase: friend and foe. *J. Leukoc. Biol.* **77**, 598-625 (2005).
- 62 Winterbourn, C. C. & Kettle, A. J. Redox Reactions and microbial killing in the neutrophil phagosome. *Antioxid. Redox Signal.* **18**, 642-660 (2013).
- 63 Lee, K.-A. *et al.* Bacterial-derived uracil as a modulator of mucosal immunity and gut-microbe homeostasis in *Drosophila*. *Cell* **153**, 797-811 (2013).
- 64 Pacelli, R. *et al.* Nitric-oxide potentiates hydrogen peroxide-induced killing of *Escherichia coli*. *J. Exp. Med.* **182**, 1469-1479 (1995).
- 65 Brownpeterson, N. J. & Salin, M. L. Purification and characterization of a mesohalic catalase from the halophilic bacterium *Halobacterium halobium*. *J. Bacteriol.* **177**, 378-384 (1995).

- 66 Gardner, P. R. & Fridovich, I. Superoxide sensitivity of the *Escherichia coli* aconitase. *J. Biol. Chem.* **266**, 19328-19333 (1991).
- 67 Roots, R. & Okada, S. Estimation of life times and diffusion distances of radicals involved in X-ray-induced DNA strand breaks or killing of mammalian-cells. *Radiat. Res.* **64**, 306-320 (1975).
- 68 Grek, C. L., Zhang, J., Manevich, Y., Townsend, D. M. & Tew, K. D. Causes and consequences of cysteine *S*-glutathionylation. *J. Biol. Chem.* **288**, 26497-26504 (2013).
- 69 Keyer, K. & Imlay, J. A. Superoxide accelerates DNA damage by elevating free-iron levels. *Proc. Natl. Acad. Sci. U.S.A.* **93**, 13635-13640 (1996).
- 70 Balasubramanian, B., Pogożelski, W. K. & Tullius, T. D. DNA strand breaking by the hydroxyl radical is governed by the accessible surface areas of the hydrogen atoms of the DNA backbone. *Proc. Natl. Acad. Sci. U.S.A.* **95**, 9738-9743 (1998).
- 71 Cooke, M. S., Evans, M. D., Dizdaroglu, M. & Lunec, J. Oxidative DNA damage: mechanisms, mutation, and disease. *FASEB J.* **17**, 1195-1214 (2003).
- 72 Sundaresan, M., Yu, Z. X., Ferrans, V. J., Irani, K. & Finkel, T. Requirement for generation of H₂O₂ for platelet-derived growth-factor signal-transduction. *Science* **270**, 296-299 (1995).
- 73 Ding, H., Hidalgo, E. & Dimple, B. The redox state of the [2Fe-2S] clusters in SoxR protein regulates its activity as a transcription factor. *J. Biol. Chem.* **271**, 33173-33175 (1996).
- 74 Gu, M. & Imlay, J. A. The SoxRS response of *Escherichia coli* is directly activated by redox-cycling drugs rather than by superoxide. *Mol. Microbiol.* **79**, 1136-1150 (2011).
- 75 Krapp, A. R., Humbert, M. V. & Carrillo, N. The *soxRS* response of *Escherichia coli* can be induced in the absence of oxidative stress and oxygen by modulation of NADPH content. *Microbiology* **157**, 957-965 (2011).
- 76 Siedler, S. *et al.* SoxR as a single-cell biosensor for NADPH-consuming enzymes in *Escherichia coli*. *ACS Synth. Biol.* **3**, 41-47 (2013).
- 77 Helmann, J. D. *et al.* The global transcriptional response of *Bacillus subtilis* to peroxide stress is coordinated by three transcription factors. *J. Bacteriol.* **185**, 243-253 (2003).
- 78 Traore, D. A. K. *et al.* Structural and functional characterization of 2-oxo-histidine in oxidized PerR protein. *Nat. Chem. Biol.* **5**, 53-59 (2009).

- 79 Imlay, J. A. Cellular defenses against superoxide and hydrogen peroxide. *Annu. Rev. Biochem.* **77**, 755-776 (2008).
- 80 Dubbs, J. M. & Mongkolsuk, S. Peroxide-sensing transcriptional regulators in bacteria. *J. Bacteriol.* **194**, 5495-5503 (2012).
- 81 Ignarro, L. J., Buga, G. M., Wood, K. S., Byrns, R. E. & Chaudhuri, G. Endothelium-derived relaxing factor produced and released from artery and vein is nitric oxide. *Proc. Natl. Acad. Sci. U.S.A.* **84**, 9265-9269 (1987).
- 82 Wink, D. A. *et al.* Reaction kinetics for nitrosation of cysteine and glutathione in aerobic nitric oxide solutions at neutral pH. Insights into the fate and physiological effects of intermediates generated in the NO/O₂ reaction. *Chem. Res. Toxicol.* **7**, 519-525 (1994).
- 83 Lancaster, J. R. Nitroxidative, nitrosative, and nitrative stress: kinetic predictions of reactive nitrogen species chemistry under biological conditions. *Chem. Res. Toxicol.* **19**, 1160-1174 (2006).
- 84 Fukuto, J. M., Switzer, C. H., Miranda, K. M. & Wink, D. A. Nitroxyl (HNO): chemistry, biochemistry, and pharmacology. *Annu. Rev. Pharmacol. Toxicol.* **45**, 335-355 (2005).
- 85 Fukuto, J. M. & Carrington, S. J. HNO signaling mechanisms. *Antioxid. Redox Signal.* **14**, 1649-1657 (2011).
- 86 Filipovic, M. R. *et al.* Beyond H₂S and NO interplay: hydrogen sulfide and nitroprusside react directly to give nitroxyl (HNO). A new pharmacological source of HNO. *J. Med. Chem.* **56**, 1499-1508 (2013).
- 87 Eberhardt, M. *et al.* H₂S and NO cooperatively regulate vascular tone by activating a neuroendocrine HNO–TRPA1–CGRP signalling pathway. *Nat. Commun.* **5** (2014).
- 88 Wong, P. S. Y. *et al.* Reaction between *S*-nitrosothiols and thiols: generation of nitroxyl (HNO) and subsequent chemistry. *Biochemistry* **37**, 5362-5371 (1998).
- 89 Filipovic, M. R. *et al.* Chemical characterization of the smallest *S*-nitrosothiol, HSNO; cellular cross-talk of H₂S and *S*-nitrosothiols. *J. Am. Chem. Soc.* **134**, 12016-12027 (2012).
- 90 Smulik, R. *et al.* Nitroxyl (HNO) reacts with molecular oxygen and forms peroxyxynitrite at physiological pH: biological implications. *J. Biol. Chem.* (2014).

- 91 Rinaldo, S. *et al.* Unusual heme binding properties of the dissimilative nitrate respiration regulator, a bacterial nitric oxide sensor. *Antioxid. Redox Signal.* **17**, 1178-1189 (2012).
- 92 Crack, J. C., Stapleton, M. R., Green, J., Thomson, A. J. & Le Brun, N. E. Mechanism of [4Fe-4S](Cys)₄ cluster nitrosylation is conserved among NO-responsive regulators. *J. Biol. Chem.* **288**, 11492-11502 (2013).
- 93 Reeves, B. D. *et al.* Conversion of *S*-phenylsulfonyleysteine residues to mixed disulfides at pH 4.0: utility in protein thiol blocking and in protein-*S*-nitrosothiol detection. *Org. Biomol. Chem.* **12**, 7942-7956 (2014).
- 94 Thi Thu Huyen, N. *et al.* Genome-wide responses to carbonyl electrophiles in *Bacillus subtilis*: control of the thiol-dependent formaldehyde dehydrogenase AdhA and cysteine proteinase YraA by the MerR-family regulator YraB (AdhR). *Mol. Microbiol.* (2008).
- 95 Potter, A. J., Kidd, S. P., McEwan, A. G. & Paton, J. C. The MerR/NmlR Family Transcription Factor of *Streptococcus pneumoniae* Responds to Carbonyl Stress and Modulates Hydrogen Peroxide Production. *J. Bacteriol.* **192**, 4063-4066 (2010).
- 96 McEwan, A. G. *et al.* Novel bacterial MerR-like regulators: their role in the response to carbonyl and nitrosative stress. *Adv. Microb. Physiol.* **58**, 1-22 (2011).
- 97 Farmer, E. E. & Davoine, C. Reactive electrophile species. *Curr. Opin. Plant Biol.* **10**, 380-386 (2007).
- 98 Wall, S. B. *et al.* Detection of electrophile-sensitive proteins. *Biochim. Biophys. Acta* **1840**, 913-922 (2014).
- 99 Higdon, A. N., Landar, A., Barnes, S. & Darley-USmar, V. M. The electrophile responsive proteome: integrating proteomics and lipidomics with cellular function. *Antioxid. Redox Signal.* **17**, 1580-1589 (2012).
- 100 LoPachin, R. M. & Gavin, T. Molecular mechanisms of aldehyde toxicity: a chemical perspective. *Chem. Res. Toxicol.* **27**, 1081-1091 (2014).
- 101 Farmer, E. E. & Mueller, M. J. ROS-mediated lipid peroxidation and RES-activated signaling. *Annu. Rev. Plant Biol.* **64**, 429-450 (2013).
- 102 Ratasuk, N. & Nanny, M. A. Characterization and quantification of reversible redox sites in humic substances. *Environ. Sci. Technol.* **41**, 7844-7850 (2007).

- 103 Nohl, H., Jordan, W. & Youngman, R. J. Quinones in biology: functions in electron transfer and oxygen activation. *Adv. Free Rad. Biol. Med.* **2**, 211-279 (1986).
- 104 Marcia, M., Ermler, U., Peng, G. & Michel, H. A new structure-based classification of sulfide:quinone oxidoreductases. *Proteins* **78**, 1073-1083 (2010).
- 105 O'Brien, P. J. Molecular mechanisms of quinone cytotoxicity. *Chem. Biol. Interact.* **80**, 1-41 (1991).
- 106 Marnett, L. J., Riggins, J. N. & West, J. D. Endogenous generation of reactive oxidants and electrophiles and their reactions with DNA and protein. *J. Clin. Invest.* **111**, 583-593 (2003).
- 107 Leelakriangsak, M. *et al.* Regulation of quinone detoxification by the thiol stress sensing DUF24/MarR-like repressor, YodB in *Bacillus subtilis*. *Mol. Microbiol.* **67**, 1108-1124 (2008).
- 108 Töwe, S. *et al.* The MarR-type repressor MhqR (YkvE) regulates multiple dioxygenases/glyoxalases and an azoreductase which confer resistance to 2-methylhydroquinone and catechol in *Bacillus subtilis*. *Mol. Microbiol.* **66**, 40-54 (2007).
- 109 Thomas, E. L. Myeloperoxidase, hydrogen peroxide, chloride antimicrobial system: nitrogen-chlorine derivatives of bacterial components in bactericidal action against *Escherichia coli*. *Infect. Immun.* **23**, 522-531 (1979).
- 110 Palm, G. J. *et al.* Structural insights into the redox-switch mechanism of the MarR/DUF24-type regulator HypR. *Nucleic Acids Res.* **40**, 4178-4192 (2012).
- 111 Gray, M. J., Wholey, W.-Y., Parker, B. W., Kim, M. & Jakob, U. NemR is a bleach-sensing transcription factor. *J. Biol. Chem.* **288**, 13789-13798 (2013).
- 112 Parker, B. W., Schwessinger, E. A., Jakob, U. & Gray, M. J. The RclR protein is a reactive chlorine-specific transcription factor in *Escherichia coli*. *J. Biol. Chem.* **288**, 32574-32584 (2013).
- 113 Kabil, O. & Banerjee, R. Redox biochemistry of hydrogen sulfide. *J. Biol. Chem.* **285**, 21903-21907 (2010).
- 114 Kolluru, G. K., Shen, X., Bir, S. C. & Kevil, C. G. Hydrogen sulfide chemical biology: Pathophysiological roles and detection. *Nitric Oxide* **35**, 5-20 (2013).
- 115 Paul, B. D. & Snyder, S. H. H₂S signalling through protein sulfhydration and beyond. *Nat. Rev. Mol. Cell Biol.* **13**, 499-507 (2012).

- 116 Czyzewski, B. K. & Wang, D.-N. Identification and characterization of a bacterial hydrosulphide ion channel. *Nature* **483**, 494-497 (2012).
- 117 Toohey, J. I. Sulfur signaling: is the agent sulfide or sulfane? *Anal. Biochem.* **413**, 1-7 (2011).
- 118 Kabil, O., Motl, N. & Banerjee, R. H₂S and its role in redox signaling. *Biochim. Biophys. Acta* **1844**, 1355-1366 (2014).
- 119 Newberry, K. J., Fuangthong, M., Panmanee, W., Mongkolsuk, S. & Brennan, R. G. Structural mechanism of organic hydroperoxide induction of the transcription regulator OhrR. *Molec. Cell* **28**, 652-664 (2007).
- 120 Lim, D., Poole, K. & Strynadka, N. C. Crystal structure of the MexR repressor of the *mexRAB-oprM* multidrug efflux operon of *Pseudomonas aeruginosa*. *J. Biol. Chem.* **277**, 29253-29259 (2002).
- 121 Chen, H. *et al.* Structural insight into the oxidation - sensing mechanism of the antibiotic resistance of regulator MexR. *EMBO Rep.* **11**, 685-690 (2010).
- 122 Ji, Q. *et al.* *Staphylococcus aureus* CymR is a new thiol-based oxidation-sensing regulator of stress resistance and oxidative response. *J. Biol. Chem.* **287**, 21102-21109 (2012).
- 123 Niu, W.-N., Yadav, P. K., Adamec, J. & Banerjee, R. S-glutathionylation enhances human cystathionine β -synthase activity under oxidative stress conditions. *Antioxid. Redox Signal.* **22**, 350-361 (2014).
- 124 Yadav, P. K., Yamada, K., Chiku, T., Koutmos, M. & Banerjee, R. Structure and kinetic analysis of H₂S production by human mercaptopyruvate sulfurtransferase. *J. Biol. Chem.* **288**, 20002-20013 (2013).
- 125 Shatalin, K., Shatalina, E., Mironov, A. & Nudler, E. H₂S: a universal defense against antibiotics in bacteria. *Science* **334**, 986-990 (2011).
- 126 Nishida, M. *et al.* Hydrogen sulfide anion regulates redox signaling via electrophile sulfhydration. *Nat. Chem. Biol.* **8**, 714-724 (2012).
- 127 Zhang, D. *et al.* Detection of protein S-sulfhydration by a tag-switch technique. *Angew Chem. Int. Ed.* **53**, 575-581 (2014).
- 128 Libiad, M., Yadav, P. K., Vitvitsky, V., Martinov, M. & Banerjee, R. Organization of the human mitochondrial hydrogen sulfide oxidation pathway. *J. Biol. Chem.* **289**, 30901-30910 (2014).

- 129 Bailey, T. S., Zakharov, L. N. & Pluth, M. D. Understanding hydrogen sulfide storage: probing conditions for sulfide release from hydrodisulfides. *J. Am. Chem. Soc.* **136**, 10573-10576 (2014).
- 130 Greiner, R. *et al.* Polysulfides link H₂S to protein thiol oxidation. *Antioxid. Redox Signal.* **19**, 1749-U1122 (2013).
- 131 Krishnan, N., Fu, C., Pappin, D. J. & Tonks, N. K. H₂S-induced sulphydration of the phosphatase PTP1B and its role in the endoplasmic reticulum stress response. *Sci. Signal.* **4**, ra86-ra86, doi:10.1126/scisignal.2002329 (2011).
- 132 Sen, N. *et al.* Hydrogen sulfide-linked sulphydration of NF- κ B mediates its anti-apoptotic actions. *Molec. Cell* **45**, 13-24 (2012).
- 133 Lowy, F. D. *Staphylococcus aureus* infections. *N. Engl. J. Med.* **339**, 520-532 (1998).
- 134 Nizet, V. Understanding how leading bacterial pathogens subvert innate immunity to reveal novel therapeutic targets. *J. Allergy Clin. Immunol.* **120**, 13-22 (2007).
- 135 Lithgow, J. K., Hayhurst, E. J., Cohen, G., Aharonowitz, Y. & Foster, S. J. Role of a cysteine synthase in *Staphylococcus aureus*. *J. Bacteriol.* **186**, 1579-1590 (2004).
- 136 Jacob, C., Giles, G. I., Giles, N. M. & Sies, H. Sulfur and selenium: the role of oxidation state in protein structure and function. *Angew Chem. Int. Ed.* **42**, 4742-4758 (2003).
- 137 Soutourina, O., Poupel, O., Coppee, J. Y., Danchin, A., Msadek, T., Martin-Verstraete, I. CymR, the master regulator of cysteine metabolism in *Staphylococcus aureus*, controls host sulfur source utilization and plays a role in biofilm formation. *Molec. Microbiol.* **73**, 194-211 (2009).
- 138 Soutourina, O., Dubrac, S., Poupel, O., Msadek, T. & Martin-Verstraete, I. The pleiotropic CymR regulator of *Staphylococcus aureus* plays an important role in virulence and stress response. *PLoS Pathog.* **6**, e1000894 (2010).
- 139 Burns, K. E. *et al.* Reconstitution of a new cysteine biosynthetic pathway in *Mycobacterium tuberculosis*. *J. Am. Chem. Soc.* **127**, 11602-11603 (2005).
- 140 Bhawe, D. P., Muse, W. B., 3rd, Carroll, K. S. Drug targets in mycobacterial sulfur metabolism. *Infect. Disord. Drug Targets* **7**, 140-158 (2007).
- 141 Senaratne, R. H. *et al.* Vaccine efficacy of an attenuated but persistent *Mycobacterium tuberculosis* *cysH* mutant. *J. Med. Microbiol.* **56**, 454-458 (2007).

- 142 Hildebrandt, T. M. & Grieshaber, M. K. Three enzymatic activities catalyze the oxidation of sulfide to thiosulfate in mammalian and invertebrate mitochondria. *FEBS J.* **275**, 3352-3361 (2008).
- 143 Jackson, M. R., Melideo, S. L. & Jorns, M. S. Human sulfide:quinone oxidoreductase catalyzes the first step in hydrogen sulfide metabolism and produces a sulfane sulfur metabolite. *Biochemistry* **51**, 6804-6815 (2012).
- 144 Liu, T. *et al.* CsoR is a novel *Mycobacterium tuberculosis* copper-sensing transcriptional regulator. *Nat. Chem. Biol.* **3**, 60-68 (2007).
- 145 Chang, F.-M. J. *et al.* Cu(I)-mediated allosteric switching in a copper-sensing operon repressor (CsoR). *J. Biol. Chem.* **289**, 19204-19217 (2014).
- 146 Higgins, K. A. & Giedroc, D. Insights into protein allostery in the CsoR/RcnR family of transcriptional repressors. *Chem. Lett.* **43**, 20-25 (2014).
- 147 Mandal, A. K., Cheung, W. D. & Argüello, J. M. Characterization of a thermophilic P-type Ag⁺/Cu⁺-ATPase from the extremophile *Archaeoglobus fulgidus*. *J. Biol. Chem.* **277**, 7201-7208 (2002).
- 148 Gonzalez-Guerrero, M., Eren, E., Rawat, S., Stemmler, T. L. & Arguello, J. M. Structure of the two transmembrane Cu⁺ transport sites of the Cu⁺-ATPases. *J. Biol. Chem.* **283**, 29753-29759 (2008).
- 149 Banci, L., Bertini, I., Ciofi-Baffoni, S., Del Conte, R. & Gonnelli, L. Understanding copper trafficking in bacteria: interaction between the copper transport protein CopZ and the N-terminal domain of the copper ATPase CopA from *Bacillus subtilis*. *Biochemistry* **42**, 1939-1949 (2003).
- 150 Ma, Z. *et al.* Unnatural Amino Acid Substitution as a Probe of the Allosteric Coupling Pathway in a Mycobacterial Cu(I) Sensor. *J. Am. Chem. Soc.* **131**, 18044-18045 (2009).
- 151 Cipollone, R., Ascenzi, P. & Visca, P. Common themes and variations in the rhodanese superfamily. *IUBMB Life* **59**, 51-59 (2007).
- 152 Dahl, J.-U. *et al.* The Identification of a Novel Protein Involved in Molybdenum Cofactor Biosynthesis in *Escherichia coli*. *J. Biol. Chem.* **286**, 35801-35812 (2011).
- 153 Dahl, J.-U. *et al.* The sulfur carrier protein TusA has a pleiotropic role in *Escherichia coli* that also affects molybdenum cofactor biosynthesis. *J. Biol. Chem.* **288**, 5426-5442 (2013).

- 154 Ikeuchi, Y., Shigi, N., Kato, J., Nishimura A., Suzuki, T. Mechanistic insights into sulfur relay by multiple sulfur mediators involved in thiouridine biosynthesis at tRNA wobble positions. *Molec. Cell* **21**, 97-108 (2006).
- 155 Shi, R., Proteau, A., Villarroya, M., Moukadiri, I., Zhang, L., Trempe, JF., Matte, A., Armengod, M. E., Cygler, M. Structural basis for Fe-S cluster assembly and tRNA thiolation mediated by IscS protein-protein interactions. *PLoS Biol.* **8**, e1000354 (2010).
- 156 Filiatrault, M. J. *et al.* *Pseudomonas aeruginosa* PA1006, which plays a role in molybdenum homeostasis, is required for nitrate utilization, biofilm formation, and virulence. *PLoS One* **8**, e55594 (2013).
- 157 Tomblin, G. *et al.* *Pseudomonas aeruginosa* PA1006 is a persulfide-modified protein that is critical for molybdenum homeostasis. *PLoS One* **8**, e55593 (2013).
- 158 Robert, X. & Gouet, P. Deciphering key features in protein structures with the new ENDscript server. *Nucl. Acids Res.* **42**, W320-W324 (2014).
- 159 Numata, T., Fukai, S., Ikeuchi, Y., Suzuki, T., Nureki, O. Structural basis for sulfur relay to RNA mediated by heterohexameric TusBCD complex. *Structure* **14**, 357-366 (2006).
- 160 Dahl, C. *et al.* Novel genes of the *dsr* gene cluster and evidence for close interaction of Dsr proteins during sulfur oxidation in the phototrophic sulfur bacterium *Allochromatium vinosum*. *J. Bacteriol.* **187**, 1392-1404 (2005).
- 161 Tiranti, V. *et al.* Loss of ETHE1, a sulfur mitochondrial dioxygenase, causes fatal sulfide toxicity in ethylmalonic encephalopathy. *Neurology* **72**, A135-A135 (2009).
- 162 Luebke, J. L., Arnold, R. J. & Giedroc, D. P. Selenite and tellurite form mixed seleno- and tellurotrisulfides with CstR from *Staphylococcus aureus*. *Metallomics* **5**, 335-342 (2013).
- 163 Mueller, E. G. Trafficking in persulfides: delivering sulfur in biosynthetic pathways. *Nat. Chem. Biol.* **2**, 185-194 (2006).
- 164 Sekowska, A., Kung, H. F. & Danchin, A. Sulfur metabolism in *Escherichia coli* and related bacteria: facts and fiction. *J. Mol. Microbiol. Biotechnol.* **2**, 145-177 (2000).
- 165 Dahl, C., Friedrich, C. G. *Microbial sulfur metabolism*. (Springer, 2008).

- 166 Zannoni, D., Borsetti, F., Harrison, J. J. & Turner, R. J. The bacterial response to the chalcogen metalloids Se and Te. *Adv. Microb. Physiol.* **Volume 53**, 1-312 (2007).
- 167 Chasteen, T. G., Fuentes, D. E., Tantaleán, J. C. & Vásquez, C. C. Tellurite: history, oxidative stress, and molecular mechanisms of resistance. *FEMS Microbiol. Rev.* **33**, 820-832 (2009).
- 168 Lindemann, T. & Hintelmann, H. Identification of selenium-containing glutathione S-conjugates in a yeast extract by two-dimensional liquid chromatography with inductively coupled plasma MS and nanoelectrospray MS/MS detection. *Anal. Chem.* **74**, 4602-4610 (2002).
- 169 Kice, J. L., Lee, T. W. S., and Pan, S. Mechanism of the reaction of thiols with selenite. *J. Am. Chem. Soc.* **102**, 4448-4455 (1980).
- 170 Larabee, J. L., Hocker, J. R. & Hanas, J. S. Mechanisms of inhibition of zinc-finger transcription factors by selenium compounds selen and selenite. *J. Inorg. Biochem.* **103**, 419-426 (2009).
- 171 Harrison, J. J., Ceri, H., Stremick, C. & Turner, R. J. Differences in biofilm and planktonic cell mediated reduction of metalloid oxyanions. *FEMS Microbiol. Let.* **235**, 357-362 (2004).
- 172 Riddles, P. W., Blakeley, R. L. & Zerner, B. Reassessment of Ellman's reagent. *Meth. Enzymol.* **Volume 91**, 49-60, doi:10.1016/s0076-6879(83)91010-8 (1983).
- 173 Wolf-Yadlin, A., Hautaniemi, S., Lauffenburger, D. A. & White, F. M. Multiple reaction monitoring for robust quantitative proteomic analysis of cellular signaling networks. *Proc. Natl. Acad. Sci. U.S.A.* **104**, 5860-5865 (2007).
- 174 Kuzmic, P. Program DYNAFIT for the analysis of enzyme kinetic data: application to HIV proteinase. *Anal. Biochem.* **237**, 260-273 (1996).
- 175 Milligan, B., Swan, J. M. The synthesis of disulphides by displacement reactions. *J. Ceramic Soc.* **1962**, 683-684 (1962).
- 176 Ba, L. A., Doring, M., Jamier, V. & Jacob, C. Tellurium: an element with great biological potency and potential. *Org. Biomol. Chem.* **8**, 4203-4216 (2010).
- 177 Freeman, F. & Angeletakis, C. N. Formation of α -disulfoxides, sulfinic anhydrides, and sulfines during the *m*-chloroperoxybenzoic acid oxidation of symmetrical S-alkyl alkanethiosulfinates. *J. Am. Chem. Soc.* **105**, 4039-4049 (1983).

- 178 Herring, C. D. & Blattner, F. R. Global transcriptional effects of a suppressor tRNA and the inactivation of the regulator *frmR*. *J. Bacteriol.* **186**, 6714-6720 (2004).
- 179 Sakamoto, K., Agari, Y., Agari, K., Kuramitsu, S., Shinkai, A. Structural and functional characterization of the transcriptional repressor CsoR from *Thermus thermophilus* HB8. *Microbiology* **156**, 1993-2005 (2010).
- 180 Dwarakanath, S. *et al.* Response to copper stress in *Streptomyces lividans* extends beyond genes under direct control of a copper-sensitive operon repressor protein (CsoR). *J. Biol. Chem.* **287**, 17833-17847 (2012).
- 181 Pan, J. & Carroll, K. S. Persulfide reactivity in the detection of protein S-sulfhydration. *ACS Chem. Biol.* **8**, 1110-1116 (2013).
- 182 Hill, B. C. *et al.* Interactions of sulfide and other ligands with cytochrome-c oxidase - an electron-paramagnetic-resonance study. *Biochem. J.* **224**, 591-600 (1984).
- 183 Miranda, K. M. & Wink, D. A. Persulfides and the cellular thiol landscape. *Proc. Natl. Acad. Sci. U.S.A.* **111**, 7505-7506 (2014).
- 184 Kelly, D. P., Chambers, L. A. & Trudinger, P. A. Cyanolysis and spectrophotometric estimation of trithionate in mixture with thiosulfate and tetrathionate. *Anal. Chem* **41**, 898-901 (1969).
- 185 Bubeck Wardenburg, J., Williams, W. A. & Missiakas, D. Host defenses against *Staphylococcus aureus* infection require recognition of bacterial lipoproteins. *Proc. Natl. Acad. Sci. U.S.A.* **103**, 13831-13836 (2006).
- 186 Toledo-Arana, A. *et al.* *Staphylococcus aureus* develops an alternative, *ica*-independent biofilm in the absence of the *arlRS* two-component system. *J. Bacteriol.* **187**, 5318-5329 (2005).
- 187 Hussain, M., Hastings, J. G. M. & White, P. J. A chemically defined medium for slime production by coagulase-negative staphylococci. *J. Med. Microbiol.* **34**, 143-147 (1991).
- 188 Chang, M. W., Toghrol, F. & Bentley, W. E. Toxicogenomic response to chlorination includes induction of major virulence genes in *Staphylococcus aureus*. *Environ. Sci. Technol.* **41**, 7570-7575 (2007).
- 189 Hochgräfe, F. *et al.* Nitric Oxide Stress Induces Different Responses but Mediates Comparable Protein Thiol Protection in *Bacillus subtilis* and *Staphylococcus aureus*. *J. Bacteriol.* **190**, 4997-5008 (2008).

- 190 Schlag, S., Nerz, C., Birkenstock, T. A., Altenberend, F. & Götz, F. Inhibition of staphylococcal biofilm formation by nitrite. *J. Bacteriol.* **189**, 7911-7919 (2007).
- 191 Wolf, C. *et al.* Proteomic analysis of antioxidant strategies of *Staphylococcus aureus*: diverse responses to different oxidants. *Proteomics* **8**, 3139-3153 (2008).
- 192 Fuchs, S. *et al.* *Aureolib* — a proteome signature library: Towards an understanding of *Staphylococcus aureus* pathophysiology. *PLoS One* **8**, e70669, doi:10.1371/journal.pone.0070669 (2013).
- 193 Hildebrandt, T., Di Meo, I., Zeviani, M., Viscomi, C. & Braun, H. P. Proteome adaptations in ETHE1 deficient mice indicate a role of sulfide signaling in lipid catabolism and cytoskeleton organization via post-translational protein modifications. *Biosci. Rep.* **31**, S42-S42 (2013).
- 194 Marcia, M., Ermler, U., Peng, G., Michel, H. A new structure-based classification of sulfide:quinone oxidoreductases. *Proteins* **78**, 1073-1083 (2009).
- 195 Rehder, D. S. & Borges, C. R. Cysteine sulfenic acid as an intermediate in disulfide bond formation and non-enzymatic protein folding. *Biochemistry* **49**, 7748-7755 (2010).
- 196 Apuy, J. L. *et al.* Pulsed-alkylation mass spectrometry for the study of protein folding and dynamics: development and application to the study of a folding/unfolding intermediate of bacterial luciferase. *Biochemistry* **40**, 15153-15163 (2001).
- 197 Ma, Z., Cowart, D. M., Scott, R. A. & Giedroc, D. P. Molecular insights into the metal selectivity of the copper(I)-sensing repressor CsoR from *Bacillus subtilis*. *Biochemistry* **48**, 3325-3334 (2009).
- 198 Xiao, Z. *et al.* Unification of the copper(I) binding affinities of the metallo-chaperones Atx1, Atox1, and related proteins: detection of probes and affinity standards. *J. Biol. Chem.* **286**, 11047-11055 (2011).
- 199 Fu, Y. *et al.* A new structural paradigm in copper resistance in *Streptococcus pneumoniae*. *Nat. Chem. Biol.* **9**, 177-183 (2013).
- 200 Senko, M., Beu, S. & McLaffertycor, F. Determination of monoisotopic masses and ion populations for large biomolecules from resolved isotopic distributions. *J. Am. Soc. Mass Spectrom.* **6**, 229-233 (1995).
- 201 Reyes-Caballero, H., Campanello, G. C. & Giedroc, D. P. Metalloregulatory proteins: metal selectivity and allosteric switching. *Biophys. Chem.* **156**, 103-114 (2011).

- 202 Apuy, J. L., Chen, X., Russell, D. H., Baldwin, T. O. & Giedroc, D. P. Ratiometric pulsed alkylation/mass spectrometry of the cysteine pairs in individual zinc fingers of MRE-binding transcription factor-1 (MTF-1) as a probe of zinc chelate stability. *Biochemistry* **40**, 15164-15175 (2001).
- 203 Chang, F.-M. J., Lauber, M. A., Running, W. E., Reilly, J. P. & Giedroc, D. P. Ratiometric pulse–chase amidination mass spectrometry as a probe of biomolecular complex formation. *Anal. Chem.* **83**, 9092-9099 (2011).
- 204 Fuchs, S., Pané-Farré, J., Kohler, C., Hecker, M. & Engelmann, S. Anaerobic gene expression in *Staphylococcus aureus*. *J. Bacteriol.* **189**, 4275-4289 (2007).
- 205 Bueno, E., Mesa, S., Bedmar, E. J., Richardson, D. J. & Delgado, M. J. Bacterial adaptation of respiration from oxic to microoxic and anoxic conditions: redox control. *Antioxid. Redox Signaling* **16**, 819-852 (2011).
- 206 Richardson, A. R., Dunman, P. M. & Fang, F. C. The nitrosative stress response of *Staphylococcus aureus* is required for resistance to innate immunity. *Mol. Microbiol.* **61**, 927-939 (2006).
- 207 Barraud, N. *et al.* Involvement of nitric oxide in biofilm dispersal of *Pseudomonas aeruginosa*. *J. Bacteriol.* **188**, 7344-7353 (2006).
- 208 Barraud, N., Kelso, M. J., Rice, S. A. & Kjelleberg, S. Nitric oxide: a key mediator of biofilm dispersal with applications in infectious diseases. *Curr. Pharm. Des.* **21**, 31-42 (2014).
- 209 Wrobel, A. T., Johnstone, T. C., Deliz Liang, A., Lippard, S. J. & Rivera-Fuentes, P. A fast and selective near-infrared fluorescent sensor for multicolor imaging of biological nitroxyl (HNO). *J. Am. Chem. Soc.* **136**, 4697-4705 (2014).
- 210 Devarie Baez, N. O., Reisz, J. A. & Furdui, C. M. Mass spectrometry in studies of protein thiol chemistry and signaling: Opportunities and caveats. *Free Rad Biol Med* (2014).
- 211 Pan, J. & Carroll, K. S. Chemical biology approaches to study protein cysteine sulfenylation. *Biopolymers* **101**, 165-172 (2014).
- 212 Rhee, K. Y., Erdjument-Bromage, H., Tempst, P. & Nathan, C. F. S-nitroso proteome of *Mycobacterium tuberculosis*: enzymes of intermediary metabolism and antioxidant defense. *Proc. Natl. Acad. Sci. U.S.A.* **102**, 467-472 (2005).
- 213 Seth, D., Hausladen, A., Wang, Y.-J. & Stamler, J. S. Endogenous protein S-nitrosylation in *E. coli*: regulation by OxyR. *Science* **336**, 470-473 (2012).

- 214 Soonsanga, S., Lee, J.-W. & Helmann, J. D. Oxidant-dependent switching between reversible and sacrificial oxidation pathways for *Bacillus subtilis* OhrR. *Molec. Microbiol.* **68**, 978-986 (2008).
- 215 Debiemme-Chouvy, C., Wartelle, C. & Sauvage, F.-X. First evidence of the oxidation and regeneration of polysulfides at a GaAs electrode, under anodic conditions. A study by *in Situ* UV–Visible spectroelectrochemistry. *J. Phys. Chem. B.* **108**, 18291-18296 (2004).

APPENDIX

```
[task]
  data = equilibria
  task = fit

[mechanism]
  P + DNA <=> DNA.P : K1 assoc.
  P + DNA.P <=> DNA.2P : K2 assoc.

[concentration]
  DNA = 10

[constants]
  K1 = 1 ?
  K2 = 1 ?

[response]
  DNA = .01257
  DNA.P = .01364
  DNA.2P = .01527

[equilibria]
  directory ./data/CstR_2014
  extension txt
  variable P
  file 10nMCstR4_apo_OP1

[output]
  directory ./output/Dynafit/Results/CstR+copper_2014/CstR_apo_OP1

[end]
```

Figure A1: Example DynaFit¹⁷⁴ script file used for fitting data obtained from fluorescence anisotropy titrations of CstR with fluorescently-labeled *cst* OP1.

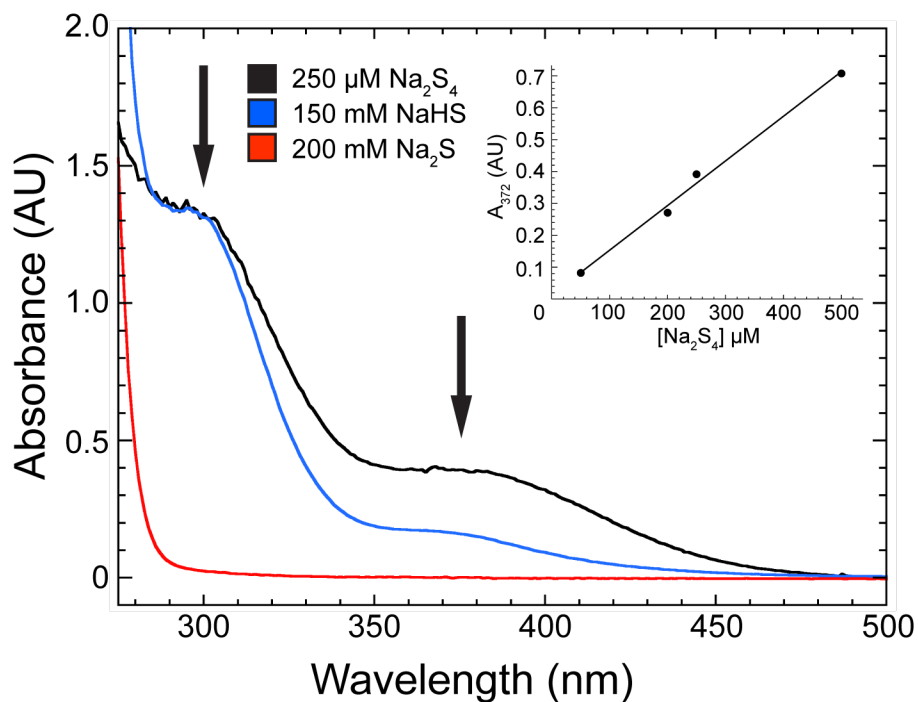


Figure A2: UV-Vis spectra of sulfur sources used. Na₂S₄ (black), NaHS (blue), and Na₂S (red) were prepared anaerobically in fully degassed 10 mM Tris-HCl at pH 8.0 containing 1 mM EDTA. The commercial preparation of NaSH used here is contaminated with detectable (0.3%) polysulfide as determined by a Na₂S₄ standard curve (inset) and gives off a light yellow hue. The yellow coloring is not present in crystalline Na₂S. Arrows indicate locations of characteristic disulfide peaks at 300 and 372 nm.^{130,215}

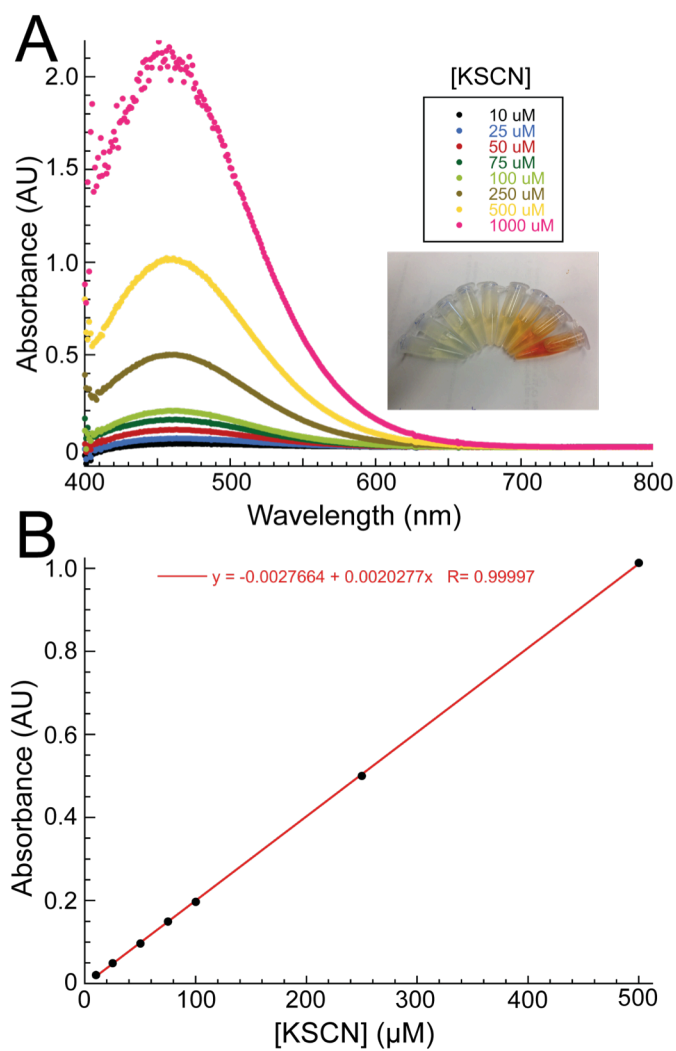


Figure A3. Cyanolysis assay standard curve for the determination of [GSSH]. At 1000 μM KSCN, detection was approaching saturation and this value was excluded from the standard curve.

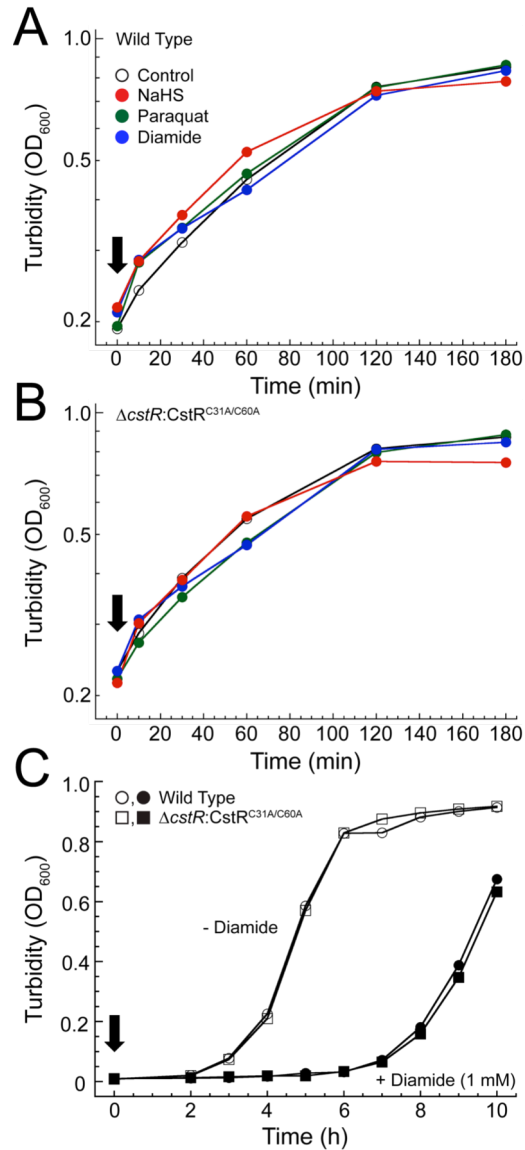


Figure A4. *Staphylococcus aureus* growth rates are not impacted by addition of oxidative stressors and growth under diamide stress is not *cst*-operon dependent. (A-B) Addition of *cst* operon inducers NaHS or diamide and non-inducers have no growth phenotype when added to mid-log cells (marked by the arrow, OD₆₀₀≈0.2). Both WT (A) and $\Delta cstR:CstR^{C31A/C60A}$ (B) strains were tested with the addition of 0.2 mM NaHS (red), 1.0 mM diamide (blue), or 25 nM paraquat (green) vs. untreated cells (black). (C) Diamide was added to a final concentration of 1 mM at the beginning of the growth (marked by the arrow, *filled* symbols) induces a growth phenotype that is equivalent in WT (circles) and $\Delta cstR:CstR^{C31A/C60A}$ (squares) strains. Thus, although diamide weakly induces the operon (Fig. 24, Chapter 3) expression of *cst* operon is not likely essential for survival under diamide stress, in contrast to NaHS sulfide stress.

```

[task]

data = equilibria
task = fit

[mechanism]

cstr + cu <==> cstr.cu : k1 assoc.
bca + bca + cu <==> bca2.cu : k2 assoc.

[concentrations]

[constants]

k1 = 1e+3?
k2 = 1.585e+5

[responses]

bca = 5.7e-5?
bca2.cu = 0.0077

[equilibria]

variable cstr
file ./data/Metal_Binding/CstR_Cu1_BCA_3.txt |concentration cu = 9.98, bca = 30
file ./data/Metal_Binding/CstR_Cu1_BCA_1.txt |concentration cu = 18.9, bca = 50
file ./data/Metal_Binding/CstR_Cu1_BCA_2.txt |concentration cu = 29.6, bca = 70

[output]

directory
./output/Dyanfit/results/Metal_Binding/CstR+Cu1_BCA/CstR+Cu1_BCA_Global_3

```

Figure A5: Representative DynaFit¹⁷⁴ script file used for a global fit to a direct competition model.

CURRICULUM VITAE

Justin Lee Luebke

Department of Chemistry
Indiana University
Bloomington, IN 47405-7003
Email: JLLuebke@indiana.edu, Tel: 612-419-1207

Education

- July 2009 – Present PhD, Chemistry, Indiana University, Bloomington, IN
Dissertation Title: Biophysical and Functional Characterization of the Persulfide Sensor CstR from *Staphylococcus aureus*
Advisor: David P. Giedroc.
- Aug 2004 – May 2009 Winona State University, Winona, MN B.S. Chemistry, B.S. Biochemistry, and B.S. Cell & Molecular Biology

Research Experience

- May 2014 – Present
May 2011 – Aug 2013 Graduate Research Assistant, Giedroc Laboratory
- Sept 2009 – May 2010 Introduction to Research Rotation Indiana University Department of Chemistry (Research Advisors: David P. Giedroc and Stephen C. Jacobson).
Research: Initial development of a csrO-PEG-fCzrA complex for the fabrication of a novel reagentless microfluidic biosensor for Zn(II)
- July 2009 – Sept 2009 Summer Research Associate – Indiana University Department of Chemistry (Research Advisor: David P. Giedroc).
Research: Initial purification and characterization of CsoR IV from *Staphylococcus aureus* (later renamed CstR)
- June 2008 – Aug 2008 University of Nebraska – Lincoln NSF Research Experience for Undergraduates (Research Advisor: Vadim Gladyshev, Redox Biology Center).
Research: Methionine sulfoxide reductase activity in mouse liver and lung

Teaching Experience

Aug 2013 – May 2014 Associate Instructor (Principles of Chemistry and Biochemistry,
Aug 2009 – May 2011 Introduction to Chemical Principles, Elementary Chemistry, Biochemistry Laboratory, Biological Chemistry)

Honors and Awards

2009 – 2011 Indiana University Dean's Allocation Fellowship

Publications

Luebke, J. L. and Giedroc, D. P. Microbial Mechanisms of Redox Sensing and Regulation.

Biochemistry – Invited Current Topics Review, Submitted

Luebke, J. L., Bruce, K. E., Shen, J., Peng, H., Karty, J., and Giedroc D. P. Kinetic Analysis of Cysteine Residue Reactivity in the Persulfide Sensor CstR from *Staphylococcus aureus*. Manuscript in preparation

Higgins, K. A., Peng, H., **Luebke, J. L.**, Chang, F. M., and Giedroc D. P. Conformational Analysis and Chemical Reactivity of the Multidomain Sulfurtransferase, *Staphylococcus aureus*, CstA. DOI: 10.1021/acs.biochem.5b00056

Luebke, J. L., Shen, J., Bruce, K. E., Kehl-Fei, T. E., Peng, H., Skaar, E. P., and Giedroc, D. P. (2014) The CsoR-like Sulfurtransferase Repressor (CstR) is a Persulfide Sensor in *Staphylococcus aureus*. *Mol. Microbiol.* 94. 1343-60

Luebke, J. L., Arnold, R. J., and Giedroc, D. P. (2013) Selenite and Tellurite Form Mixed Seleno- and Tellurotrisulfides with CstR from *Staphylococcus aureus*. *Metallomics.* 5. 335-342

Wilson, T. **Luebke, J. L.**, Morcomb, E. F., Carrell, E. J., Leveranz, M. C., Kobs, L., Schmidt, T. P., Limburg, P. J., Vorsa, N., and Singh, A. P. (2010) Glycemic Responses to Sweetened Dried and Raw Cranberries in Humans with Type 2 Diabetes. *J. Food Sci.* 75. H218-223

Presentations

2014 – Nov 11th **Justin L. Luebke**
“Hydrogen Sulfide Sensing and Regulation in *Staphylococcus aureus*”

Oral presentation for the ChemGRC Seminar Series, Indiana University, Bloomington, IN

- 2014 – Oct 11th **Justin L. Luebke**, Jiangchuan Chen, Kevin E. Bruce, Thomas Kehl-Fie, Hui Peng, Randy J. Arnold, Eric P. Skaar, and David P. Giedroc
“Persulfide Sensing and Regulation in *Staphylococcus aureus* by the Transcription Repressor CstR”
Poster presentation at the August M. Watanabe Symposium in Biotechnology at Indiana University, Bloomington, IN
- 2013 – Sept 10th **Justin L. Luebke**, Randy J. Arnold, and David P. Giedroc.
“Hydrogen Sulfide, Selenite, and Tellurite form mixed Disulfides and Seleno- and Tellurotrisulfides with the Transcriptional Repressor CstR from *Staphylococcus aureus*”
Poster presentation at the 2013 American Chemical Society Fall National Meeting and Exposition, Indianapolis, IN
- 2013 – Jan 23rd **Justin L. Luebke**, Randy J. Arnold, and David P. Giedroc.
“Hydrogen Sulfide, Selenite, and Tellurite form mixed Disulfides and Seleno- and Tellurotrisulfides with the Transcriptional Repressor CstR from *Staphylococcus aureus*”
Poster presentation at the 2013 Winter Conference on Medicinal & Bioorganic Chemistry (WCMBC) in Steamboat Springs, CO
- 2012 – Sept 29th **Justin L. Luebke** and David P. Giedroc.
“Comparative Analysis of *Staphylococcus aureus* Transcriptional Repressors CstR and CsoR.”
Poster presentation at the August M. Watanabe Symposium in Biotechnology at Indiana University, Bloomington, IN
- 2011 – Nov 5th **Justin L. Luebke**
“Characterization of CstR (CsoR-like sulfur transferase repressor) and CstA from *Staphylococcus aureus*”
Oral presentation for fulfillment of IU Chemistry 5th Semester Candidacy Requirements and Indiana University, Bloomington, IN
- 2011 – Aug 8th **Justin L. Luebke** and David P. Giedroc.
“Characterization of a Trisulfide-like Selenium Bridge in the *Staphylococcus aureus* Transcriptional Repressor CstR.”
Poster presentation at the 2011 International Conference on Biological Inorganic Chemistry (ICBIC) in Vancouver, British Columbia, Canada

- 2011 – June 10th **Justin L. Luebke** and David P. Giedroc.
 “Characterization of a Trisulfide-like Selenium Bridge in the *Staphylococcus aureus* Transcriptional Repressor CstR.”
 Poster presentation at the 2011 American Chemical Society Central Region Meeting (CERM), Indianapolis, IN
- 2009 **Justin L. Luebke** and Mark A. Engen.
 “Natural Flux of Greenhouse Gasses”
 Oral presentation at the 2009 Celebration of Research and Creative Scholarship at Winona State University, Winona, MN
- 2009 Ted Wilson, Erin F. Morcomb, Travis P. Schmidt, **Justin L. Luebke**, Emily J. Carrell, Megan C. Leveranz, Lisa Kobs, Ajay P. Singh, and Paul J. Limburg.
 “Glycemic Response of Type 2 Diabetics to Sweetened Dried Cranberries”
 Poster presentation at the 2009 Celebration of Research and Creative Scholarship at Winona State University, Winona, MN
- 2009 Ted Wilson, Erin F. Morcomb, Travis P. Schmidt, **Justin L. Luebke**, Emily J. Carrell, Megan C. Leveranz, Lisa Kobs, Ajay P. Singh, and Paul J. Limburg.
 “Glycemic Response of Type 2 Diabetics to Sweetened Dried Cranberries”
 Poster presentation at the 2009 Experimental Biology Conference in New Orleans, LA
- 2008 **Justin L. Luebke**, Byung Cheon Lee, and Vadim Gladyshev.
 “MsrA and MsrB Protein Activity in Mouse Liver and Lung”
 Poster presentation at the 2008 University of Nebraska – Lincoln NSF Summer Research Experience for Undergraduates Symposium, Lincoln, NE

Professional Activities

- 2014 – 2015 Indiana University Chemistry Career Development Symposium, Planning Committee and Founding Member, Indiana University, Bloomington, IN
- Mar 2014 2014 Kelley School of Business Johnson Center for Entrepreneurship and Innovation Velocity Conference, University of California Berkeley, Berkeley, CA
- Dec 12 – 15th 2011 “Mass Spectrometry in Proteomics & Protein Structure Analysis” Short Course presented by Dr. Michael Przybylski,

University of Konstanz, Germany. Indiana University
Department of Chemistry, Bloomington, IN

2009 – Present

ACS, Member

2008 – 2009

Chemistry Club ASO (Association of Student Organizations)
Representative, Winona State University, Winona, MN

Skill and Expertise

Molecular Biology, Microbiology, and Biochemistry

- PCR amplification/cloning
- Site-directed mutagenesis
- Recombinant protein expression and purification from *E. coli*
- Äkta FPLC (affinity, ion exchange, and size exclusion chromatography)
- Biosafety level 2 work with *Staphylococcus aureus*

Spectroscopy

- UV-Vis (metal binding and competition experiments)
- Fluorescence anisotropy
- Atomic absorption
- Circular dichroism

Spectrometry

- LC-ESI-MS
- MALDI-TOF MS
- Tandem MS (LTQ-Orbitrap, LTQ-Velos)
- Synapt G2
- Ion mobility MS

Software

- DynaFit
- MassLynx
- Xcalibur
- Protrawler
- FlexAnalysis
- Pymol
- Prism
- Adobe Illustrator

Other

- Protein work under anaerobic conditions (glovebox, argon)
- Glovebox maintenance
- Solid-phase oligonucleotide synthesis

- Laboratory safety officer

References

David P. Giedroc

Department of Chemistry
Indiana University
Simon Hall 320A
212 South Hawthorn Drive
Bloomington, IN 47405
giedroc@indiana.edu
Tel: (812) 856-3178

Khadine A. Higgins

Department of Chemistry
Salve Regina University
O'Hare Academic Center 233
Shepard Avenue
Newport, RI 02840
khadine.higgins@salve.edu
Tel: (401) 341-3215

Ted Wilson

Department of Biology
Winona State University
Pasteur Hall 232
175 West Mark Street
Winona, MN 55987
twilson@winona.edu
Tel: (507) 457-2485